

**PRECLINICAL BIOCOMPATIBILITY ASSESSMENT OF CARDIOVASCULAR
DEVICES**

by

Trevor Arnoult Snyder

B.S., Tulane University, 1997

Submitted to the Graduate Faculty of
The School of Engineering in partial fulfillment
of the requirements for the degree of
Doctor of Philosophy

University of Pittsburgh

2006

UNIVERSITY OF PITTSBURGH
SCHOOL OF ENGINEERING

This dissertation was presented

by

Trevor Arnoult Snyder

It was defended on

March 31, 2006

and approved by

James F. Antaki, Ph.D.

Professor, Departments of Biomedical Engineering & Computer Science, Carnegie Mellon University; Associate Professor Departments of Bioengineering & Surgery; University of Pittsburgh

Franklin A. Bontempo, M.D.

Associate Professor of Medicine, Department of Medicine

Harvey S. Borovetz, Ph.D.

Professor & Chair, Department of Bioengineering; Robert L. Hardesty Professor, Department of Surgery; Professor, Department of Chemical & Petroleum Engineering

William J. Federspiel, Ph.D.

Professor & CNG Faculty Fellow Department of Chemical & Petroleum Engineering; Professor, Departments of Bioengineering & Surgery

Robert L. Kormos, M.D.

Professor, Department of Surgery

William R. Wagner, Ph.D.

Dissertation Director

Associate Professor, Departments of Bioengineering, Chemical & Petroleum Engineering, & Surgery

Copyright © by Trevor Arnoult Snyder

2006

PRECLINICAL BIOCOMPATIBILITY ASSESSMENT OF CARDIOVASCULAR DEVICES

Trevor Arnoult Snyder, Ph.D.

University of Pittsburgh, 2006

Bleeding and thromboembolism remain major complications of ventricular assist device (VAD) support. The amount of biocompatibility information that may be collected during preclinical studies is limited due to a lack of available assays, leaving the evaluation of investigational devices incomplete. To address these issues, flow cytometric assays were developed to quantify bovine circulating activated platelets, platelet microaggregates, platelet-leukocyte aggregates, and monocytes expressing tissue factor. Platelet lifespan was determined using an *ex vivo* biotinylation technique.

These assays were applied in 50 animals receiving the Nimbus/Heartmate II axial flow VAD, 29 receiving the SunMedical EVAHEART centrifugal VAD, over 20 animals receiving a variety of other cardiovascular devices, and eight animals that underwent a sham VAD implantation procedure. The results demonstrated significantly increased circulating activated platelets and leukocytes, and cell aggregates following VAD implantation, which then usually declined to a lower but still significantly elevated level. Deviations from this pattern were observed in several pumps with obstructive thrombi in the blood flow path. Platelet life span decreased and platelet consumption correspondingly increased. The sham studies demonstrated that the effects of the implant procedure abated within three weeks. Thus, the ongoing platelet and leukocyte activation and aggregation, and decreased platelet life span could be attributed to the VADs, even while accounting for surgical effects.

To identify the potential causes of the observed cellular activation, VAD surface modifications, revolutions per min increases, and anticoagulant regimen changes were evaluated *in vivo*. Two blood-shearing devices were constructed to investigate the effects of the supraphysiologic shear field within rotary VADs, although heat generation and sealing issues

limited their effectiveness. Flow visualization of the Heartmate II VAD revealed vortices developed at low flow rates, frequently encountered *in vivo*.

In conclusion, the propensity of cardiovascular devices to activate platelets and leukocytes was quantified, while accounting for the effects of the implant procedure. Through *in vivo* and *in vitro* investigations, it was demonstrated that the blood-contacting surface and adverse flow effects each contributed to the observed cellular activation. Thus, applying novel biocompatibility assays to preclinical studies, including those evaluating design enhancements and refinements, may be used to develop safer cardiovascular devices.

TABLE OF CONTENTS

PREFACE.....	XXII
1.0 INTRODUCTION.....	1
1.1 THE CLINICAL NEED.....	1
1.1.1 First Generation Devices	2
1.1.1.1 The Jarvik-7 Total Artificial Heart.....	2
1.1.1.2 Pulsatile Ventricular Assist Devices.....	4
1.1.2 Second Generation Devices	6
1.1.3 Third Generation Devices	7
1.2 BIOCOMPATIBILITY CHALLENGES.....	7
1.2.1 Surface	9
1.2.1.1 The Intrinsic Coagulation Cascade.....	9
1.2.1.2 Cell Adhesion	10
1.2.1.3 Interface with Injured Tissue and the Extrinsic Cascade.....	10
1.2.1.4 Coatings	11
1.2.2 Flow Effects	11

1.2.2.1	Stagnation Zones and Vortices	11
1.2.2.2	Shear	12
1.2.3	Anticoagulation	14
1.3	PREVIOUS PRECLINICAL BIOCOMPATIBILITY STUDIES	15
1.4	SPECIFIC AIMS	15
2.0	BIOCOMPATIBILITY ASSAY DEVELOPMENT.....	16
2.1	INTRODUCTION	16
2.2	FLOW CYTOMETRIC QUANTIFICATION OF CIRCULATING ACTIVATED PLATELETS AND PLATELET MICROAGGREGATES .	17
2.2.1	Washington State University Monoclonal Antibody Center Antibodies	17
2.2.1.1	Methods	17
2.2.1.2	Results.....	19
2.2.1.3	Discussion	21
2.2.2	Annexin V	21
2.2.2.1	Methods	22
2.2.2.2	Results.....	22
2.2.2.3	Discussion	23
2.2.3	Anti-P-Selectin.....	24
2.2.3.1	Methods	24
2.2.3.2	Results.....	24

2.2.3.3	Discussion	25
2.2.4	Anti-bovine CD63.....	26
2.2.4.1	Methods	26
2.2.4.2	Results.....	26
2.2.4.3	Discussion	27
2.2.5	Platelet Microaggregates	27
2.3	PLATELET LIFE SPAN DETERMINATION BY <i>EX VIVO</i> BIOTINYLATION	28
2.3.1.1	Methods	29
2.3.1.2	Results.....	30
2.3.1.3	Discussion	31
2.4	QUANTIFICATION OF BOVINE LEUKOCYTE PLATELET AGGREGATES AND MONOCYTES EXPRESSING TISSUE FACTOR BY FLOW CYTOMETRY	32
2.4.1	Granulocyte-Platelet Aggregates.....	33
2.4.1.1	Methods	33
2.4.1.2	Results & Discussion.....	33
2.4.2	Monocyte-Platelet Aggregates	34
2.4.2.1	Methods	34
2.4.2.2	Results & Discussion.....	34
2.4.3	Monocytes Expressing Tissue Factor	34

2.4.3.1	Methods	34
2.4.3.2	Results & Discussion.....	35
3.0	BIOCOMPATIBILITY ASSESSMENT OF THE HEARTMATE II AXIAL FLOW VENTRICULAR ASSIST DEVICE	36
3.1	SPECIFIC AIMS	41
3.1.1	Quantification of Circulating Activated Platelets, Platelet Microaggregates, and Platelet Life Span.....	41
3.2	TEMPORAL STUDIES QUANTIFYING CIRCULATING ACTIVATED PLATELETS, PLATELET MICROAGGREGATES, AND PLATELET LIFE SPAN IN BOVINES RECEIVING THE HEARTMATE II.....	42
3.2.1	Methods.....	42
3.2.1.1	VAD Implant Procedure and Animal Care.....	42
3.2.1.2	Sham Surgical Implant Procedure.....	43
3.2.1.3	Study Termination and Necropsy	43
3.2.1.4	Blood Sampling and Assay Preparation.....	44
3.2.1.5	Statistical Analysis.....	44
3.2.2	Results.....	44
3.2.2.1	Uneventful Post-operative Course Data	44
3.2.2.2	Sham Surgical Implant Procedure.....	47
3.2.2.3	Comparison of Uneventful VAD Course and Sham Surgical Procedure Studies	48
3.2.2.4	Adverse Events.....	48

3.2.2.5	Platelet Life Span.....	53
3.2.2.6	The Effects of Step Increases in VAD RPM.....	54
3.2.2.7	Surface Comparisons.....	56
3.3	LEUKOCYTE PLATELET AGGREGATES AND MONOCYTE TISSUE FACTOR	57
3.3.1	Methods.....	57
3.3.2	Results	57
3.3.3	Discussion.....	58
3.4	FLOW VISUALIZATION OF THE HEARTMATE II	59
3.4.1	Methods.....	59
3.4.2	Results	60
3.5	DISCUSSION OF THE OVERALL HEARTMATE II FINDINGS	62
4.0	BIOCOMPABILITY ASSESSMENT OF THE SUNMEDICAL EVAHEART CENTRIFUGAL VAD	67
4.1	SPECIFIC AIMS	69
4.1.1	Quantify Circulating Activated Platelets, Platelet Microaggregates, Platelet Life Span, Leukocyte Platelet Aggregates, and Monocytes Expressing Tissue Factor.	69
4.1.2	Compare DLC vs. MPC Coated Pumps.	69
4.1.3	Assess the Impact of Using No Post-Operative Anticoagulation.....	69
4.2	BIOCOMPATIBILITY ASSAYS	69

4.2.1	Methods.....	69
4.2.2	Results	69
4.3	SURFACE COMPARISON OF DLC VS. MPC	72
4.3.1	Methods.....	73
4.3.2	Results	73
4.4	NO POST-OPERATIVE ANTICOAGULATION	74
4.4.1	Methods.....	75
4.4.2	Results	75
4.5	DISCUSSION OF OVERALL EVAHEART FINDINGS	76
5.0	BIOCOMPATIBILITY ASSESSMENT OF THE STREAMLINER VAD	78
5.1	SPECIFIC AIMS	79
5.1.1	Quantify Circulating Activated Platelets, Platelet Microaggregates, and Platelet Life Span in Bovines Implanted with the Streamliner VAD.....	79
5.1.2	Investigate the Effect of the Impeller Blade Tip Gap Width on Blood Damage and Platelet Activation.	79
5.2	BIOCOMPATIBILITY ASSAYS	79
5.2.1	Methods.....	79
5.2.2	Results	80
5.2.3	Discussion.....	81
5.3	INVESTIGATION OF THE EFFECTS OF IMPELLER BLADE TIP GAP ON PLATELET ACTIVATION AND BLOOD DAMAGE.....	82

5.3.1	Introduction.....	82
5.3.2	Methods.....	83
5.3.2.1	Streamliner Implant, Operation, and Blood Sample Collection	83
5.3.2.2	Blood Biocompatibility Assays	85
5.3.3	Results	87
5.3.3.1	Changes in Circulating Activated Platelets and Platelet Count with Decreases in Impeller Gap	87
5.3.3.2	Effect of Decreases in the Impeller Blade Tip Gap on Plasma Free Hemoglobin	89
5.3.3.3	Effect of Impeller Touchdown on Circulating Platelet Activated and Platelet Count	90
5.3.4	Discussion.....	93
6.0	BLOOD SHEARING DEVICES	97
6.1	SPECIFIC AIMS	98
6.1.1	Develop a Device to Expose Blood to the High Shear, Millisecond Exposure Time Environment Which Occurs in Rotary Blood Pumps..	98
6.1.2	Measure the Heat Generation and Reduce this Generation to Acceptable Levels for Blood Testing.....	98
6.1.3	Characterize the Flow Field in the Device.....	98
6.1.4	Apply Biocompatibility Assays to Quantify Activated Platelets and Microaggregates in Blood Passing through the Blood Shearing Device.	98
6.2	THE HEMOLYZER	98

6.2.1	Heat Generation Testing	99
6.2.1.1	Introduction.....	99
6.2.1.2	Methods	100
6.2.1.3	Results.....	101
6.2.1.4	Discussion	102
6.2.2	Visualization of the flow patterns within the Hemolyzer.....	102
6.2.2.1	Introduction.....	102
6.2.2.2	Methods	102
6.2.2.3	Results.....	103
6.2.2.4	Discussion	108
6.2.3	Platelet Activation and Microaggregate Formation Following Exposure to High Shear for Short Time Durations	109
6.2.3.1	Introduction.....	109
6.2.3.2	Methods	109
6.2.3.3	Results.....	110
6.2.3.4	Discussion	111
6.3	THE BLOOD SHEARING INSTRUMENT (BSI).....	112
6.3.1	Introduction.....	112
6.3.2	Sealing and heat generation issues	117

7.0	BIOCOMPATIBILITY ASSESSMENT OF AN INTRAVASCULAR ARTIFICIAL LUNG	121
7.1	SPECIFIC AIMS	121
7.1.1	Quantify Circulating Activated Platelets and Platelet Microaggregates with the Artificial Lung Following Implantation in Bovines.....	121
7.1.2	Development and Implementation of a Rapid Method for Assessing the Relative Biocompatibility of Several Coatings Applied to Hollow Fiber Membranes.....	121
7.2	BIOCOMPATIBILITY ASSAYS	121
7.2.1	Introduction.....	121
7.2.2	Methods.....	122
7.2.2.1	Device Insertion and Blood Sampling.....	122
7.2.2.2	Anticoagulation.....	122
7.2.2.3	Quantification of Circulating Activated Platelets and Platelet Microaggregates.....	122
7.2.2.4	Post-Explant Analysis.....	122
7.2.2.5	Scanning Electron Microscopy	123
7.2.2.6	Statistical Analysis	124
7.2.3	Results	125
7.2.3.1	Flow cytometric assays	125
7.2.3.2	Post-Explant Analysis.....	126
7.2.3.3	Scanning Electron Microscopy Findings.....	127

7.2.4	Potential Coatings for the Artificial Lung HMFs	128
7.2.4.1	Methods	129
7.2.4.2	Results.....	130
7.3	DISCUSSION.....	131
8.0	SUMMARY	133
8.1	CONCLUSIONS.....	133
8.2	FUTURE STUDIES.....	134
	BIBLIOGRAPHY.....	136

LIST OF TABLES

Table 5-1. Blood samples collected during acute Streamliner study.....	85
Table 6-1. Locations of hemolyzer temperature measurements.	100
Table 6-2. Performance characteristics of the BSI.	116
Table 7-1. Fiber/coating combinations tested in the <i>in vitro</i> rocker studies.....	130

LIST OF FIGURES

Figure 1-1. The Jarvik-7 TAH.	2
Figure 1-2. The Abiomed Abiocor TAH. (<i>AP Photo</i>)	3
Figure 1-3. Thoratec pneumatic VADs are shown in the left and right VAD configurations.....	4
Figure 1-4. Novacor (left) and Heartmate I (right) VADs are shown with external components. .	6
Figure 2-1. Flow cytometry analysis plots.....	18
Figure 2-2. The effect of sample washing on ColiS69 binding to platelets.....	19
Figure 2-3. Detection of <i>in vitro</i> activated bovine platelets with monoclonal antibodies BAQ125 and GC5.	20
Figure 2-4. Annexin V binding to <i>in vitro</i> activated platelets.	23
Figure 2-5. Anti-CD62P binding to <i>in vitro</i> activated platelets.....	25
Figure 2-6. Anti-CD63 binding to <i>in vitro</i> activated platelets.	27
Figure 2-7. Percent of biotinylated platelets detected by flow cytometry using SA-PE and SA-FITC, with and without washing.	30
Figure 2-8. Platelet life span determination following <i>ex vivo</i> biotinylation normalizing the one hour sample to 100% and using for different labeling techniques.....	31

Figure 3-1. The Heartmate II VAD with cannulae attached shown next to a D-cell battery.....	36
Figure 3-2. The Heartmate II pump with the stators and impeller shown above.....	37
Figure 3-3. The Heartmate II impeller and stators, without the bearings, are shown.....	38
Figure 3-4. The Heartmate II impeller and stators, without the bearings, are shown.....	39
Figure 3-5. H-Q curves provided by the manufacturer for the Heartmate II.....	40
Figure 3-6. The chart shows the temporal results of 3 platelet activation indicators and platelet microaggregates for an uneventful course animal, A063.	45
Figure 3-7. Combined temporal circulating activated platelet and platelet microaggregate data for 10 studies with uneventful post-operative courses.	46
Figure 3-8. Temporal data from 3 circulating activated platelet indicators and platelet microaggregates for 8 sham surgical procedure animals.....	47
Figure 3-9. Flow cytometric assay data from study A058 is shown.....	49
Figure 3-10. Three images from the necropsy of study A058 are shown.....	50
Figure 3-11. Flow cytometric study data from study A056 is shown.....	51
Figure 3-12. Data is shown from case A042, where pre-operative values were elevated, and the animal died from bleeding on POD16.	52
Figure 3-13. Pre-operative and post-implant platelet life spans in 8 animals receiving the Heartmate II.	53
Figure 3-14. Circulating activated platelets and platelet microaggregate following a step increase in VAD RPM.	55
Figure 3-15. Data from three platelet life span determinations are shown.....	56

Figure 3-16. Combined temporal data from 4 Heartmate II implanted animals is shown.....	58
Figure 3-17. The schematic shows the set-up for flow visualization imaging of the flow through the Heartmate II.....	60
Figure 3-18. The images show particles tracks indicating the flow patterns within the pump.....	61
Figure 3-19. A summary H-Q curve displaying under what conditions disturbed flow occurred in the inlet of the Heartmate II.....	62
Figure 4-1. The upper image shows a view of the interior of the EVAHEART. The lower image shows the recirculating Cool-Seal purge flow system.....	67
Figure 4-2. Temporal circulating activated platelet and platelet microaggregate data collected from an uneventful post-operative course animal is shown.....	70
Figure 4-3. Temporal graph of leukocyte platelet aggregates or monocyte tissue factor is shown for study D054.	71
Figure 4-4. Temporal plots of annexin V and anti-p-selectin binding to platelets from studies using DLC- (solid lines) or MPC- (dashed lines) coated components.	74
Figure 4-5. Temporal antibody and annexin V binding data for study D033.....	76
Figure 5-1. A cross-section of the Streamliner is shown.....	78
Figure 5-2. Three indicators of circulating activated platelets and platelet microaggregates for Streamliner study T004 are shown.	80
Figure 5-3. Change in circulating activated platelets as indicated by CD62P expression with variation in the impeller blade tip gap.	87
Figure 5-4. Platelet counts for the time points described in Table 5-1 are shown.....	88
Figure 5-5. Plasma free hemoglobin (PlfHb), standardized to a hematocrit of 36%, the time points are described in Table 5-1.....	89

Figure 5-6. The percent of platelets expressing CD62P from venous and arterial samples during continuous touchdown of the Streamliner impeller is shown.	91
Figure 5-7. Platelet counts from venous (CVP) and arterial blood samples collected during continuous touchdown of the Streamliner impeller.	92
Figure 5-8. The plasma free hemoglobin, standardized to a 36% hematocrit, for venous (CVP) and arterial samples during continuous touchdown of the Streamliner impeller is shown.	93
Figure 6-1. A high-shear couette flow device, the hemolyzer, is shown.	98
Figure 6-2. Temperature of the hemolyzer surfaces, indicated in Table 6-1, after 30 mins of motor operation are shown.	101
Figure 6-3. H-Q for the hemolyzer with a 0.005” rotor gap.	103
Figure 6-4. Flow through the inlet of the hemolyzer with a 0.010” rotor gap, 10,500 RPM, Q=4.5 lpm	104
Figure 6-5. CFD prediction of the axial velocity of the primary flow path in the hemolyzer.	105
Figure 6-6. A disturbed flow pattern at the tip of the rotor.	106
Figure 6-7. The flow pattern from the rotor surface extending to the housing is shown for the same conditions as in Figure 6-5.	107
Figure 6-8. Flow visualization (left) and CFD predicted axial velocity contours (right) of the flow through the high shear gap in the hemolyzer.	108
Figure 6-9. Changes in activated platelets and microaggregates following hemolyzer passage.	110
Figure 6-10. The platelet activation dependency on shear rate and exposure time is shown.	111
Figure 6-11. A schematic of the blood shearing device is shown in cross section.	114

Figure 6-12. The modified BSI with temporary blocks added to permit introduction of lubricant into the cavities between the labyrinth seal and the bearings to prevent purge fluid ingress into the motor chamber..... 119

Figure 7-1. The plot shows the percent of circulating activated platelets, as indicated by annexin V binding, versus the time from implant. 125

Figure 7-2. The plots show the percent of circulating platelet microaggregates versus the implant duration. 126

Figure 7-3. The images show the appearance of sections excised from the device following explant after a 6 hour study..... 127

Figure 7-4. A micrograph is shown of the device which completed the 96 hour study. 128

Figure 7-5. The chart displays the percent of surface area covered by visible thrombus following rocking a 3 cm diameter swatch of knitted hollow fiber membranes in bovine blood for 2 hours..... 131

PREFACE

I like to thank all of those who have contributed to my learning and development during the past several years. My advisor, Dr. William R. Wagner, has my sincerest gratitude for his guidance, assistance, and patience. His direction has been invaluable the experimental design, data analysis, abstract and manuscript writing, and conference presentations which form the basis for this thesis and my future pursuits in the field.

Along with Dr. Wagner, I would like to thank my committee for their assistance with this project. Dr. Borovetz, Dr. Antaki, Dr. Federspiel, Dr. Kormos, and Dr. Bontempo provided valuable guidance in the development of my academic career, the construction of this dissertation, and the completion of my doctorate. Dr. Borovetz has provided so many opportunities for graduate students at the University of Pittsburgh. I was fortunate to take advantage of just some of those opportunities. Dr. Antaki has always been generous with his limited time and place enough trust in me to twice relinquish possession of his cherished Streamliner to me for experiments which surely made him wince. Dr. Federspiel was kind enough to repeatedly take the product of his laboratory's efforts and dissect it. Dr. Kormos has always been patient enough to answer an Engineer's questions even in the middle of the night standing bedside with a patient. I would also like to thank Dr. Kameneva who has taught me a tremendous amount about blood and I look forward to continuing to work with her in the future.

I would sincerely like to thank everyone at the McGowan Institute who helped with this research especially the staff of the Experimental Surgery Center (now the Center for Preclinical Studies). Dr. Kenneth Litwak, Dr. Take Akimoto, Dr. Shin Kihara, Dr. Hiro Tsukui, Mary Watach, Lisa Gordon, Shawn Bengston, Kevin McHugh, Joe Hanke, Aaron Dean, and Erin Myers especially deserve thanks for their assistance. This research simply could not have been accomplished without them. Dr. Litwak has also been extremely helpful in reviewing manuscripts. I would also like to thank all of interns who have worked with me in the lab: Eric Miller, Aisha Moore, Mirrhet Birru, Claudia Grossman, Nicole Price, Anika Joseph, Peter Huhr, and Hiroki Meguro. I would also like to thank Karen Masterson, Doug Thomas, and Ken Butler from Nimbus/TCI/Thoratec and for allowing me to study their pump so completely. Funding for this research was provided by the NIH and the Commonwealth of Pennsylvania.

I would also like to thank my labmates, past and present, Dr. Carl Wilhelm, Julie Buchanan, Dr. Tim Deglau, Patrick McGinley, Dr. Greg Weller, Dr. Jianjun Guan, Ken Gage, Alexa Polk, John Stankus, Eric Tom, Priya Ramaswami, Carl Johnson, and Joshua Woolley for their support and assistance.

I'd also like to thank Steve Winowich, Dr. Rick Schaub, and Don Severyn for the opportunity to work in the Artificial Heart Program and the clinical transport team. The experiences and opportunities afforded by the program have been outstanding and one of the most cherished portion of my experience.

I want to offer a special thought to my grandparents. My sister has always there to remind me no matter how far I go, I'm still Tursha. I would never have reached this point without the strength and encouragement of my mother. For everything she had to overcome and all of her hard work to help me reach this point I cannot thank her enough. Finally, to the person who deserves this the most, my wonderful wife, Sara. Thank you for your love, patience, and sacrifice.

1.0 INTRODUCTION

*“For it stirs the blood in an old man’s heart,
And makes his pulses fly,
To catch the thrill of a happy voice
And the light of a pleasant eye.”*

-Nathaniel Parker Lewis

1.1 THE CLINICAL NEED

Cardiovascular disease ranks as the leading cause of mortality in the Western world [1]. As medical technology advances, a growing number of patients may be sustained in spite of severe cardiovascular disease states, included in this group are patients suffering from end stage heart failure requiring a heart transplant. Between 30,000 – 70,000 patients in the United States (US) and 100,000 – 200,000 patients worldwide could potentially benefit from a heart transplant [2]. Unfortunately the number of donor hearts available in the US each year has reached a plateau of about 2,200 [3] and this number is not expected to increase significantly in the near future [4]. The gap between available donor hearts and patients who require a transplant has increased waiting times to six months on average [5]. Several mechanical circulatory assist devices currently on the market provide a “bridge-to-transplant” by providing left ventricular or biventricular circulatory assistance until a donor organ becomes available [6]. The success of these devices combined with the growing number of patients on transplant waiting lists has provided the impetus to develop a circulatory assist device capable of providing long-term support exceeding five years [7, 8].

The advent of “destination therapy,” implanting a VAD in transplant ineligible patients as an alternative to cardiac transplant, could dramatically increase the potential patient population. A small portion of patients placed on mechanical circulatory support eventually recover adequate cardiac function to permit removal of support without transplantation. The mechanism(s) of recovery remains unclear; however, there appears to be a population for which temporary circulatory support may provide therapy to prevent further cardiac function deterioration and potentially offers the hope of restoration of some cardiac function.

1.1.1 First Generation Devices

1.1.1.1 The Jarvik-7 Total Artificial Heart

Many investigators during the twentieth century attempted to construct heart replacement devices. Such a concept became clinically feasible with the successful development of

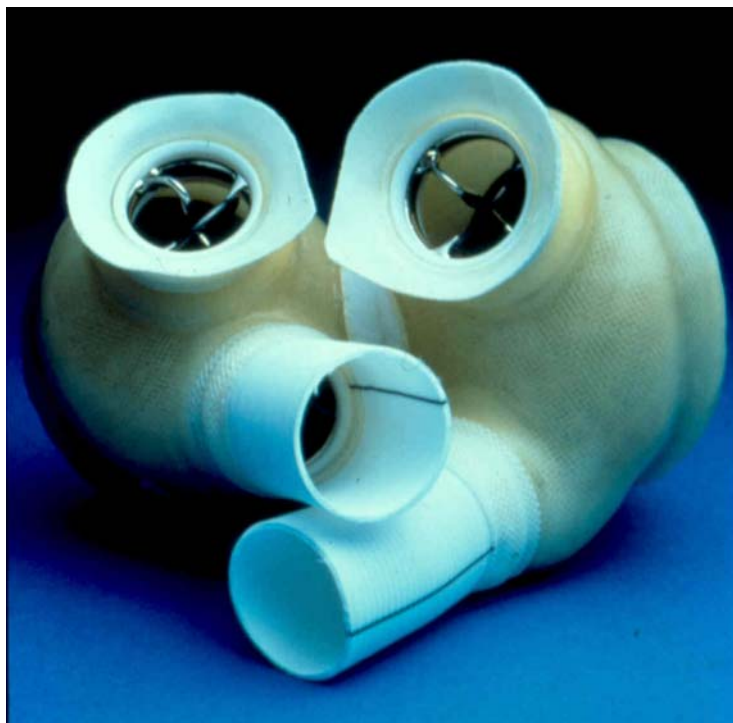


Figure 1-1. The Jarvik-7 TAH.

cardiopulmonary bypass. Cooley performed the first implant of an artificial heart in 1969; the patient received a human heart transplant 64 hours later, marking the first successful “bridge-to-transplant” use of a total artificial heart (TAH) [9]. The Jarvik-7 TAH, shown in Figure 1-1, became the first device to initiate a clinical trial to serve as a permanent replacement for the failing native heart. The first Jarvik-7 was implanted in Dr. Barney Clarke by William DeVries in Salt Lake City in 1982 [10]. The Jarvik-7 helped extend Dr. Clarke’s life 112 days, but caused multiple strokes and severely limited mobility. About 90 additional patients also received a Jarvik-7, the longest surviving 632 days. However, thromboembolic events (strokes) and infections were frequent complications [11]. Thrombus formation on the mechanical valves of the device were the primary cause of the embolic events, while passage of large bore pneumatic tubes extending from the implanted device, through the skin, to an external console left the patient vulnerable to infection at the exit site of the tubing from the body. The high complication rates, quality of life concerns, and limited support durations called into question the practicality of a TAH, at least with the existing technology. These same issues arose again during the more recent clinical trial of the totally implantable Abiomed Abiocor TAH, shown in Figure 1-2 [12, 13].



Figure 1-2. The Abiomed Abiocor TAH. (AP Photo)

During the efforts to develop safe mechanical circulatory support devices, concurrently pioneering transplant surgeon Dr. Thomas Starzl and others were investigating and refining immune suppression methods to make solid organ transplantation more feasible [14, 15]. Drs. Hardesty, Griffith, and Kormos here at the University of Pittsburgh first successfully used the Jarvik-7 as a bridge-to-transplant [16]. While several dozen additional patients were supported in this manner, the size of the TAH restricted the potential patient population usually to large males and the complication rate remained elevated. It was also recognized that a majority of patients with severe heart failure only required support for the left ventricle [17].

1.1.1.2 Pulsatile Ventricular Assist Devices

Subsequently, three pulsatile ventricular assist devices (VADs) gained wider clinical use. The three – the Novacor, Heartmate I, and Thoratec pneumatic – operate in a similar manner to the native heart. A chamber within the device fills with blood which is ejected by pneumatic or

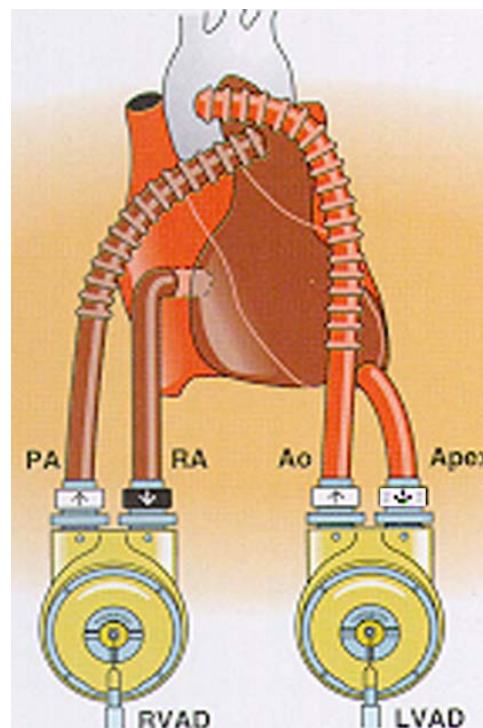


Figure 1-3. Thoratec pneumatic VADs are shown in the left and right VAD configurations.

electromechanical compression of the chamber. The devices interface with the circulation through an inflow cannula inserted through the apex into the left ventricle and an outflow cannula anastomosed onto the aorta. The cannulae contain valves to prevent retrograde flow. The Thoratec pneumatic VAD (pVAD), shown in Figure 1-3, can also be deployed to provide support to the right side of the heart, or bi-ventricular support. Together these three devices have been used in nearly 7,000 patients worldwide. However, bleeding, thromboembolism, and infection remain major complications associated with these VADs [18]. Thromboembolism rates vary by device and center but generally range from 5 – 30% [19]. Infection rates increase dramatically with implantation time reaching over 60% at eight months post-implantation [20, 21].

As the support duration for bridge to transplant applications increases and with the emergence of destination therapy, durability concerns have risen substantially. Over 40 changes have been implemented to the Heartmate I VAD, shown in Figure 1-4, to increase the average device half-life from 8 months to 1.5 years [22]. The Novacor VAD, shown in Figure 1-4, has a projected life span of at least three years [23]. The Thoratec pVAD has an estimated life span of up to five years, and with extracorporeal placement can be much more readily exchanged than the other VADs, which require extensive surgery to remove the faulty device and place a new one [24].

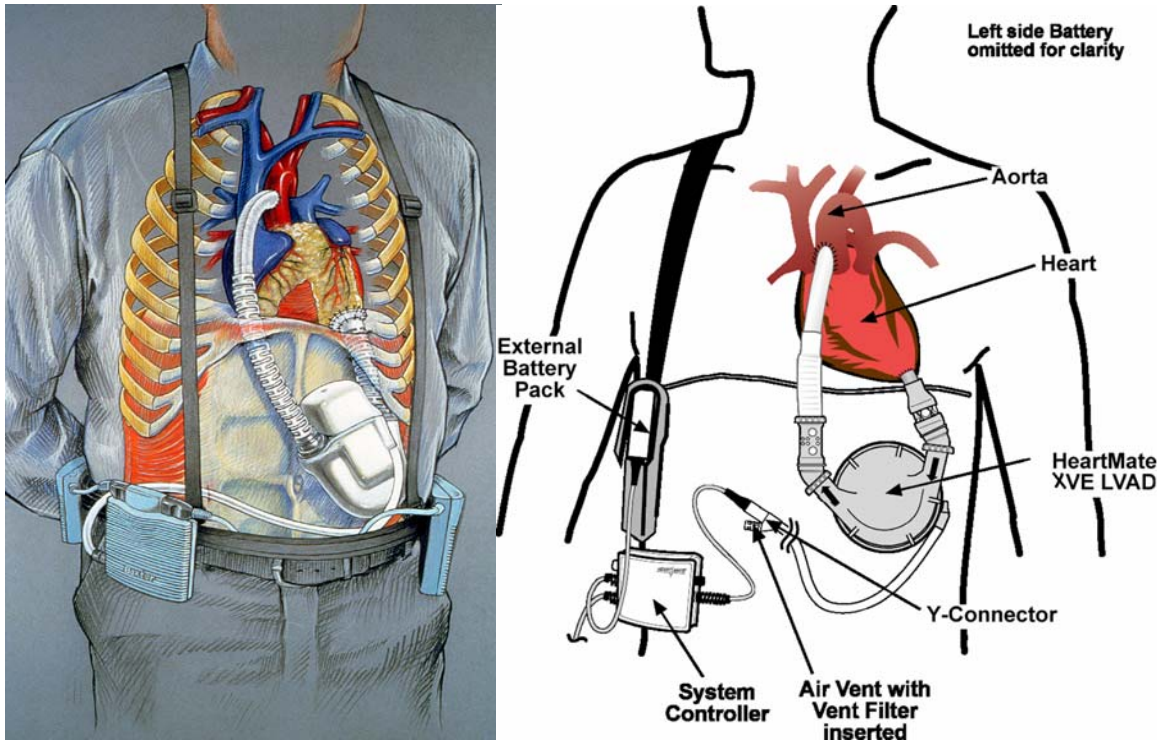


Figure 1-4. Novacor (left) and Heartmate I (right) VADs are shown with external components.

1.1.2 Second Generation Devices

Second generation VADs use a rotating impeller to generate blood flow and are alternately referred to as rotary, continuous flow, or non-pulsatile VADs. The final term is a misnomer and is not appropriate although it still appears in the literature. This type of pump is also frequently referred to by the pump topology (e.g. centrifugal or axial). Blood enters the pump and then momentum is imparted to the blood by a rotating member (usually with 2 or more blades). In the centrifugal configuration the blood exits tangentially from the impeller. An axial flow pump induces helical flow which is recovered by curved stators at the end of the impeller which redirect the helical flow in the axial direction. The impeller rotation rate is generally between 1,500 – 5,000 revolutions per min (RPM) for centrifugal pumps and 7,000 – 15,000 RPM for axial flow pumps, although this depends on the impeller diameter, cannula diameter and length, and the patient’s blood pressure. The impeller is either mounted on a shaft, which requires a mechanical seal in the blood flow path, or on a set of bearings, again in the blood flow path.

Commutation of the impeller is usually driven by a brushless direct current motor. Rotary blood pumps also do not require valves or either a compliance chamber or external venting. There is only a single moving part, so that with adequate bearing or seal design, the pumps can last several years.

1.1.3 Third Generation Devices

Pumps in which the contact bearings have been replaced with non-contacting magnetic bearings are called third generation devices [25]. By eliminating the friction point(s) in the design, the life span of the device is theoretically unlimited, but practically limited by internal pump components. Nevertheless, ten plus year useful device life spans are anticipated. The trade off from implementing a magnetically levitated impeller is the substantial increase in device complexity. The position of the impeller must be maintained within the pump and controlled in 6 degrees of freedom while it is rotating at several thousand RPM. Loss of impeller levitation or failure to adequately maintain impeller position results in the impeller crashing into the stationary housing, termed touchdown. Touchdown may result in mechanical damage to the contacting surfaces, resulting in scratches, gouges, or even fracture and particle release.

1.2 BIOCOMPATIBILITY CHALLENGES

Continuous flow devices present a different set of challenges when compared to the pulsatile VADs. Implementing a control algorithm to regulate pump output, remains a significant hurdle. In addition to control issues, the high RPM required to generate biologically relevant flow rates expose blood to extremely high shear levels (in excess of 6,000 dynes/cm²) for relatively short exposure times (less than 10 ms). Mechanical damage to red blood cells due to the operation of this type of pump has previously been examined and quantified [26, 27]. The potential effects of this shear environment on platelets and leukocytes have not been thoroughly investigated. Preliminary investigations demonstrate that significant platelet activation occurred *in vitro* with centrifugal pumps and rotablation without a concomitant increase in hemolysis [28, 29]. Takami

and colleagues found mechanical leukocyte damage without significant changes in hemolysis in a rotary blood pump [30]. Bonaros et al. reported no correlation between platelet activation and hemolysis parameters, despite periods of platelet hypo- and hyperaggregability [31]. These findings suggest platelets and leukocytes may be more susceptible to mechanical damage (including lysis) and activation than red blood cells in the flow environment generated within rotary blood pumps.

Examining results from two axial flow VADs, which are currently being used clinically, revealed several potential concerns. Koster et al. found significant elevations of β -thromboglobulin (β -TG), platelet factor 4 (PF-4), factor XIIa, and plasmin/ α_2 -antiplasmin (PAP), in patient plasma following implantation of the DeBakey axial flow VAD when compared to the pulsatile Novacor VAD, in spite of the smaller surface area and lack of valves in the DeBakey pump [32]. Additionally thrombin-antithrombin (TAT) and d-dimer were elevated in both groups compared to baseline. These indicators suggested increased platelet granule secretion (β -TG and PF4), thrombin generation (TAT), contact activation (factor XIIa), and fibrinolysis (d-dimer and PAP).

The same researchers also found significant increases in IL-6 and C5a in patients with the DeBakey VAD compared to the Novacor [33]. Rothenburger et al. describe using thrombolytic therapy in response to significant declines in pump output attributed to device-related thrombus formation in eight of 22 DeBakey VAD recipients [34]. To attempt to alleviate this issue, the inflow cannula of the DeBakey was coated with heparin. The Jarvik 2000 axial flow VAD has not been as thoroughly investigated as the DeBakey, although reports have described occasional transient ischemic episodes, neurologic deficits, and the requirement for thrombolytic therapy [35-38].

The observed platelet activation may be attributable to several causes: the interaction with artificial surfaces, recirculation regions or stasis within the pump, interaction with platelet agonists released from lysed red blood cells or platelets, or shear-induced platelet activation and aggregation. An understanding of the contribution of each of these factors to the thrombotic disturbances observed in early clinical use cannot be drawn from the currently available data. Virchow's triad of surface, flow, and condition of the blood still provide a framework for understanding the underlying causes of thromboembolism and bleeding observed clinically [39]. This approach remains useful to analyze the biocompatibility of any blood-contacting device.

1.2.1 Surface

Immediately following blood contact with foreign material plasma proteins adsorb onto the surface. The composition of the adsorbed protein layer can change with time, known as the Vroman effect [40]. Protein adsorption is a thermodynamically driven process in which proteins may adopt altered configurations or orientations to reduce their surface free energy, mainly through hydrophobic/hydrophobic, ionic, and hydrogen bonding interactions [41]. The result is proteins on a surface may have peptide sequences accessible to the plasma which are normally not available. Thus the protein layer can alternately promote or inhibit cell adhesion to the surface or acquire increased or diminished enzymatic activity.

1.2.1.1 The Intrinsic Coagulation Cascade

The intrinsic coagulation cascade is initiated when high molecular weight kininogen (HMWK) and prekallikrein (PK) adsorb to a surface and PK is converted to kallikrein. The kallikrein can then catalyze conversion of factor XII (FXII) to FXIIa. FXIIa can then hydrolyze PK to kallikrein establishing a feedback mechanism to increase the forward reaction rate. FXIIa promotes conversion of FXI to FXIa. FXIa then in turn can promote the release of bradykinin from HMWK and conversion of FIX to FIXa in the presence of a divalent calcium ion. It is important to recognize that these reactions occur in close proximity to the surface, allowing for local concentrations of the activated factors to be substantially increased over the bulk plasma concentration.

The FIXa then complexes with FVIIIa on the surface of activated platelets, endothelial cells, or some leukocytes again in the presence of Ca^{++} to form the intrinsic tenase complex. The tenase complex converts FX to FXa beginning the common pathway (described below) of the coagulation cascade. FVIIIa in this process comes from activation of FVIII to FVIIIa by thrombin. Thus, the reactions proceed relatively slowly initially, but with positive feedback, the reaction rate accelerates. Thrombin can also inactivate FVIIIa providing negative feedback to thrombin generation as the concentration increases.

Thus, through initiation of the intrinsic cascade a surface may become thrombogenic because of the proteins which absorbed onto it. Often this behavior has been ascribed to

negatively charged surfaces, but this view is not wholly accurate. The current understanding of this adsorption behavior remains inadequate to predict if a given surface will demonstrate this behavior or the magnitude of the effect [42].

1.2.1.2 Cell Adhesion

Cells may adsorb onto a surface through the interaction of cellular receptors with adsorbed proteins. Many investigators believe cell adhesion onto blood-contacting materials is primarily through adsorbed fibrinogen, although other adhesive proteins such as fibronectin, vitronectin, collagen, and von Willebrand Factor (vWF) may be involved as well [43]. Platelet adhesion, primarily through the GPIIb/IIIa (CD41/61) integrin receptor, can lead to cell activation and granule release, initiating thrombus formation. Leukocytes may also interact with adhesive proteins through a variety of receptors again potentially activating the cell and initiating an inflammatory response. Denaturation of surface proteins may provoke an opsonizing response in which the cell attempts to phagocytose the foreign material. The response is termed frustrated phagocytosis and includes release of free radicals and superoxide ions which may damage or degrade the material or adjacent cells and tissue [44]. Activation of leukocytes results in the release of inflammatory mediators which provoke a continued inflammatory response.

The adhesion of cells onto a surface does not definitely result in thrombogenesis and an inflammatory response. Again, the complex interplay of protein concentrations, conformations, and adhesive ligands with blood cells and their varied receptors is not completely understood. Some biomaterials which have been designed to limit fibrinogen adsorption offer promising results to begin to control these interactions, however, none of the materials has yet been used clinically to demonstrate the advantage of this approach [45].

1.2.1.3 Interface with Injured Tissue and the Extrinsic Cascade

For a device to interface with the circulation, of necessity, an injury must be made to access the normally closed vasculature. Thus, a biomaterial surface is placed immediately adjacent to injured tissue which can promote the extrinsic coagulation cascade. Damaged tissue (and activated monocytes) express and release tissue factor, which complexes with FVIIa to convert

FX to FXa. The FVIIa comes from enzymatic cleavage of FVII by thrombin or FXa, again providing positive feedback to accelerate thrombin generation.

Platelets adhere to damaged tissue through collagen and vWF, among other proteins, in the exposed extracellular matrix. The activated platelets release coagulation factors and provide a catalytic surface for further coagulation cascade reactions. FXa forms the prothrombinase complex on the surface of activated platelets in the presence of Ca^{++} with FVa to cleave prothrombin (FII) into thrombin (FIIa). Thrombin cleaves two sites on fibrinogen to form fibrin, the polymer which acts as a mesh to hold the growing thrombus together. Thrombin converts FXIII to FXIIIa which crosslinks fibrin strands increasing the tensile strength of the clot [42].

1.2.1.4 Coatings

Coatings have been applied to medical devices for a variety of reasons, but primarily to enhance biocompatibility or serve a mechanical purpose. Titanium nitride for example, has been widely used to coat surgical instruments to reduce wear on the instrument surfaces. Many coatings have been used which claimed to improve biocompatibility. Long-chain polymers of polyethylene glycol (PEG) have been applied to surfaces to prevent cellular adhesion [46]. This type of coating acts in a passive manner by serving as a physical obstacle to a cell interfacing directly with a surface. The PEG molecules do not serve a biologic function. Heparin has been widely used as a "bioactive" coating. That is, the heparin molecule contains 2 active sites which catalyze the inactivation of thrombin by anti-thrombin III. The heparin molecule is also a linear hydrophilic chain, similar to the PEG molecule, so it also may provide a physical barrier limiting cellular access to a surface [47].

1.2.2 Flow Effects

1.2.2.1 Stagnation Zones and Vortices

It has long been recognized in artificial organ design that fluid stagnation within the blood flow path will lead to thrombus formation [48]. This is due to a combination of local increase in thrombogenic agonist concentration and cellular deposition in the low shear environment. Many

flow characterization and visualization techniques have been developed to observe the character of the fluid flow through prototype medical devices. Flow visualization by laser illumination of microscopic, fluorescent beads suspended in blood analogue fluids circulated through cardiovascular devices has emerged as one of the most frequently applied prototype analysis tools [49]. Often several design iterations may be evaluated in a single experimental set-up over the entire anticipated device operating range.

1.2.2.2 Shear

Blood exposure to elevated shear stress can lead to hemolysis, the mechanical compromise of red blood cells leading to the release of hemoglobin, although the amount of damage is related to both the magnitude of the applied shear stress and the length of time the cell is exposed to the stress. Many investigators have attempted to define the relation using a power-law relation:

$$D.I. = a \tau^b t^c \quad \text{(Equation 1.1)}$$

where D.I. is a damage index which correlates to hemoglobin release, τ is the local shear stress, t is the exposure time, and a , b , & c are coefficients obtained from regression fit to available data.

Several different sets of coefficients have been published, indicating an influence of experimental set-up [50]. Yeleswarapu integrated the above relation to produce an accumulated damage function using a Lagrangian solution for flow field through an axial flow VAD produced by computational fluid dynamic (CFD) analysis [51]. This approach has been modified and repeated by others and utilized to improve the design of blood pump flow paths [52].

Shear-induced platelet activation occurs when the soluble plasma protein vWF binds to the GPIb-IX-V complex on the platelet surface during exposure to elevated shear levels [53]. This binding begins a cascade of intercellular events within the platelet leading to activation of integrin GPIIb/IIIa, platelet activation and degranulation [54, 55]. Shear induced platelet activation can be suppressed by blocking vWF binding to the GPIb-IX-V complex [56]. Material

selection may influence shear-induced platelet activation through platelet degranulation, as vWF is one of the granule constituents released following activation. Additionally platelets will adhere to surface bound vWF and become activated in the presence of elevated shear rates [57]. While this process has clearly been demonstrated at shear rates relevant to biologic processes such as stenosis of an artery, most shear-induced platelet activation studies have been carried out with cone-and-plate viscometers, which expose the blood to elevated shear rates for seconds to mins [58]. This time exposure is orders of magnitude greater than the millisecond exposure individual blood elements experience *in vivo* in many cardiovascular devices.

Several researchers have used other approaches to investigate platelet responses to high shear, short time duration exposure. Wurzinger et al. performed a series of studies demonstrating that at high shear stresses (570 to 2550 dynes/cm²) platelet activation, as measured with β -TG, correlated with lactate dehydrogenase (LDH), an indicator of platelet lysis [59-62]. They also concluded that substrates which removed adenosine diphosphate (ADP) from the suspension medium suppressed platelet activation, implicating hemolysis as a significant contributing factor. However, the couette test apparatus employed in their studies had significant limitations, including uncertain flow pattern and time exposure, as well as exposure of blood elements to rotor/seal interfaces. The results from these studies did show the importance of accounting for shear-induced platelet lysis as well as the difficulty in designing an appropriate test apparatus. Klaus et al. also utilized a couette test apparatus, but implemented a fluid seal to eliminate the effects of the hard mechanical seal [63]. They examined platelet count and PF-4 release for shear rates from 1,800 to 110,000 s⁻¹ with an exposure time of 400 msec and found significant elevations in PF-4 concentration and significant decreases in platelet count with increasing shear rate. They found a much lower index of hemolysis than the Wurzinger studies, but did not measure LDH and only stated that cell fragments were not observed during cell counting procedures. However, 400 msec remains much longer than the actual exposure time to elevated shear rates in most cardiovascular devices. Neither group was able to discern the cause of the platelet activation, although Wurzinger et al. attributed it to platelet and red blood cell lysis.

Sakarissen et al. utilized plane and stenotic parallel-plates to show significantly increased platelet activation following exposure of whole blood to a shear rate of 10,500 s⁻¹ (corresponding shear stress was 315 dyn/cm²) for 75 and 609 msec [64]. Again, this time exposure was greater

than that in rotary blood pumps while not applying maximum exerted shear stresses. The parallel plate approach also required multiple chambers with varied dimensions to generate a range of shear rates (420 to 10,500 s⁻¹).

1.2.3 Anticoagulation

Anticoagulation regimens for VADs range from aspirin alone for the Heartmate I, to a complex and comprehensive strategy developed by Copeland and colleagues for patients receiving the SynCardia TAH (the continued evolution of the Jarvik-7), which utilizes combinations of heparin, coumadin, aspirin, ticlopidine, dipyridamole, and pentoxifylline [65]. Aspirin therapy is desirable because of oral administration of a single dose and it does not require monitoring; however a significant portion of long-term VAD supported patients appear to develop aspirin resistance [66]. Aspirin inhibits the formation of thromboxanes in platelets, reducing the recruitment of other platelets following activation. Coumadin (warfarin) is often used in outpatients and is desirable because of oral intake. It prevents the carboxylation of vitamin K dependent coagulation factors (FVII, FIX, FX, FII) in the liver extending the time required for blood clot formation. Patient anticoagulation must be monitored through serial blood collections, dosage frequently changes, and dietary restrictions of vitamin K intake must be followed. However, it is important to recognize the potential stimulus for thrombus formation in attempting to reduce artificial organ associated adverse events. For instance, aspirin has been shown to be ineffective in preventing shear-induced platelet activation.

Inadequate anticoagulation is not the sole concern. Bleeding is a frequent complication and can be difficult to appropriately treat. The bleeding source in VAD patients often cannot be located and normalization of the patient hemostatic system can leave the patient vulnerable to thromboembolic events associated with the device. An understanding of the mechanism(s) of platelet activation in artificial organs could be used to better target anticoagulation and anti-platelet strategies to reduce both bleeding episodes and thromboembolic events.

1.3 PREVIOUS PRECLINICAL BIOCOMPATIBILITY STUDIES

Biocompatibility issues in the development of new cardiovascular devices previously have been examined through *in vitro* testing and by gross observations in pre-clinical animal studies, such as platelet counts and thrombus deposition found on the device at necropsy [19, 67-71]. Platelet counts, however, do not usually provide an accurate measure of thromboembolism and it is difficult to assess the potentially subtle effects of strokes and infarcts on an animal [72]. Indicators of end organ function, such as creatinine, blood urea nitrogen (BUN), and bilirubin, remain within normal limits even with infarcts apparent on over 20% of the kidney surface [73]. Previous studies attempted to use assays developed for use in humans to measure coagulation products, platelet activation, release of platelet granule contents, and fibrinolytic products [74, 75]. Both groups found a thrombin-anti-thrombin III (TAT, indicative of thrombin generation and subsequent inactivation) and thromboxane B2 could be measured in bovines. Through these measures as well as platelet aggregometry both studies indicated platelet activation following implantation of TAHs in bovines. Bovines have been shown to have a diminished response to thrombotic stimuli when compared to humans; however, the differences between the bovine model and humans with respect to issues such as relative reactivity to blood-contacting materials and applied shear stress have not been studied [75-77].

1.4 SPECIFIC AIMS

The purpose of this dissertation is to expand the range of information which may be collected during preclinical investigational device studies, when modifications and refinements can be implemented without endangering human life or incurring a regulatory burden. The assays can then be used with several blood-contacting devices undergoing development and testing at the University of Pittsburgh to quantify the effects of the device on platelets and leukocytes.

2.0 BIOCOMPATIBILITY ASSAY DEVELOPMENT

2.1 INTRODUCTION

Previously the only measures of thrombosis regularly utilized in preclinical studies were clotting time tests (e.g. activated clotting time (ACT)), platelet counts, and plasma fibrinogen concentration. In attempt to extend the range of available assays, our laboratory obtained a panel of potential anti-bovine platelet antibodies from the Washington State University Monoclonal Antibody Center (WSUMAC). After testing, three antibodies (BAQ56, BAQ125, GC5) were found to display an increase in binding to platelets activated with either 20 μ M ADP or 3 μ M phorbol 12-myristate 13-acetate (PMA), both known platelet agonists, as detected with flow cytometry [78]. These antibodies were then used to measure platelet activation temporally in three animals receiving a VAD. Additionally the WSUMAC had identified an anti-bovine CD41/61 antibody, CAPP2A. CD41/61 (GPIIb/IIIa) is an integrin expressed on the surface of all platelets. A flow cytometric assay was developed to use this antibody to identify platelet microaggregates, small aggregates of platelets which have remained in circulation [78]. These assays provide two methods for identifying *in vivo* platelet activation. The circulating activated platelet indicators (BAQ56, BAQ125, GC5) and the microaggregate assay significantly increased following VAD implantation and remained elevated throughout the post-operative period.

2.2 FLOW CYTOMETRIC QUANTIFICATION OF CIRCULATING ACTIVATED PLATELETS AND PLATELET MICROAGGREGATES

2.2.1 Washington State University Monoclonal Antibody Center Antibodies

These antibodies were previously used in our laboratory to identify bovine activated platelets. To initiate the research, it was attempted to reproduce the previously obtained results.

2.2.1.1 Methods

Bovine blood samples were collected via jugular venipuncture using an 18 gauge 1 ½ inch needle into a syringe. 2.7 mL of blood was transferred into a 3 mL monovette (collection vial) containing 0.3 mL of 0.106 M trisodium citrate (Sarstedt, Newton, NC). 5 µL of citrated blood was added to 12 x 75 mm round bottom polystyrene tubes, containing 30 µL phosphate buffered saline, pH 7.4, (PBS; Gibco BRL, Grand Island, NY); 5 µL of the monoclonal antibody of interest, BAQ125, GC5, BAQ56A, or ColiS69 (Washington State University Monoclonal Antibody Center, Pullman, WA); and 5 µL of platelet agonist, for a final concentration of 20 µM ADP or 1 U thrombin (Sigma-Aldrich, St. Louis, MO). Initially 15 µg/mL of antibody was added to each sample tube for activation studies; subsequently concentrations of 0.75, 1.5, and 7.5 µg/mL were also used. ColiS69 served as a mouse IgG isotype control. After incubation with whole blood in PBS buffer, the samples were washed and a fluorescein-isothiocyanate (FITC) conjugated secondary antibody, goat anti-mouse IgG (GαM-IgG-FITC; Pierce, Rockford IL) was added to each tube. Control samples received an additional 5 µ of PBS rather than agonist. The samples were incubated for 30 mins then washed and fixed with 500 µL of 1% paraformaldehyde (PF). Four tubes were prepared for each sample.

Flow cytometric analysis was performed on a FACScan flow cytometer (Becton-Dickinson, La Jolla, CA). A region was drawn around single platelet events in a logarithmic plot of forward versus side scatter. The FL-1 channel (520 nm) photomultiplier tube voltage was adjusted so that the isotype control sample fluorescence fell primarily in the 1st decade of an intensity histogram shown in Figure 2-1. Five thousand single platelet events were collected. A mark was set below which 98% of the platelets incubated with the isotype control fluorescence

intensity values fell. In subsequent samples, platelets with fluorescence intensity values greater than this mark were considered positive for the antibody of interest.

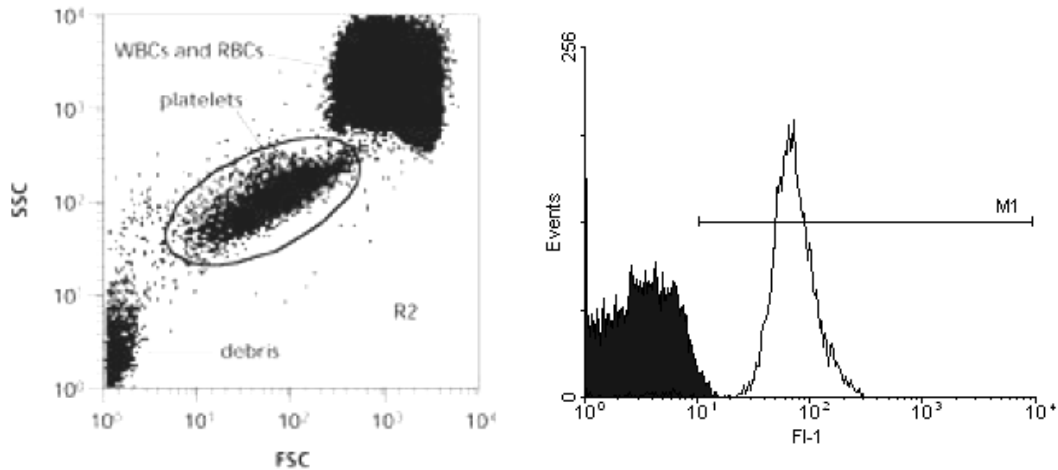


Figure 2-1. Flow cytometry analysis plots.

The image on the left is a dot plot of forward scatter (FSC; x-axis) versus side scatter (SSC; y-axis). Each dot represents a single event (cell, aggregate, or debris) detected by the flow cytometer. Forward scatter is indicative of physical size, while side scatter reflect cell granularity or complexity. An elliptical region is drawn around single platelet events. Events with greater forward and side scatter than platelets are mostly red blood cells, leukocytes, and cellular aggregates. Events with very low forward scatter are sub-micron debris particles. The image on the right is a histogram of fluorescence intensity for ColiS69 (black filled) and BAQ125 (white). The fluorescence intensity of the ColiS69 is a combination of autofluorescence, non-specific antibody binding, and specific antibody binding, which all should be relatively low. The BAQ125 intensity is a combination of autofluorescence and non-specific binding (which should be the same as in ColiS69) and specific binding, which in this case is very high. M1 indicates the 98% mark set for ColiS69. Thus, in this particular sample over 95% of the platelets were identified as positive for the BAQ125.

The percent of positive platelet events were averaged for each experiment. Tests were repeated with blood from at least 3 animals. The mean percent labeled platelets for each antibody were compared using an unpaired, two sample Student's *t*-test assuming unequal variances with two-tailed distribution with Bonferroni correction. Data presented are mean + standard deviation.

2.2.1.2 Results

Using the concentrations of primary antibodies (BAQ56A, BAQ125, and GC5) given by Baker [78] yielded 80+% labeling of platelets with or without added agonist, which was not useful to attempt to identify activated platelets. Initially, there was no washing step in the labeling protocol. To attempt to reduce non-specific binding of the antibodies to the platelets, the effect of washing (adding 1 mL of PBS, centrifuging the sample, and removing the

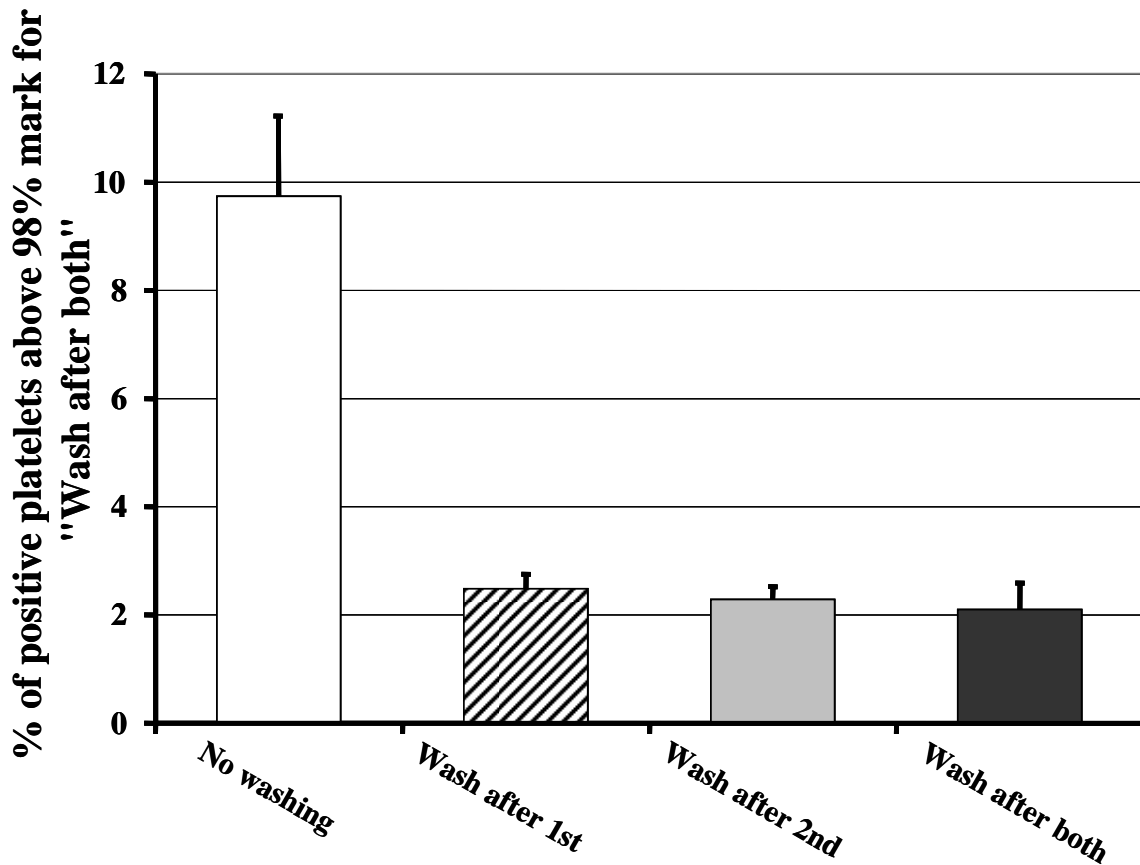


Figure 2-2. The effect of sample washing on ColiS69 binding to platelets.

supernatant) were examined. The results are shown in Figure 2-2. After comparing binding in isotype control samples with washing after incubation with the primary antibody, after

incubation with the secondary antibody, and after both incubations, a single wash step was added as described above.

The addition of the wash step still resulted in 80+% binding of BAQ125, GC5, and BAQ56A to unactivated platelets, so antibody titration was performed with the concentrations described above. The results of labeling with 1.5 $\mu\text{g}/\text{mL}$ of BAQ125 and GC5 using 20 μM ADP as the stimulatory agonist are shown in Figure 2-3.

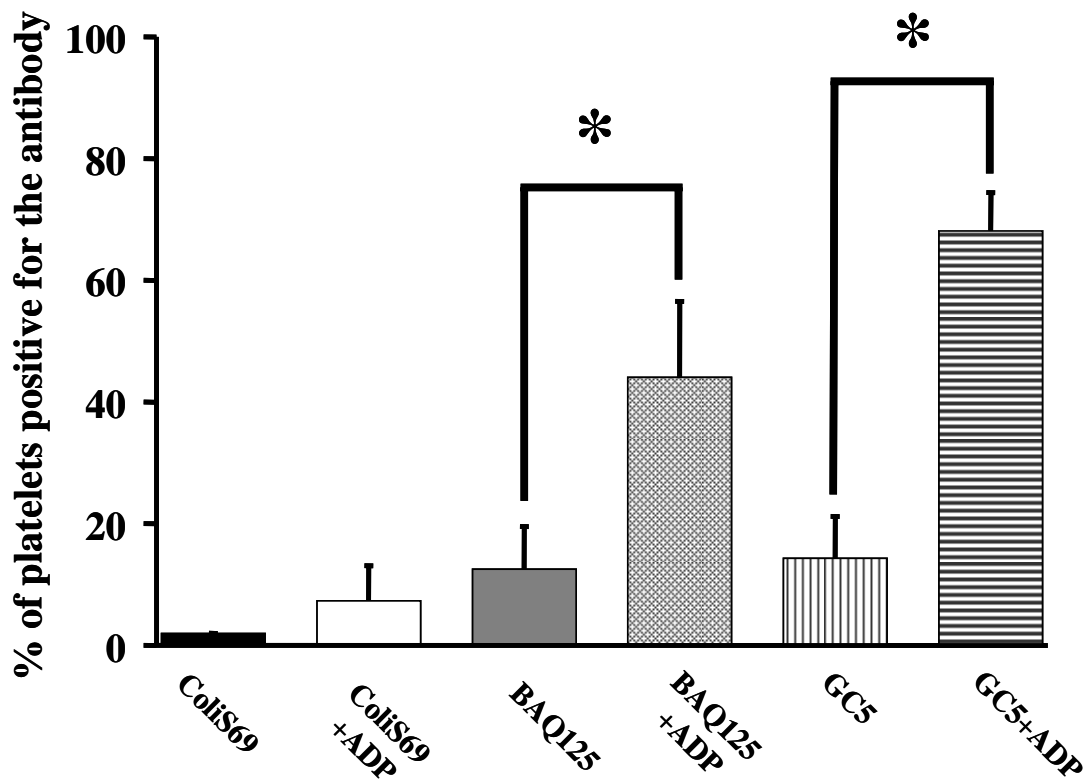


Figure 2-3. Detection of *in vitro* activated bovine platelets with monoclonal antibodies BAQ125 and GC5.

* indicates significant difference between control and activated samples.

During these repeated experiments it was noted that BAQ56A samples contained far fewer platelets than those for other antibodies. After repeated attempts to identify potential causes, it was observed that addition of BAQ56A antibody resulted in the formation of large

aggregates which could be observed using a fluorescent microscope after the addition of a fluorochrome-conjugated secondary antibody.

2.2.1.3 Discussion

While the initial finding of different results with several antibodies compared to previous work in the laboratory was concerning, it is a recommended practice in flow cytometry to perform antibody titrations upon receipt of new lots (or batches) of antibody. Unfortunately this recommendation is not found in the literature but is common knowledge among clinical cytometrists.

Having addressed the concentration issues, the data did confirm the previous finding that BAQ125 and GC5 could be used to identify activated bovine platelets. Antibody BAQ56A produced *in vitro* aggregation of platelets, and thus could not be used to identify activated platelets. It is possible that this antibody bound to a receptor site which induced activation. This type of antibody induced platelet activation has been reported previously with other antibodies [79].

2.2.2 Annexin V

Annexin V is a 36 kDa protein found in all mammals that binds to negatively charged phospholipids such as phosphatidyl serine in the presence of calcium ions. Quiescent platelets possess an enzyme to maintain negatively charged phospholipids on the inner leaflet of the cell membrane. Following activation of the platelet, the enzyme is inactivated and phosphatidyl serine and other negatively charged phospholipids rapidly diffuse to the external leaflet of the cell membrane. These phospholipids provide a catalytic surface supporting coagulation cascade reactions. Binding of annexin V to a platelet indicates the cell has “flipped” its membranes and become activated [80].

Annexin V has been widely used clinically to identify activated platelets. Harasaki and colleagues reported annexin V binding to 12.9% of calcium ionophore A23187 stimulated bovine platelets [75]. However, that report does not describe or reference the preparation or analysis methods.

2.2.2.1 Methods

Whole blood was collected as described in Section 2.2.1.1. The blood was diluted tenfold with PBS, PBS + 20 μ M ADP, or PBS + 0.1 U/mL thrombin. Following a 20 min incubation, 20 μ L diluted blood was added to tubes containing 250 μ L annexin V binding buffer and 5 μ L annexin V-FITC (BD-Pharmingen, San Diego, CA). After a 20 min incubation, samples were fixed with 500 μ L 1% PF. Samples were analyzed on a flow cytometer within 1 hour of fixation. Annexin V binding buffer is HEPES tyrode's buffer containing 140 mM NaCl and 2.5 μ M CaCl_2 with pH 7.4.

There was considerable difficulty in preventing activated platelets from aggregating in the annexin V binding buffer. To alleviate this issue, two calcium ionophores, A23187 and ionomycin (Sigma), were employed. In these studies, 10 μ L calcium ionophore (5 μ M final concentration) was added to the sample tubes prior to adding diluted blood.

Twenty total samples from five animals were analyzed. A threshold mark was set based on the control samples using the method described in Section 2.2.1.1. Since annexin V is not an antibody, an isotype control was not required.

Statistical comparisons were performed as described in Section 2.2.1.1.

2.2.2.2 Results

Initially, attempting to add *in vitro* activated blood to a buffer containing Ca^{++} resulted in rapid clotting of the sample. It was found that diluting the whole blood 1:10 prior to activation and increasing the amount of annexin V binding buffer somewhat tempered this problem, although thrombin results were still inconsistent. The use of calcium ionophores did not result in sample clotting if the sample was gently agitated immediately after the addition of blood and periodically through the incubation period. The annexin V binding buffer causes some shrinkage of the cells so that the platelet region had slightly reduced forward scatter and the identifying region was adjusted accordingly. Annexin V binding to *in vitro* activated platelets is shown in Figure 2-4.

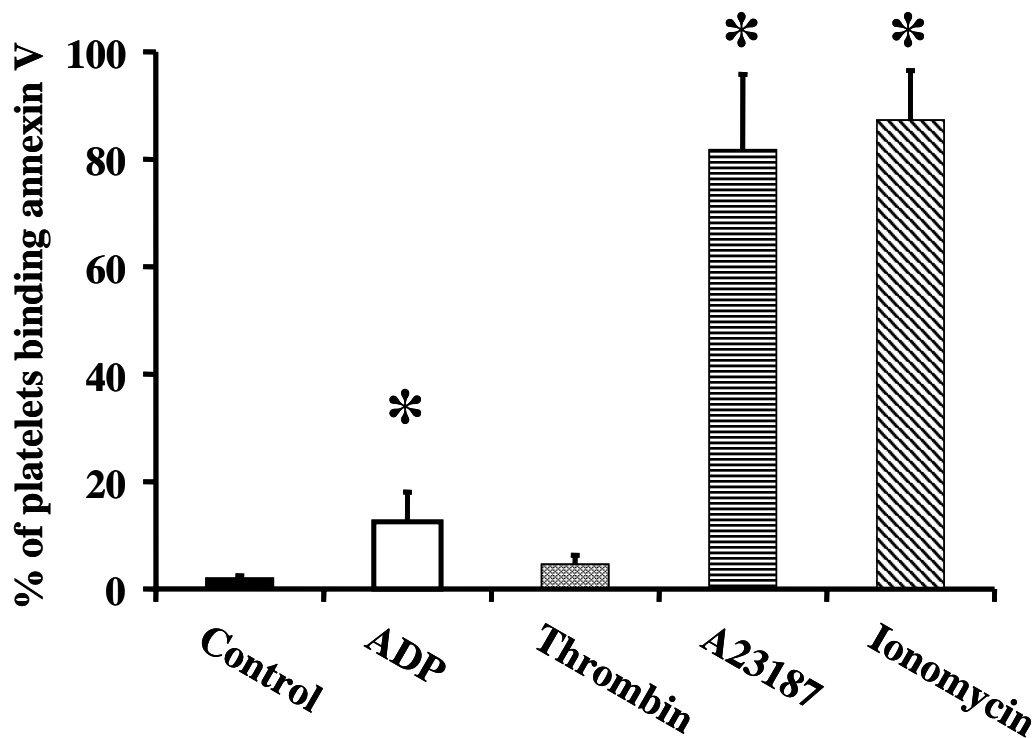


Figure 2-4. Annexin V binding to *in vitro* activated platelets.

* indicates significantly increased versus control.

2.2.2.3 Discussion

Annexin V binding to activated platelets increased compared to unstimulated platelets, however, the need for calcium ions in the buffering solution proved problematic, especially with potent agonists ADP and thrombin. In the ADP and thrombin stimulated samples, despite the precautions described, some aggregation still likely occurred. Stimulation of platelets with calcium ionophores resulted in binding to over 80% of platelets. A desirable aspect of this assay is the known binding epitope. Unlike the previously described antibodies, BAQ125, GC5, and BAQ56, there is a clear understanding to what the annexin V binds and the implications of the binding. Additionally, as mentioned above annexin V can be applied in human studies, so that the process of comparing the responses of the healthy juvenile bovines in which cardiovascular devices are tested to the infirm humans who receive them for life support may be advanced.

2.2.3 Anti-P-Selectin

Flow cytometric detection of platelets expressing surface p-selectin (also known as CD62P, GMP-140, PADGEM protein) is frequently used in clinical studies of human platelet activation, including several examining the effects of VAD support [66, 81]. P-selectin is a component of the α -granule and is absent from the surface of resting platelets. Following activation and degranulation of the platelet, p-selectin is expressed on the surface. Several reports have attempted to use anti-human p-selectin antibodies with *in vitro* activated bovine platelets, but no change in antibody binding was observed [75, 78]. An anti-p-selectin antibody, clone NPL44-10, from Takara Biochemicals (Tokyo, JP) has been reported to cross-react with human, beagle, rabbit, and guinea pig activated platelets, appearing to bind to a highly conserved portion of the protein. This antibody was purchased and tested for reactivity with bovine platelets.

2.2.3.1 Methods

Bovine blood was collected from three pre-operative animals as described in Section 2.2.1.1. Five μ L of blood was added to tubes containing 35 μ L PBS, 35 μ L PBS + thrombin (0.05, 0.1, 0.5, 1.0 U/mL), or 35 μ L PBS + 20 μ M ADP; and 5 μ L 10 μ g/mL anti-CD62P (as recommended by the supplier). Samples were incubated for 30 mins then washed with 1000 μ L PBS. Then 5 μ L G α M-IgG-FITC was added, the samples incubated for 30 mins, followed by fixation with 500 μ L 1% PF. Isotype control preparation, flow cytometric data acquisition and analysis, and statistical comparisons were carried out as described in Section 2.2.1.1.

2.2.3.2 Results

The anti-CD62P antibody binding to platelets significantly increased following *in vitro* activation. While increases were observed with all concentrations of thrombin used, the two highest concentrations (0.5 and 1.0 U/mL) also produced aggregation, so those concentrations were only employed in a single study. The combined results from the three experiments are shown in Figure 2-5.

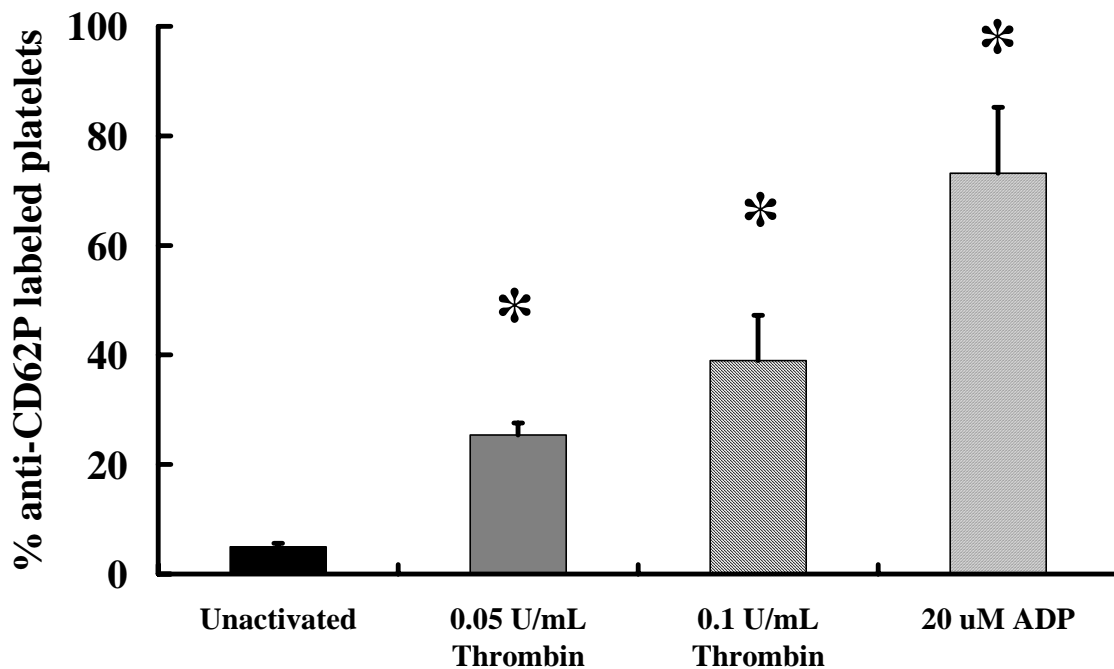


Figure 2-5. Anti-CD62P binding to *in vitro* activated platelets.

* indicates significantly increased versus unactivated sample.

2.2.3.3 Discussion

The NPL44-10 clone clearly bound to activated bovine platelets. It was reasonable to assume the antibody bound to the bovine homologue of p-selectin. Bovine platelets possess intracellular granules, similar to humans and other mammals [82]. These granules merge with the cell membrane following activation. Thus binding of the anti-p-selectin antibody following activation likely indicates degranulation and secretion by the bovine platelets. Thus, this antibody offers similar advantages to annexin V, in that the antibody target is known and direct comparisons to human studies may be made.

2.2.4 Anti-bovine CD63

CD63 (also known as LAMP-1), similar to p-selectin, is a protein expressed on the platelet surface following activation and degranulation. An antibody to the bovine homologue of CD63 was developed by Brooke and colleagues and commercialized by Serotec [83].

2.2.4.1 Methods

Bovine blood was collected from three pre-operative animals as described in Section 2.2.1.1. Five μL of blood was added to tubes containing 35 μL PBS, 35 μL PBS + agonist, and 5 μL anti-CD63 (undiluted; Serotec, Raleigh, NC). The agonists used were 20 μM ADP (N=2), 0.1 U/mL thrombin (N=1), thrombin receptor agonist peptide (TRAP; N=2), 3 μM phorbol 12-myristate 13-acetate (PMA, N=1). Samples were incubated for 30 mins (120 mins for PMA study) then washed with 1000 μL PBS. Then 5 μL G α M-IgG-FITC was added, the samples incubated for 30 mins, followed by fixation with 500 μL 1% PF. Isotype control preparation, flow cytometric data acquisition and analysis, and statistical comparisons were carried out as described in Section 2.2.1.1.

2.2.4.2 Results

Anti-CD63 binding increased significantly in response to all four agonists, however, not to the same degree as previously indicated with the anti-p-selectin antibody with ADP and thrombin. TRAP was employed because of prior issues with samples clotting when attempting to activate platelets with thrombin concentrations exceeding 0.1 U/mL. PMA was previously used to stimulate bovine platelets in our laboratory [78]. The combined results are shown in Figure 2-6. Note that the y-axis range is 0 to 50%.

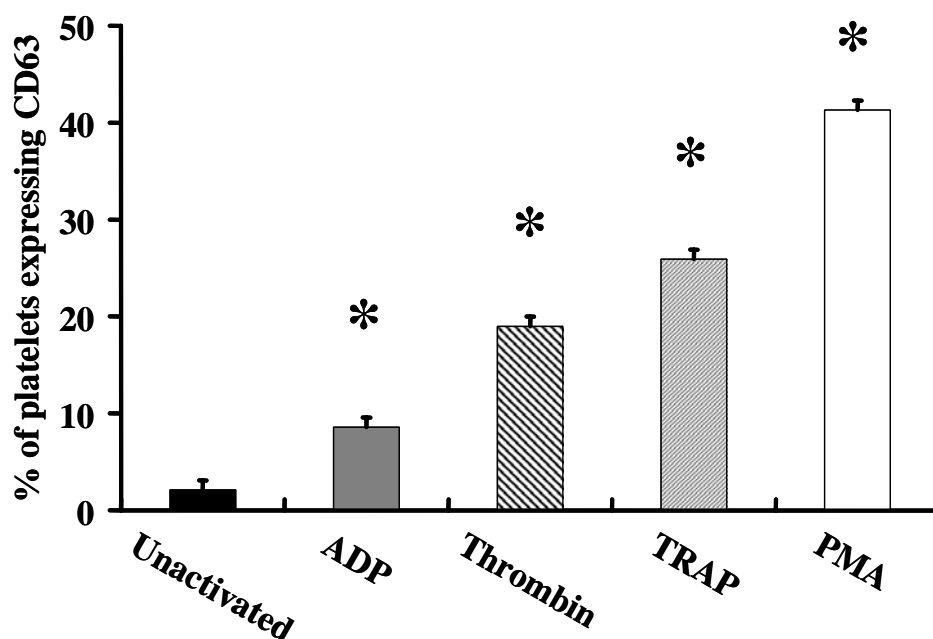


Figure 2-6. Anti-CD63 binding to in vitro activated platelets.

* indicates significantly different versus unactivated samples.

2.2.4.3 Discussion

In humans CD63 appears on the platelet membrane following dense granule content secretion. Analogous dense granules appear in micrographs of bovine platelets, thus it is likely CD63 expression reflects a similar occurrence in bovines [82]. As with the anti-p-selectin antibody and annexin V, this marker possess two desirable attributes, known binding target and potential to perform direct comparison with human data. CD63 expression is also frequently used to quantify platelet activation in humans, including while on VAD support [81].

2.2.5 Platelet Microaggregates

Platelet microaggregates were quantified as described previously without modification [78, 84]. CAPP2A, an anti-ruminant CD41/61 antibody (VMRD Inc., Pullman, WA), labels all bovine platelets. The forward scatter parameter of the flow cytometer was used to discriminate between

single platelet events and platelet aggregates. The samples were prepared from platelet-rich plasma (PRP), thus aggregates containing cells other than platelets would not be present in the sample.

2.3 PLATELET LIFE SPAN DETERMINATION BY *EX VIVO* BIOTINYLATION

In the past *in vivo* cell life span studies required radiolabeling of the population of interest [85, 86]. The use of radioactive substances adds a considerable cost and regulatory burden to already expensive preclinical studies. Several investigators have biotinylated cells in a variety of species as an alternative approach, including our laboratory which previously adapted this technique for bovines [87].

Biotin (vitamin H) has many attractive features for cell labeling. It is widely dispersed in animal tissues as well as present in vegetables and legumes. Thus, it is very unlikely to provoke an antigenic response. The biotinylation technique employed here uses biotin to which a nucleophilic leaving group, N-hydroxysuccinimide (NHS), has been attached. This leaving group preferentially attacks ϵ -amine groups present in the amino acid lysine. A sulfo group is added to the compound to make it water soluble, alleviating the need for dissolution in inorganic solvents. Chain extenders can also be included to avoid steric hindrance in attempting to detect the biotin. Thus, the water soluble sulfo-NHS-biotin can be added to a suspension of cells or proteins, resulting in biotinylation of the lysine residues within the proteins in solution or expressed on cell surfaces.

The presence of biotin is readily detected with avidin, or its derivatives. Avidin is a tetrameric protein composed of four subunits, each containing a single biotin binding site, found in egg whites. The interaction of biotin and avidin is one of the strongest noncovalent bonds in protein chemistry. Avidin contains a substantial number of carbohydrate moieties which can contribute to non-specific binding to cells. Several commercial sources offer a similar, bacterially-derived avidin-like proteins (e.g. Streptavidin), while others process avidin to remove the carbohydrate moieties to reduce non-specific interactions (e.g. Neutravidin from Pierce). Thus, fluorochrome-labeled avidin derivatives are used to detect biotinylated cells.

2.3.1.1 Methods

Ex vivo biotinylation was performed as described previously reported [78, 84]. 360 mL of whole blood was collected via jugular venipuncture using an 18 gauge 1 ½” needle (Becton-Dickinson) and a 60 mL syringe into a 600 mL blood transfer pack (Baxter) containing 40 mL of acid citrate dextrose (ACD, Gambro BCT, Lakewood, CO). Three mL of blood was collected at this time and placed in a citrated monovette to serve as an unlabeled control. 100 mg of the sulfo-NHS-biotin was dissolved in ~15 mL of phosphate buffered saline by vortexing for one min. The biotin solution was added to the blood by drawing 10 mL of blood from the blood transfer pack, then infusing the biotin solution through a 0.2 µm filter. The 10 mL of blood was reinfused to ensure all of the solution was washed into the blood transfer pack. The blood transfer pack was manually inverted several times and incubated for 10 mins. Three mL of blood was collected to measure labeling efficiency. The remaining blood was then reinfused into the jugular vein through a 16 gauge 140 mm i.v. catheter (usual time for reinfusion is 10 – 15 mins). Subsequent 3 mL blood samples were collected by jugular venipuncture using an 18 gauge 1 ½” needle and immediately transferring the blood to a citrated monovette containing 3.8% trisodium citrate. Blood draws were collected one hour after reinfusion and at least daily until the no biotin labeled platelets could be detected. If the animal had an indwelling vascular access line, it was used instead of jugular venipuncture for blood collection.

The blood was prepared for flow cytometric analysis by adding into six 12x75mm polystyrene tubes 250 µL of phosphate-buffered saline (PBS) pH 7.4 containing 1mg/mL bovine serum albumin, 20 µL of 0.1 mg/mL Streptavidin-FITC (SA-FITC) or Streptavidin-PE (SA-PE, Calbiochem), and 20µL of blood diluted 1:10 with PBS. After 30 mins 1000 µL of PBS was added to each sample tube and the sample were centrifuged for 5 mins at 190 x g. The supernatant was removed with a transfer pipette. 500 µL of 1% PF was then added to all sample tube for fixation. The tubes were shielded from light and stored at 2 – 8° C until analysis could be performed on the flow cytometer.

In one study performed on animal A040, four sets of samples were prepared as above using SA-PE with no wash step, SA-PE with the above wash step, SA-FITC with no wash step, and SA-FITC with the above wash step. This was done to determine if using FITC instead of PE, as employed by Baker, and addition of a wash step would reduce non-specific binding.

The sample collected prior to biotin labeling was used to set a fluorescence intensity threshold, above which 2% of non-biotin-labeled platelets fell. The percent of platelets exceeding the threshold in the hour one sample minus 2% was normalized to 100%. Subsequent samples were normalized using the above calculation. Samples were collected until the normalized percentage returned to zero (2% positive platelets).

2.3.1.2 Results

Results from the A040 study indicated insufficient amounts of SA were added to measure labeling efficiency (from the sample obtained following biotinylation, but prior to re-infusion). In later studies, more SA-FITC was used (0.5 mg/mL), and it was found over 95% of platelets were labeled with biotin. The percent of biotin labeled platelets detected is shown in Figure 2-7.

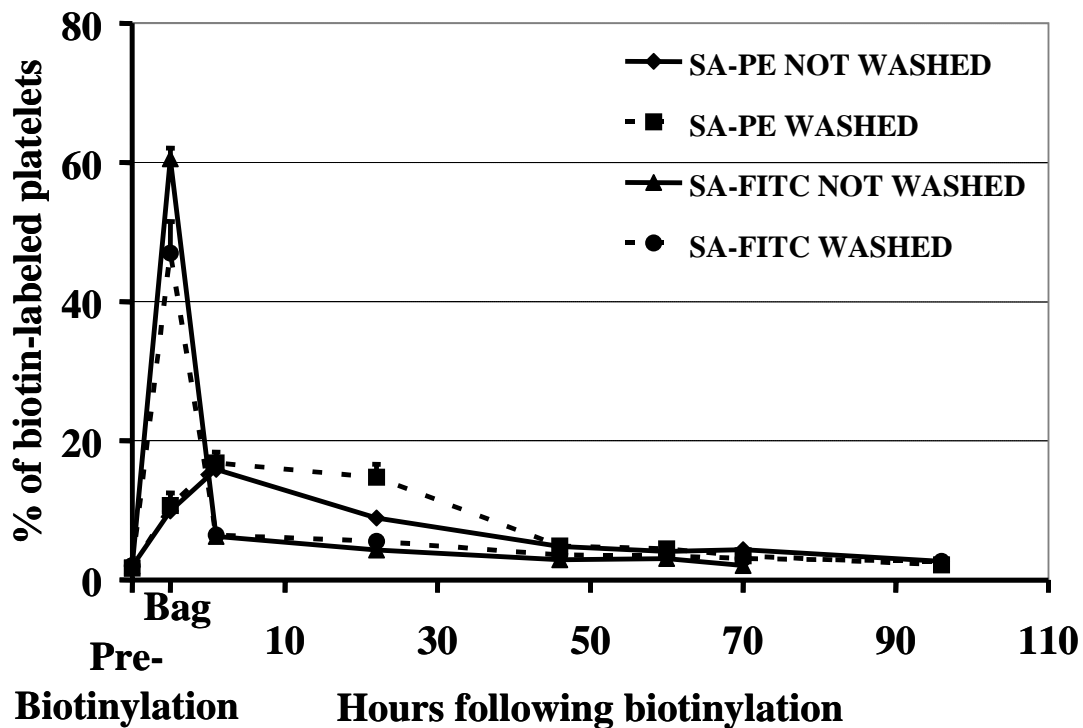


Figure 2-7. Percent of biotinylated platelets detected by flow cytometry using SA-PE and SA-FITC, with and without washing.

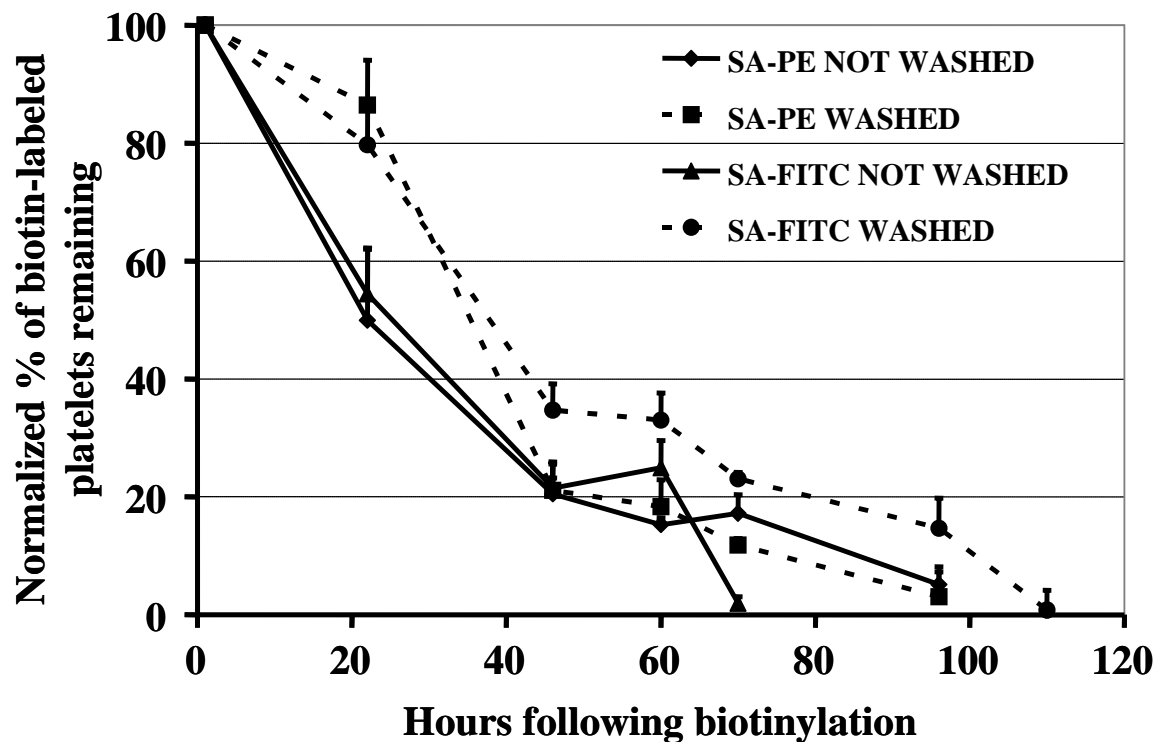


Figure 2-8. Platelet life span determination following *ex vivo* biotinylation normalizing the one hour sample to 100% and using for different labeling techniques.

The normalized percent of biotin-labeled platelets remaining is shown in Figure 2-8. The life spans using the different detection agents ranged for 70 to 110 hours. The SA-FITC without a wash step produced the shortest estimated life span, while the SA-PE with or without a wash step similar end results, despite substantial differences in the early portion of the study.

2.3.1.3 Discussion

Additional life span data using the refinements to the technique described here will be presented below. The *ex vivo* biotinylation technique offers several advantages over alternative radiolabeling techniques. Blood did not require centrifugation and time outside of the body was minimized. Magnusson and colleagues reported biotinylation of platelets could cause platelet activation and impaired response to agonists; however, the concentration employed here was half of the smallest amount examined in that study that was found to induce only minor effects [88].

The labeling technique had a considerable influence on the results. PE has a higher fluorescence intensity per mole than FITC, so PE provides a “brighter” label. However, PE has a molecular weight nearly three times larger than FITC, and thus is more likely to encounter steric hindrance. Washing SA-PE samples did not produce different results with both methods indicating ~100 hour life span. Washing SA-FITC samples produced dramatically different results ~110 hours versus ~70 hours without washing. Of course, the issue then becomes which data are most likely to be correct? It seems reasonable to assume that the SA-FITC with washing was most useful in detecting biotin-labeled platelets, as it combines the measure more likely to be able access biotin on the platelet surface, with apparently reduced non-specific binding. Verification of this assumption would require using another platelet life span determination technique which would have similar or lower measurement error. Obviously, radiolabels were to be avoided and lipophilic dyes, which are also used for blood cell life span studies, require the use of organic solvents. Baker [87] reported that the use of an organic solvent for (non-water soluble) biotin labeling of blood resulted in renal distress following reinfusion. Thus, alternate methods for determining platelet life span were not attempted.

2.4 QUANTIFICATION OF BOVINE LEUKOCYTE PLATELET AGGREGATES AND MONOCYTES EXPRESSING TISSUE FACTOR BY FLOW CYTOMETRY

Platelets and leukocyte serve dual roles in thrombotic and inflammatory states. There can be considerable interaction through several proteins and receptors. Elevated levels of monocyte- and granulocyte-platelet aggregates have been demonstrated in patient with severe heart failure, vascular disease, arterial stents, or supported by mechanical circulatory assistance [89-93]. Granulocyte-platelet aggregates have been observed in acute and chronic inflammatory states in bovines [94].

2.4.1 Granulocyte-Platelet Aggregates

2.4.1.1 Methods

Granulocyte-platelet aggregates were identified with an anti-bovine granulocyte antibody CH138A (VMRD) and the anti-ruminant CD41/61 antibody used in Section 2.2.5 [95]. Blood collected as described previously from four pre-operative bovines was used for *in vitro* activation studies. 100 μ L blood was added to tubes containing 25 μ L 15 μ g/mL CH138A and 25 μ L 15 μ g/mL CAPP2A (anti-CD41/61) or ColiS69 (isotype control) and 50 μ L PBS or PBS+ 5 μ M TRAP. The samples were incubated for 20 mins then washed with 1000 μ L PBS. 25 μ L of 15 μ g/mL goat anti-mouse IgM-FITC and 25 μ L of 15 μ g/mL goat anti-mouse IgG1-PE were added and samples were again incubated for 20 mins. Two mL ammonium chloride potassium (ACK) buffer (8.29 g NH₄Cl, 1.0 g KHCO₃, 0.0372 g disodium EDTA per L distilled H₂O) were added to lyse the red blood cells, then the samples were washed 3 times with PBS and fixed with 500 μ L 1% PF. Compensation controls were simultaneously prepared.

Flow cytometric analysis was performed by gating on CH138A positive events and setting a threshold fluorescence intensity in the FL-2 channel (the channel in which PE fluorescence can be detected) above which 2% of the CH138A events fell. Statistical comparisons were performed using two-sample, unpaired *t*-test assuming unequal variances with significance assumed for $p < 0.05$.

2.4.1.2 Results & Discussion

It was found that an average of $4.5 \pm 1.2\%$ (mean \pm st. dev.) of unstimulated granulocytes were positive for platelets. The number increased significantly to 9 ± 2 following stimulation with TRAP ($p < 0.05$). Although the difference was significant, the quantitative change was relatively small. However, the goal was to develop an assay which could identify granulocyte-platelet aggregates, not stimulate maximum formation of these aggregates *in vitro*.

2.4.2 Monocyte-Platelet Aggregates

2.4.2.1 Methods

Identification of monocyte-platelet aggregates was achieved using a procedure similar to that of Section 2.4.1.1. Monocytes were identified with an anti-CD14 (an IgG2 antibody), reported to cross-react with bovines, conjugated to FITC (Serotec), obviating the need for one of the secondary antibodies. CAPP2A (anti-ruminant CD41/61) plus goat anti-mouse IgG1-PE was used as above to identify platelets. TRAP served as the agonist again.

2.4.2.2 Results & Discussion

A larger quantitative difference was observed in the formation of monocyte-platelet aggregates than was previously found for granulocyte platelets. $7 \pm 3\%$ of unstimulated monocytes were positive for platelets. This number significantly increased to $45 \pm 4\%$ following activation with TRAP. Having successfully developed an assay to quantify monocyte-platelet aggregates, no additional *in vitro* activation studies were pursued.

2.4.3 Monocytes Expressing Tissue Factor

2.4.3.1 Methods

Blood aliquots from four bovines were incubated 1:1 with PBS containing 1 mM CaCl_2 + 3 μM PMA + 5 mM A23187 for 120 mins. Control sample was mixed 1:1 with PBS. The samples were then washed three times with PBS and resuspended 1:1 in PBS. 200 μL blood: PBS mixture was added to tubes containing 25 μL anti-CD14-FITC (Serotec) and 25 μL anti-bovine tissue factor (obtained from Dr. Stephen Carson, University of Nebraska Medical Center) or ColiS69 (isotype control) [96]. Samples were washed and then 25 μL of 15 $\mu\text{g}/\text{mL}$ goat anti-mouse IgG-PE was added and the samples incubated for 20 mins. ACK buffer was added to lyse the red blood cells and then the samples were washed three times with PBS. Fixation was accomplished by addition of 500 μL of 1% PF. Flow cytometric analysis and statistical comparisons were performed as above.

2.4.3.2 Results & Discussion

Tissue factor was expressed on $2.0 \pm 0.9\%$ of unstimulated monocytes. Expression significantly increased to $23 \pm 3\%$ ($p < 0.05$) following stimulation. The appearance of tissue factor in the blood stream initiates the extrinsic coagulation cascade. Thus, monocytes expressing tissue factor reflect activation of a cell which serves both pro-inflammatory and pro-thrombotic functions [97].

3.0 BIOCOMPATIBILITY ASSESSMENT OF THE HEARTMATE II AXIAL FLOW VENTRICULAR ASSIST DEVICE



Figure 3-1. The Heartmate II VAD with cannulae attached shown next to a D-cell battery.

The Heartmate II is an axial flow VAD developed to provide long-term support (> 5 years) to patients with severe heart failure [98, 99]. The implanted portion of the system, shown in Figure 3-1, consists of a 16 mm diameter cylindrical inflow cannula (left side of the pump) inserted by coring of the apex into the left ventricle, the actual pump and an outflow cannula. The surface of the inflow cannula has 100 μm diameter titanium (Ti) beads sintered to the surface, based on the cannula and pump housing developed for the Heartmate I VAD. The white section in Figure 3-1 of the inflow conduit is a flexible strain relief section which contains a compressed Dacron (C. R. Bard, Haverhill, PA) vascular graft “recovery” segment. In the event a patient could be weaned from Heartmate II support, the strain relief can be removed to access the recovery graft. The graft would be allowed to expand and then be cut and sewn shut while allowing the ventricular portion of the inflow cannula to remain in place. The strain relief segment connects to a titanium elbow, which makes a right angle turn toward the actual pump. The interior of the inflow elbow was also coated with the sintered Ti beads.

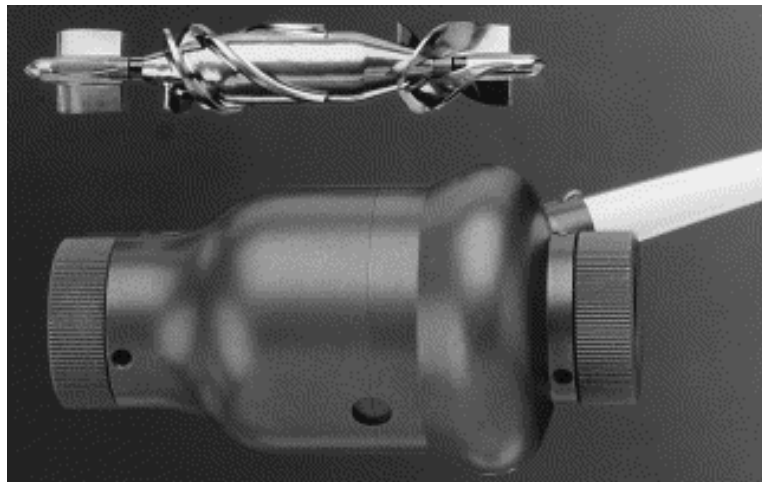


Figure 3-2. The Heartmate II pump with the stators and impeller shown above.

Blood enters the pump (left side in Figure 3-2) and flows past the airfoil-shaped inflow stators. Making the 90° turn proximal to the pump in the inflow elbow induces secondary flows. The stators “straighten” the flow, so that it is aligned in the axial direction prior to encountering

the impeller. The stators also serve as struts to support the jeweled hydrodynamic bearing. The rotating portion of the bearing has a hemispherical shape at the end, setting into a cup-shaped mating surface. During operation a thin film of liquid separates the moving and stationary surfaces to prevent wear. In some studies the sintered Ti beads were applied to the inlet of the pump and the stators (both inflow and outflow), this configuration will be referred to as a “textured pump.” In the rest of the studies the inlet, outlet, and stator surfaces were all smooth, polished surfaces, which will be referred to as a “smooth pump.”

The impeller and blades induce helical (circumferential) flow as shown in Figure 3-3. The blades extend about $2/3$ of the length of the cylindrical middle portion of the impeller.

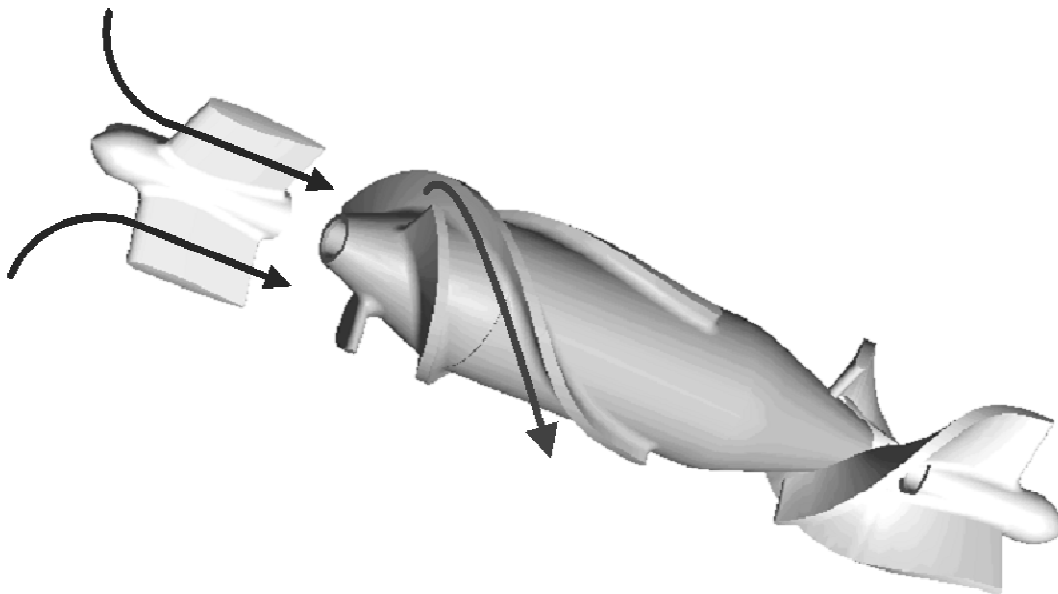


Figure 3-3. The Heartmate II impeller and stators, without the bearings, are shown.

The arrows indicate the direction of motion of fluid into the pump.

Inside the impeller at this position is the rotor of the DC brushless motor which provides commutation to generate the impeller rotation. The rear stators collect the helical flow and redirect it in the axial direction, recovering the pressure developed by the impeller as shown in Figure 3-4.

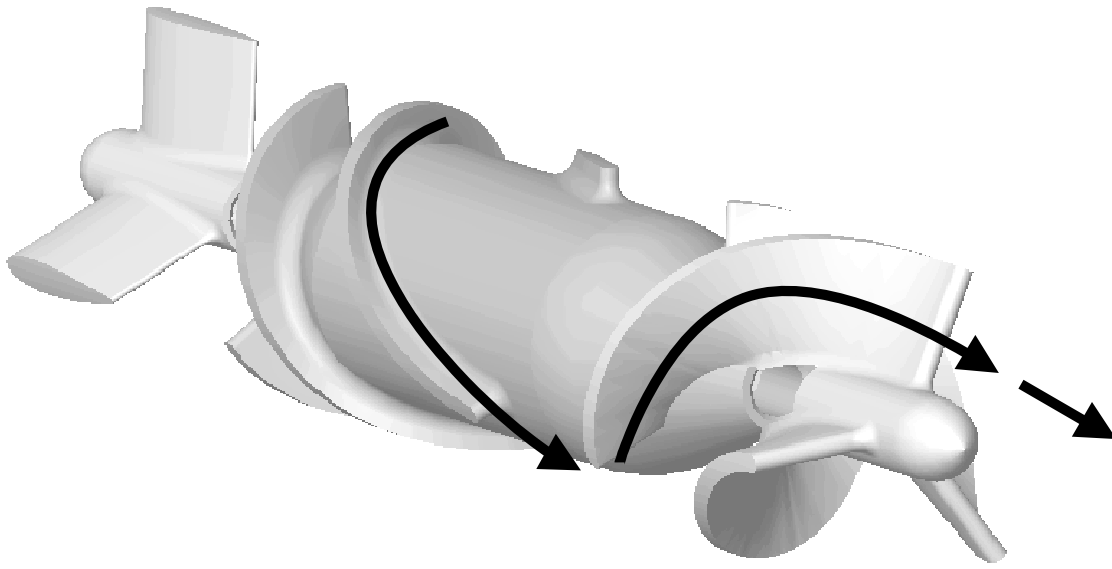


Figure 3-4. The Heartmate II impeller and stators, without the bearings, are shown.

The arrows indicate the direction of flow through the blade passage and the outflow stators.

Blood then exits the pump into another sintered Ti-coated elbow to make a 90° turn connecting with a Dacron outflow graft anastomosis to the aorta. In humans, the anastomosis site most commonly is the ascending aorta. In bovines the ascending aorta is too short to receive the graft, and so the anastomosis site was the descending aorta. A bend relief surrounds the proximal (to the pump) portion of the outflow graft to prevent kinking [100].

The Heartmate II pump RPM range is 6,000 - 15,000 RPM. However, the clinical RPM range is limited to 8,000 - 12,000 RPM. The pump flow rate is a function of several variables, but substantially, the pressure difference across the pump (aortic pressure minus left atrial pressure) and the pump speed. The curves demonstrating the relation between pump differential pressure, pump RPM, and flow rate are called H-Q curves (head pressure, H, versus flow rate, Q), shown in Figure 3-5.

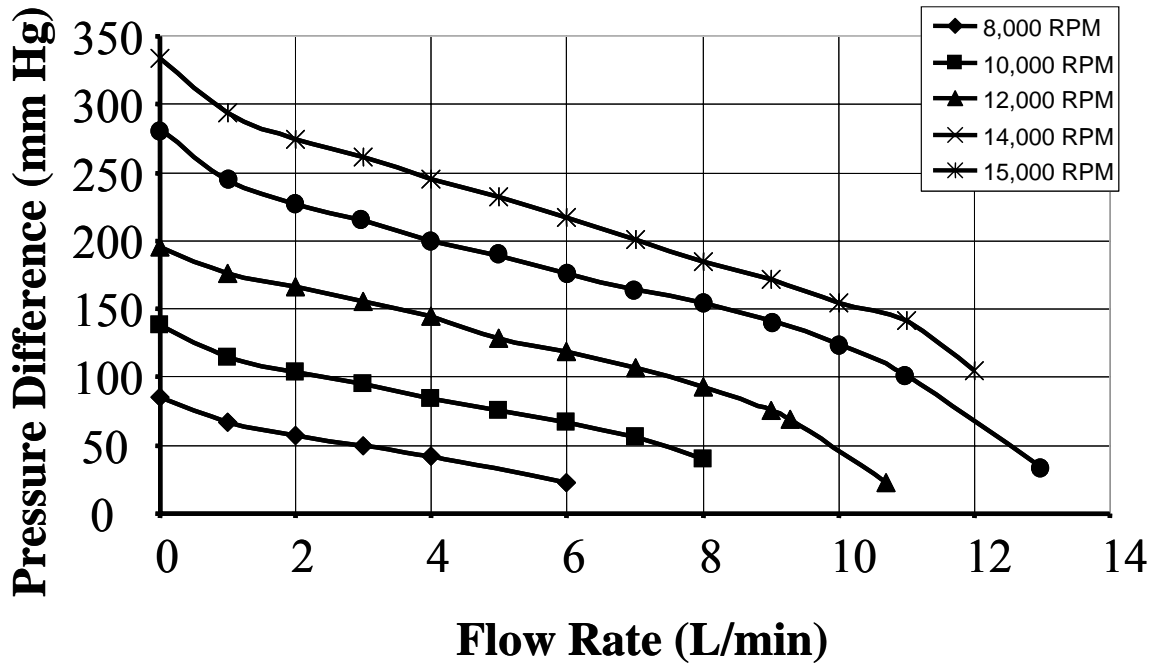


Figure 3-5. H-Q curves provided by the manufacturer for the Heartmate II.

The variation in flow rates at a given pump RPM with a variation in the differential pressure result in the flow rate can vary substantially over a single cardiac cycle. Even severely compromised myocardial tissue usually retains contractile function. For example, a patient whose pump is operating at 10,000 RPM may have an arterial pressure of 100/70 (patients with rotary pumps have a diminished pulse pressure, but still usually retain a pulsatile waveform) will have pump outputs that vary from 2 to 5 liters per min over a cardiac cycle (based on the data in Figure 3-5). If the pump speed is set too high the pump will generate negative pressure, causing the apical cannula to pull the septum into the orifice or the ventricle to collapse [101]. If the pump is operated with the RPM set too low, the flow through the pump may become retrograde allowing blood to flow back into the ventricle. In either case cardiac output is compromised and the situation must be remedied to insure adequate perfusion.

The potentially wide variation in flows and the desire to use the Heartmate II for chronic support point to the need for exceptional biocompatibility. The reduced size of the pump and the smaller diameter percutaneous lead compared to previous pulsatile pumps, will likely lead to a reduced rate of exit site and pump pocket infections. This remains to be demonstrated clinically.

The Heartmate I VAD, produced by the same manufacturer, uses textured surfaces on the blood flow path to encourage the formation of a “pseudo-neointima.” The surface promotes cellular deposition, forming a large coagulum on the textured materials [102]. Patients supported with this device only require aspirin therapy and thromboembolic events have been relatively low. While a single report claims the presence of endothelial cells on the surface, the actual description of the lining suggests a largely acellular fibrous material with interspersed fibroblasts and occasionally other nucleated cells [103]. Patients supported with the Heartmate I, have elevated thrombin generation and substantially elevated fibrinolysis [104]. Thus, it is likely that the hemostatic balance in Heartmate I patients has shifted toward fibrinolysis, the cleavage of blood clots. While the protective mechanism of the lining which develops in the Heartmate I is not completely understood, the pump has now been implanted in several thousand patients and the thromboembolic rate has reported as below 10% [105].

Based on the previous performance of the approach, the Heartmate II developers applied the sintered titanium beads to the blood-contacting surfaces of the pump, with the exception of the area immediately adjacent to the impeller, to enhance the biocompatibility of the device. The biocompatibility assays developed in the previous chapter were used to evaluate to the Heartmate II and several aspects of its performance.

3.1 SPECIFIC AIMS

3.1.1 Quantification of Circulating Activated Platelets, Platelet Microaggregates, and Platelet Life Span.

The hypothesis that the Heartmate II causes increased levels of circulating activated platelets and platelet microaggregates and decreased platelet life span was tested. Based on previous work in our laboratory and the evidence that all VADs in clinical use provoke a thrombotic disturbance to some level, the hypothesis was very likely to be true; however, the key finding would be the degree of activation and whether the extent of the observed alteration was clinically relevant.

3.2 TEMPORAL STUDIES QUANTIFYING CIRCULATING ACTIVATED PLATELETS, PLATELET MICROAGGREGATES, AND PLATELET LIFE SPAN IN BOVINES RECEIVING THE HEARTMATE II

3.2.1 Methods

3.2.1.1 VAD Implant Procedure and Animal Care

The following description is based largely on the method given in Snyder et al. [84]. Fifty Jersey calves were housed in the large animal facilities of the University of Pittsburgh. All procedures involving animals were conducted in compliance with the “Guide for the Care and Use of Laboratory Animals” published by the National Institutes of Health. Prophylactic antibiotics and the first coumadin dose (5 or 10 mg) were administered prior to surgery. The calves were implanted with the Heartmate II axial flow VAD (Thoratec, Pleasanton, CA) described above in Section 3.0. The Dacron portions of the cannulae were preclotted with the animal’s blood before implantation. The calves were premedicated with 45 mg of atropine sulfate (American Pharmaceutical Partners, Schaumburg, IL), 45 mg. Anesthesia was induced with methohexital sodium (Jones Pharma Inc, St. Louis, MO), 10 mg/kg. Following intubation, anesthesia was maintained with isoflurane in oxygen and room air. The chest was entered through the fifth intercostal space. The descending aorta was isolated to receive the outflow cannula. All blood-contacting surfaces of the pump were rinsed three times with saline. A plastic anti-kinking guard was placed around the outflow cannula, which was then sutured to the aorta end-to-side with 4-0 monofilament polypropylene. Heparin at 1.5 mg/kg was administered when the aorta was partially clamped and then again when the anastomosis was completed. The heart was then prepared with four size 0 braided Dacron pledgeted sutures. The pump was pre-assembled to both cannulae after being filled with saline. The apex of the left ventricle was cored and the inflow cannula was inserted. The pledgeted sutures were attached to the sewing ring, then the pump was de-aired and started. A Transonic flow probe (Transonic Systems Inc, Ithaca, NY) was attached around the distal section of the outflow graft. Warfarin (DuPont Pharma, Wilmington, DE) was administered daily to maintain an international normalized ratio of 2.5 to 3.5. Typical target operating measurements were volumetric flow rates of 4 to 7 L per min at 9,000 to 12,000 RPMs.

Post-operatively, the animal was placed on a heparin infusion to maintain ACTs of 200-250 seconds until coumadin dose became therapeutic. The animal was encouraged to stand and eat within a few hours of surgery. Electrolytes, nasal oxygen, and fluids were given as needed. Bovine blood was administered if excessive bleeding continued unabated. Chest drainage tubes were removed when bleeding was less than 50 mL/hr for several hours. Initially, the speed was set around 8000 in the operating room, and increased to between 9,000 and 10,000 RPMs as the animal improved. Drive line exit sites were sprayed with betadine daily and more frequently if there was evidence of infection. Implant durations ranged from 0 to 136 days.

3.2.1.2 Sham Surgical Implant Procedure

8 surgical sham calves the same underwent the same surgical procedure as in Section 3.2.1.1 with the following alterations. After the preclotted Dacron cannula was sutured to the aorta it was sutured shut approximately 3 centimeters distal to the anastomosis with a running suture of 4-0 monofilament polypropylene. One pledgeted 0 braid Dacron suture was placed in the apex of the heart in a horizontal mattress pattern. A stab incision was then made in the apex of the heart. The sutures were tied, thus closing the incision in the heart. Two sham cables were tunneled into the intercostal muscles before chest closure. These animals also received the same prophylactic antibiotic treatment and anticoagulation therapy as the VAD implanted calves. The animals were allowed recover from the procedure were housed for up to 183 days before necropsy.

3.2.1.3 Study Termination and Necropsy

In both elective and premature study terminations, the animal was administered a bolus (50,000 U) of heparin, followed by sedation with a barbiturate, and an overdose of potassium chloride. The animal was then exsanguinated by jugular laceration. The position and condition of the pump, cannula, and any transcutaneous lines were noted and photograph if significant. The heart, lung, liver, kidneys, spleen, and adrenals were examined visually by serial section if necessary. Tissue samples were submitted for histology studies. The number and size of any infarcts or lesions were noted.

3.2.1.4 Blood Sampling and Assay Preparation

Blood samples were collected at least once pre-operatively, daily during the immediate post-operative period, and subsequently twice weekly. If the study was still ongoing after 90 days, only one sample was collected weekly. Pre-operatively and after the removal of indwelling vascular access lines, samples were collected via jugular venipuncture as described in Section 2.2.1.1. Between 13 and 30 mL of blood was collected, with 3 mL being transferred into a citrated monovette. The rest of the blood was used for other studies. When an animal had indwelling lines, blood samples were obtained by drawing 20 mL of fluid (blood plus saline in the line) into a syringe through the 72" extension tubing line. The syringe was removed and 15-30 mL of blood was drawn into a new, unused syringe. A 3 mL sample was then transferred to a citrated monovette. The blood contained in the first syringe was reinfused into the animal and the line flushed with 0.9% saline containing 20 U/mL heparin. Vascular access lines were usually available for the first post-operative week.

The assays developed in Chapter 2.0 were applied to the blood samples collected from all the animals receiving implants or undergoing sham implant procedures; however, the assays were developed over time, so not all assays were used in all animals.

3.2.1.5 Statistical Analysis

Analysis of variance with post-hoc Newman Keuls testing was used to determine significant differences between pre-operative and post-operative values for each assay. The same testing was also used to compare aggregated uneventful post-operative course assay values versus sham surgical procedure animals for pre-operative values and on post-operative days 1, 3, 5, 10, 14, 17, 20, 24, and 27. Significance was assumed for $p < 0.05$ for all statistical comparisons.

3.2.2 Results

3.2.2.1 Uneventful Post-operative Course Data

An uneventful post-operative course was defined as one with no significant bleeding episodes; no infections or prolonged periods of body temperature exceeding 40° C; minimal septal

scarring; no prolonged periods of low (< 3 lpm); fewer than 10 small (2x2 mm or smaller) infarcts; and no occlusive thrombus in the VAD blood flow path.

An example of an uneventful post-operative course is shown in Figure 3-6. The graphs show that the three platelet activation indicator and microaggregates are relatively low pre-

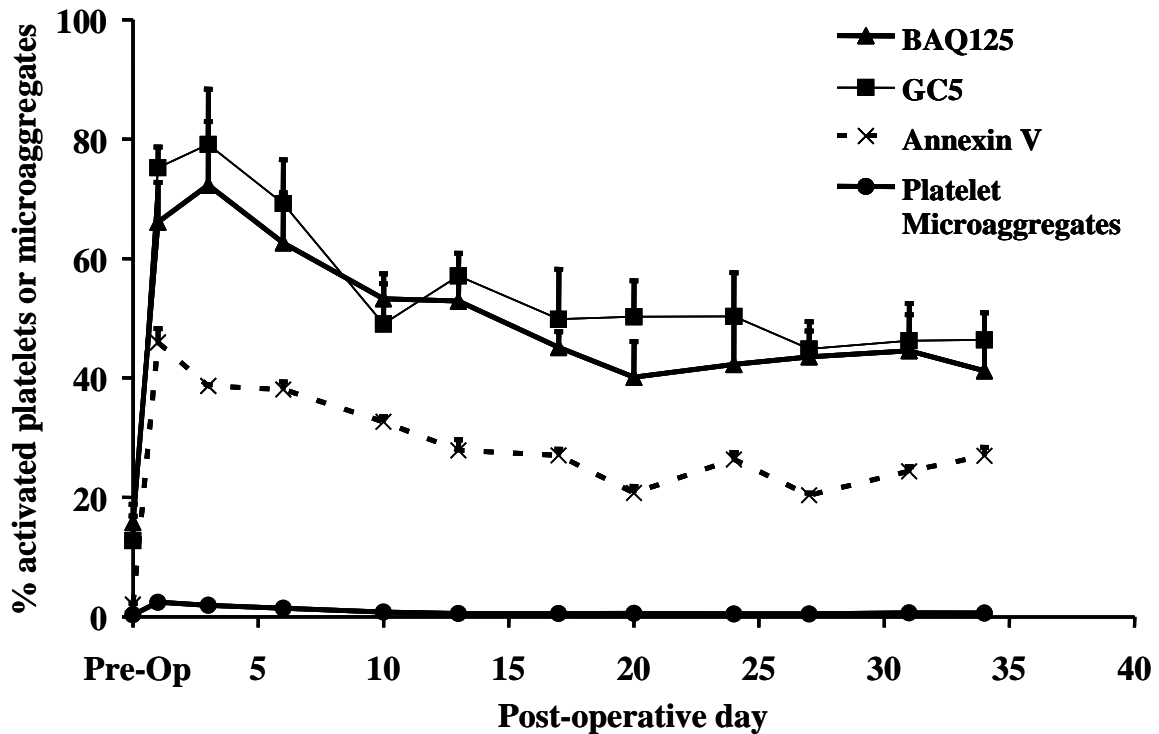


Figure 3-6. The chart shows the temporal results of 3 platelet activation indicators and platelet microaggregates for an uneventful course animal, A063.

operatively. Of course, this is to be expected when testing healthy juveniles. The effect of the implant caused profound activation of platelets. BAQ125 and GC5 exceed 60% for at least the first 6 days. Annexin V also increased notably, but not to the extent of the two indicators of platelet activation. All three circulating activated platelet indicators trend downward after the early post-operative period and appear to plateau after about POD20. Microaggregates increased significantly following the implant and remained elevated until POD13.

Ten studies met the criteria for an uneventful post-operative course. The combined temporal data from these studies is shown in Figure 3-7. The data demonstrate the same overall

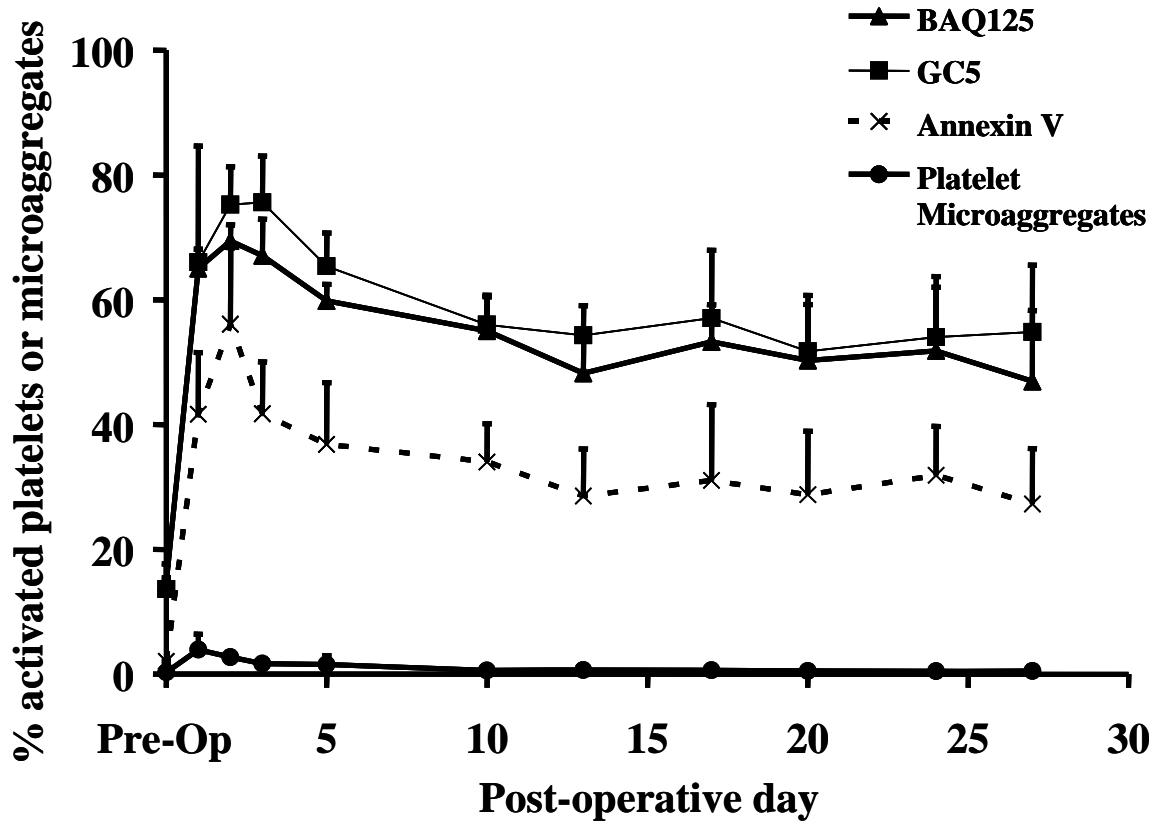


Figure 3-7. Combined temporal circulating activated platelet and platelet microaggregate data for 10 studies with uneventful post-operative courses.

pattern observed in Figure 3-6. That is, relatively low pre-operative values, followed by a substantial increase following implantation. Microaggregates remain significantly elevated versus pre-operative values until POD10, whereas the three indicators of activated platelets were significantly elevated throughout the post-operative period, but did decline from the peak peri-operative values. The results suggest that the Heartmate II causes ongoing platelet activation and

early post-operative platelet microaggregate formation. However, it is obvious that the implant procedure likely contributes to these effects.

3.2.2.2 Sham Surgical Implant Procedure

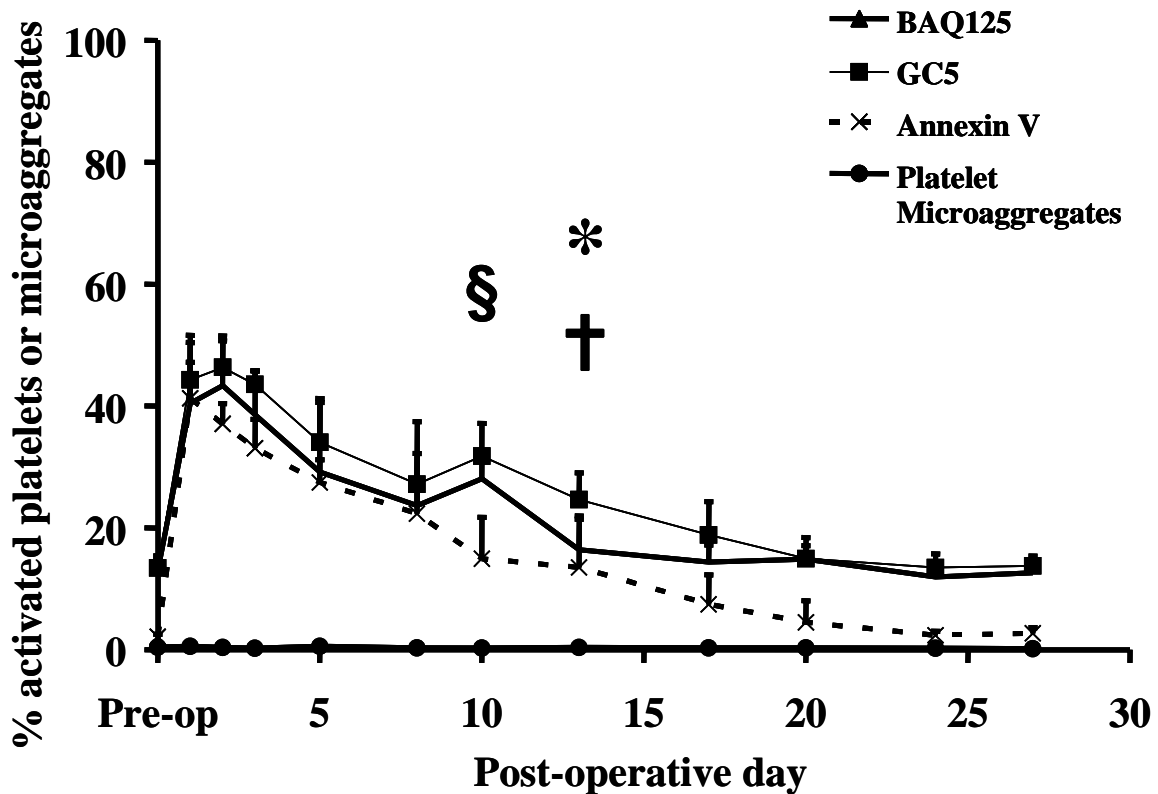


Figure 3-8. Temporal data from 3 circulating activated platelet indicators and platelet microaggregates for 8 sham surgical procedure animals.

The final datum point which was significantly elevated versus pre-operative control is indicated by *, † and § for GC5, Annexin V, and BAQ125, respectively.

Combined temporal results for the 8 sham surgical implant procedure are shown in Figure 3-8. The surgical sham procedure results demonstrate a substantial effect due to the implant procedure. Pre-operative values were, as expected, relatively low. An increase following the surgical procedure is apparent, although qualitatively the peak levels attained by the three circulating activated platelet indicators is not as elevated as in the uneventful VAD course

animals. Following the initial peak, and unlike the VAD-implanted animal, all three platelet activation indicators returned to pre-operative levels. This demonstrates that the effects of the implant procedure dissipate between two and three weeks later. Microaggregates were never observed to be significantly elevated versus pre-operative levels. During necropsy examinations, no renal lesions were found in any of the animals.

3.2.2.3 Comparison of Uneventful VAD Course and Sham Surgical Procedure Studies

In comparing the results from these two groups, it should be first noted that there was no statistical difference in the pre-operative values. Thus, there was no apparent difference in circulating activated platelets and platelet microaggregates between the two groups prior to surgery, although the study was not randomized. Both groups experience substantial increases in platelet activation following surgery. Only the group receiving the pump had a significant increase in platelet microaggregates. By POD3 for GC5, POD5 for BAQ125, and POD13 for Annexin V, the VAD-implanted group assay values are significantly increased compared to the sham surgery group. Thus, the ongoing platelet activation observed in VAD-implanted bovine may be attributed to the device and its operation, even accounting for the substantial impact of the implant procedure.

3.2.2.4 Adverse Events

In examining the number of animals described in Section 3.2.1 it is apparent that the vast majority of animals studied did not fit into the uneventful post-operative course category. The attempt was made to determine if the flow cytometric assays could yield additional insight into the problems encountered. Nearly all of the animals implanted with the Heartmate II system had some evidence of septal scarring. Frequently, there were multiple episodes of suspected suction (sudden decrease in pump flows, or fluctuating flows) especially associated with position changes. Often, the flow cytometric assays displayed a deviation from the pattern established with the uneventful post-operative course studies – dramatic increases immediately after implant, followed by a downward trend to a “plateau,” which is still significantly elevated versus pre-operative values. A dramatic example of this is illustrated by case A058. In this 10 day study the flows were > 4 LPM in the OR. The animal was following a normal post-operative course, until the pump flows began to drop on POD7. After increasing the RPM from 9,000 to 10,000

(attempting to increase the pump flows), pump flows dropped to < 2.7 LPM. After consultation with the corporate sponsors, the RPM was decreased to 8500, but flows were only ~1.3 LPM. The animal was sacrificed on POD9. Results from the flow cytometric assays are shown in Figure 3-9. Pre-operative assay data for this animal was normal. Following implantation, the 3 circulating activated platelet assays all increased to at least 80%, which was qualitatively higher than was usually observed. The three assays decreased on POD6, but then substantially

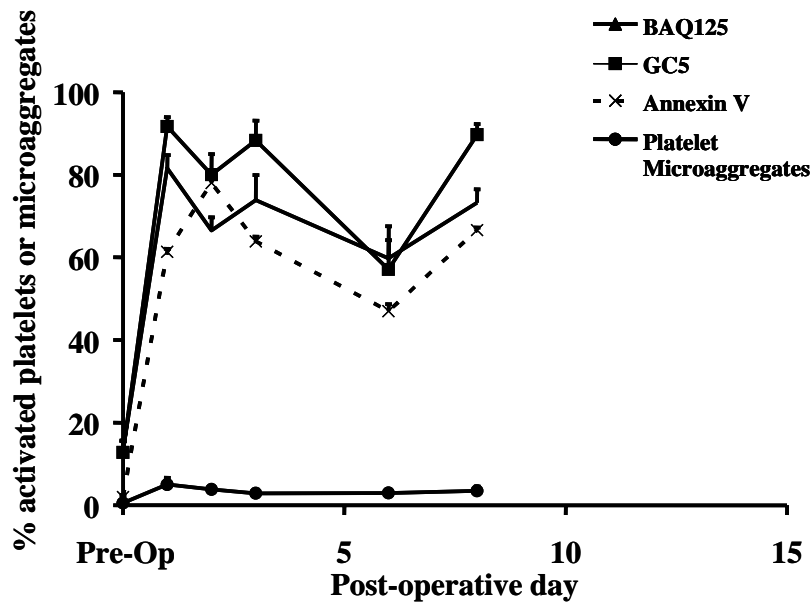


Figure 3-9. Flow cytometric assay data from study A058 is shown.

increased on POD8 (GC5 and Annexin V were significantly increased on POD8 vs. POD6). Microaggregates also remained significantly elevated compared to pre-operative control. At necropsy, a ring of scarred damaged tissue was found on the septal wall, where the apical cannula orifice was completely impinged on the septum. A partially occlusive thrombus was found attached to the outflow stators. Images of these results are shown in Figure 3-10.

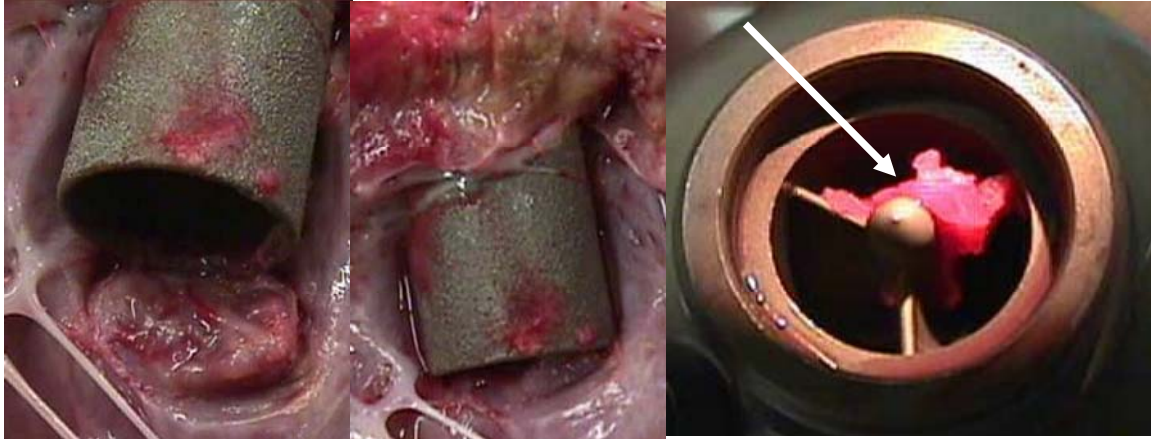


Figure 3-10. Three images from the necropsy of study A058 are shown.

The left image shows septal scarring in a ring-shaped pattern matching the orifice of the apical cannula. The middle image shows how the cannula and septum interacted. The right image shows a partially occlusive thrombus on the outflow stators.

Assay data collected at discrete time points may not capture all events that pose a serious concern; however, as occurred in this case, the assays were at least reflective of the ongoing adverse event associated with the obstruction of the inflow. Unfortunately, there were many studies that encountered inflow obstruction, septal scarring, and suction events.

In study A056, the flow cytometric assays appeared to be following an uneventful post-course; until after POD30, when the three indicators of circulating activated platelets began to trend upward, as seen in Figure 3-11. The study was electively terminated on POD62 due to low

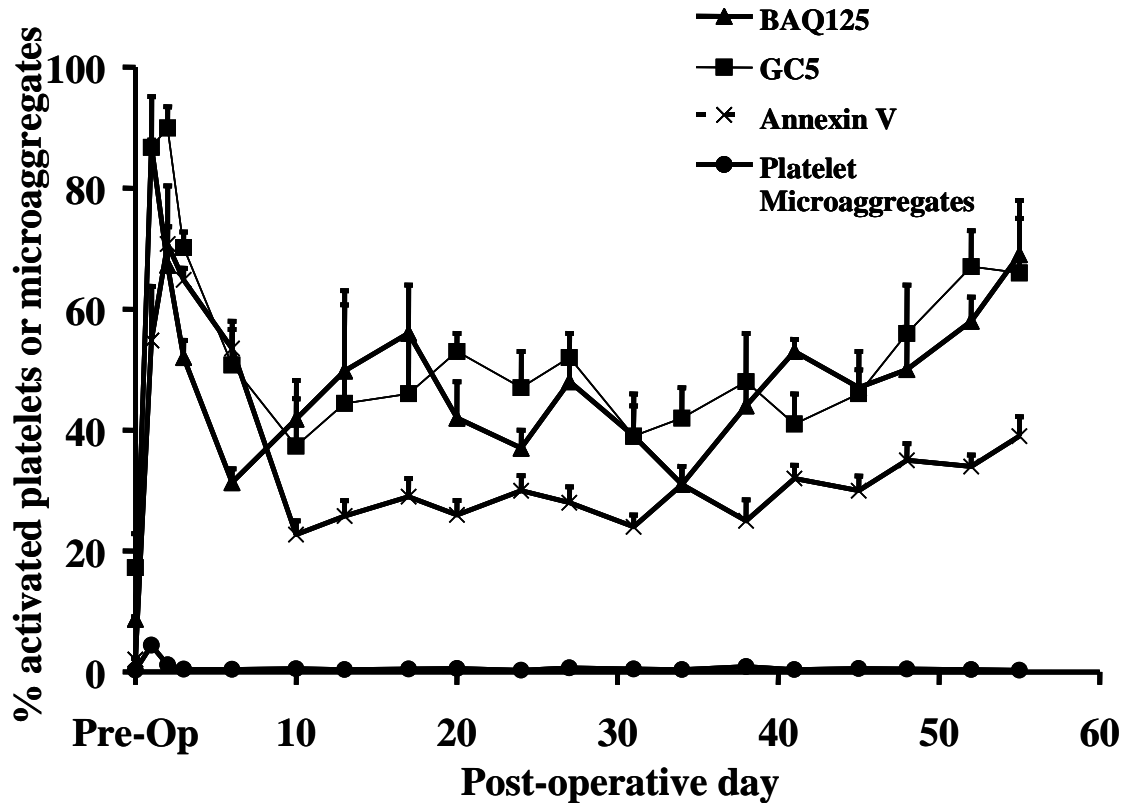


Figure 3-11. Flow cytometric study data from study A056 is shown.

pump flows. During the necropsy, it was observed that the luminal diameter of the compressed Dacron section of the inflow cannula had been reduced to 8 mm from 16 mm. The corporate sponsor requested the pump and cannulae to be returned intact, so no observations of the pump itself were made. There upward trend of circulating activated platelets may have correlated with the over-development of the neo-intima on the Dacron portion of the conduit. Of course, it is not possible to know when the overgrowth occurred. Yet, there may be some value in the information provided by the assays to reflect more subtle events, such as exaggerated neo-intima growth, which evolve over a period of days to weeks. Partial luminal occlusion of either cannula occurred in 5 animals, including A056.

During the recounting of the flow cytometric assay results, it has been noted several times pre-operative values were relatively low and this was consistent across the studies considered to this point. There were three cases in which an animal's blood clotted in citrate

tubes (not attributable to blood collection difficulties), had confirmed platelet counts exceeding 999,000, or the BAQ125, GC5, and Annexin V assay values were significantly elevated pre-operatively. All three of these animals were used for implants, after receiving what was thought to be appropriate medical treatment. Two animals died on the day of surgery, both with substantial thrombus throughout the cannulae and pump. The third animal died of massive bleeding on POD16. Assay data from that study is shown in Figure 3-12. It is readily apparent

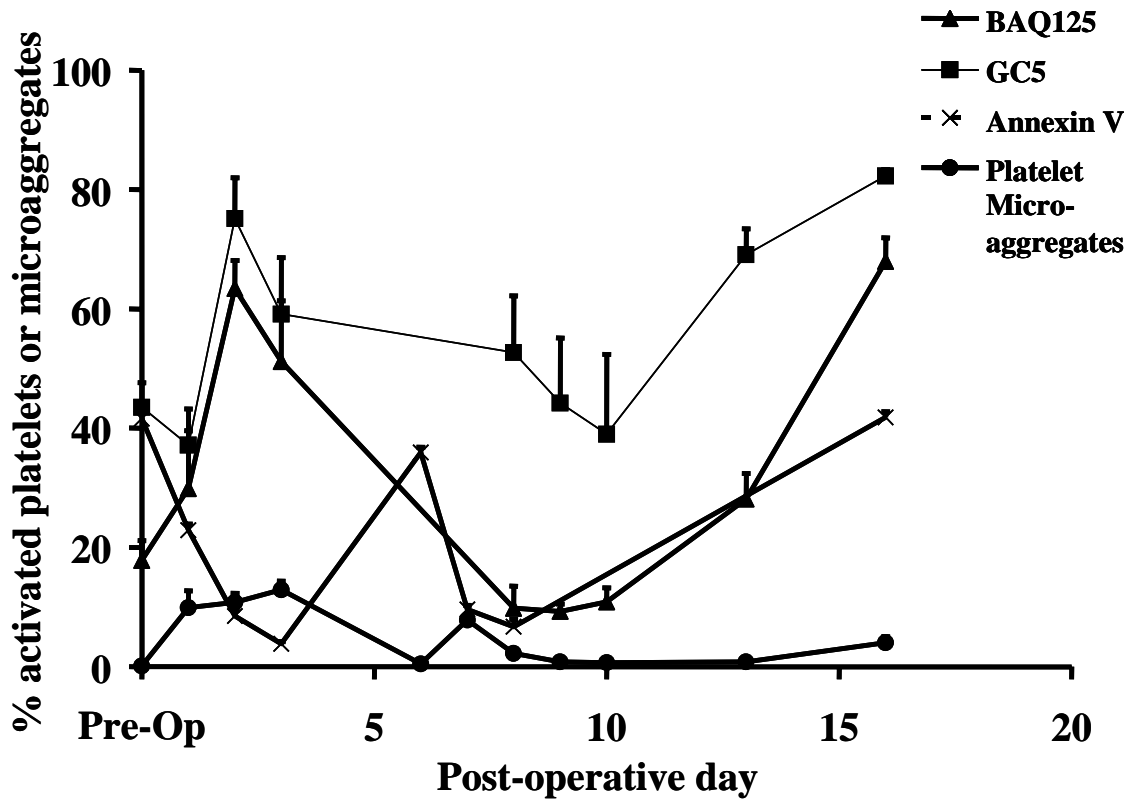


Figure 3-12. Data is shown from case A042, where pre-operative values were elevated, and the animal died from bleeding on POD16.

that, in addition to significantly elevated pre-operative values, this data deviates considerably from the usual pattern observed with the uneventful post-operative course animals. Microaggregates were elevated far beyond levels normal observed following the implant,

reaching 13% on POD3. Microaggregates also spiked to 8% on POD7 and 4% on POD13. The source of bleeding was not found during the necropsy, but in this case, both the pre-operative and post-operative data, pointed to unusual platelet activation and microaggregate behavior.

3.2.2.5 Platelet Life Span

Platelet life span was measure pre-operatively and post-operative after at least POD14 in 8 animals. The results are shown in Figure 3-13. The results support the previous findings with

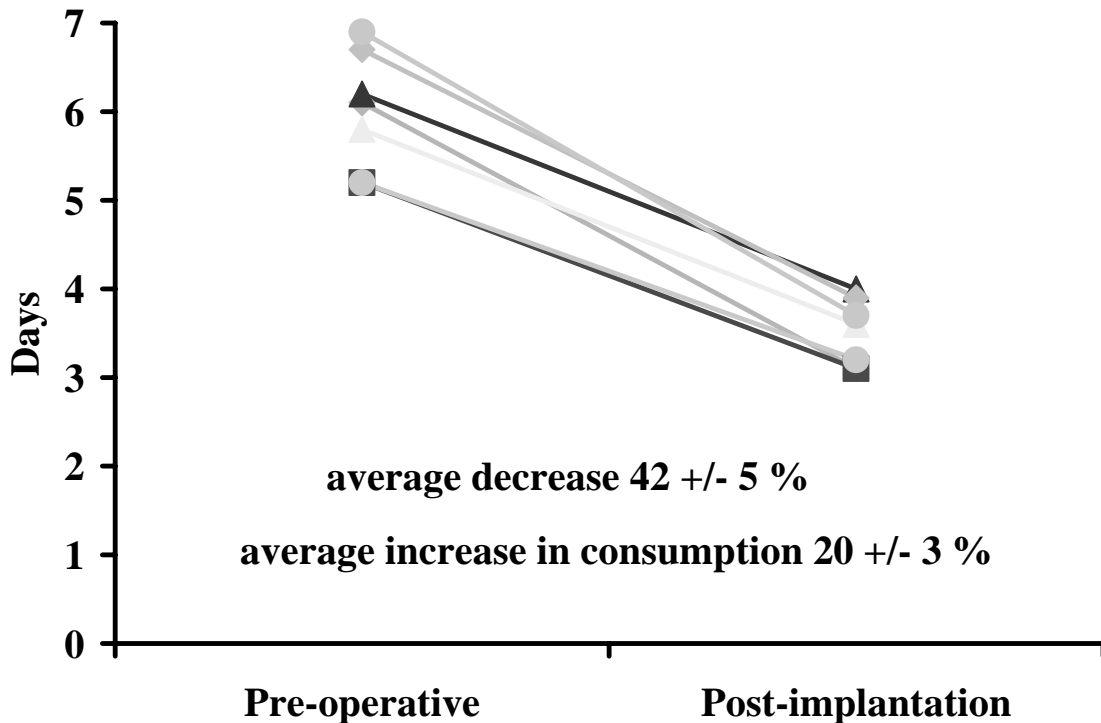


Figure 3-13. Pre-operative and post-implant platelet life spans in 8 animals receiving the Heartmate II.

the flow cytometric assays that there is ongoing platelet activation associated with VAD support. In these 8 animals the post-operative platelet life span decreased an average 42±5%. Using

Hanson and Harker's formula to calculate platelet consumption, it was found that there was a $20\pm 3\%$ increase in platelet consumption.

Platelet life span determinations were performed in 5 of the 8 sham surgical implant animals. The average pre-operative life span was 6.1 days. Post-operative life spans were determined on POD7 (N=3), 12, 14, 21 (N=2), and 32. The POD7 life spans were 3.9, 4.2, and 4.4 days. The remaining life spans were determined to be 5.5 (POD12), 5.4 (POD14), 5.7 (POD21), 6.8 (POD21), and 6.0 (POD32). The life spans for POD12 and later were significantly elevated compared to the post-operative platelet life spans of all pump implanted animals and were not significantly different from the pre-operative life spans of either the sham or device-implanted bovines.

3.2.2.6 The Effects of Step Increases in VAD RPM

In three cases, which had met the criteria for uneventful post-operative course, an *ex vivo* biotinylation was performed with the VAD speed set to 9000 RPM. Circulating activated platelets and platelet microaggregates were quantified for each blood collection. At the end of the platelet life span, another biotinylation was performed. After the 360 mL of blood was collect, but prior to re-infusion, the VAD set speed was increased to 11,500 RPM, but this produced suction, so the speed was decreased to 10,500 RPM. The results from one of the studies appear in Figures 3-14 and 3-15. In all three studies, suction occurred when attempting to increase the pump RPMs to 11,000 or higher produced suction. The initial aim of the study was to determine if the increased shear stresses to which the blood would be exposed at the higher RPM would cause increased platelet activation. In fact, these studies demonstrate the combined effects of producing ventricular suction (which results in wild swings in pump outputs), increased shear stresses, and potentially adverse flow effects.

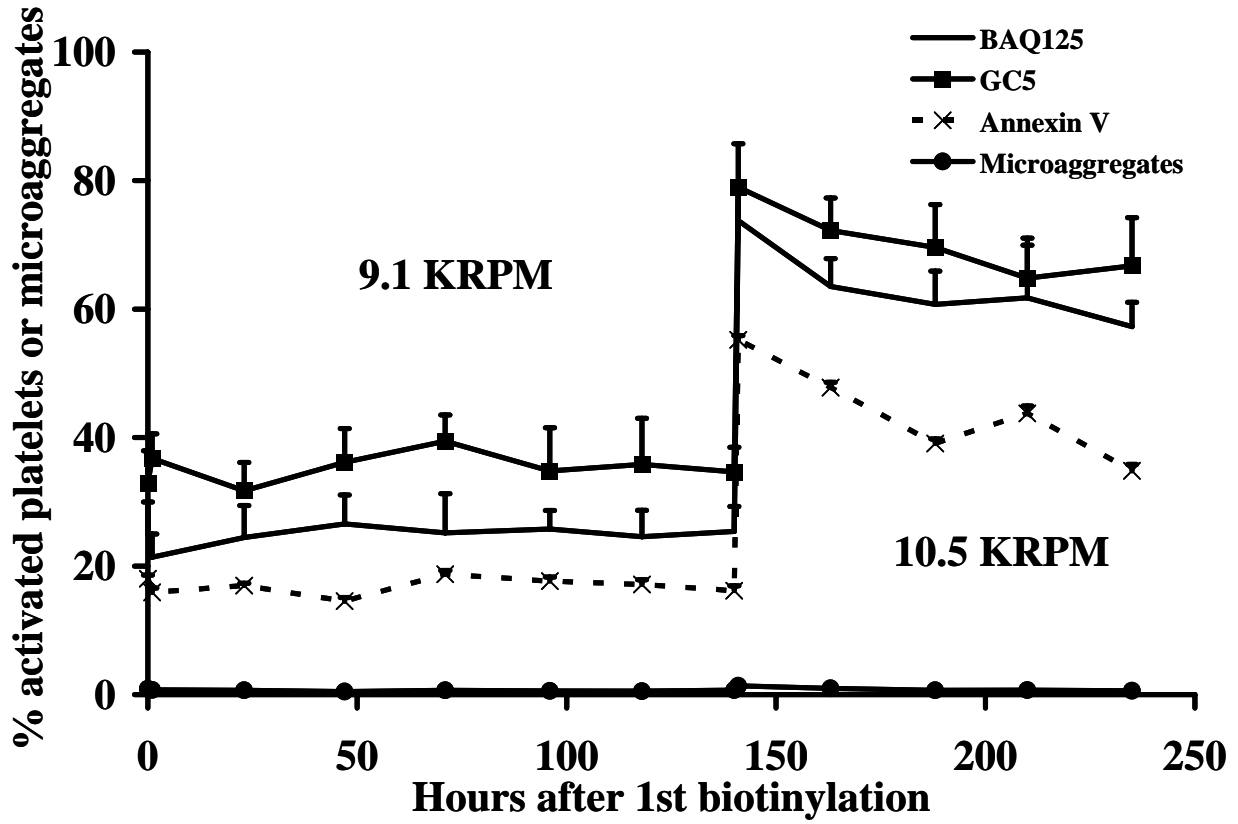


Figure 3-14. Circulating activated platelets and platelet microagregate following a step increase in VAD RPM.

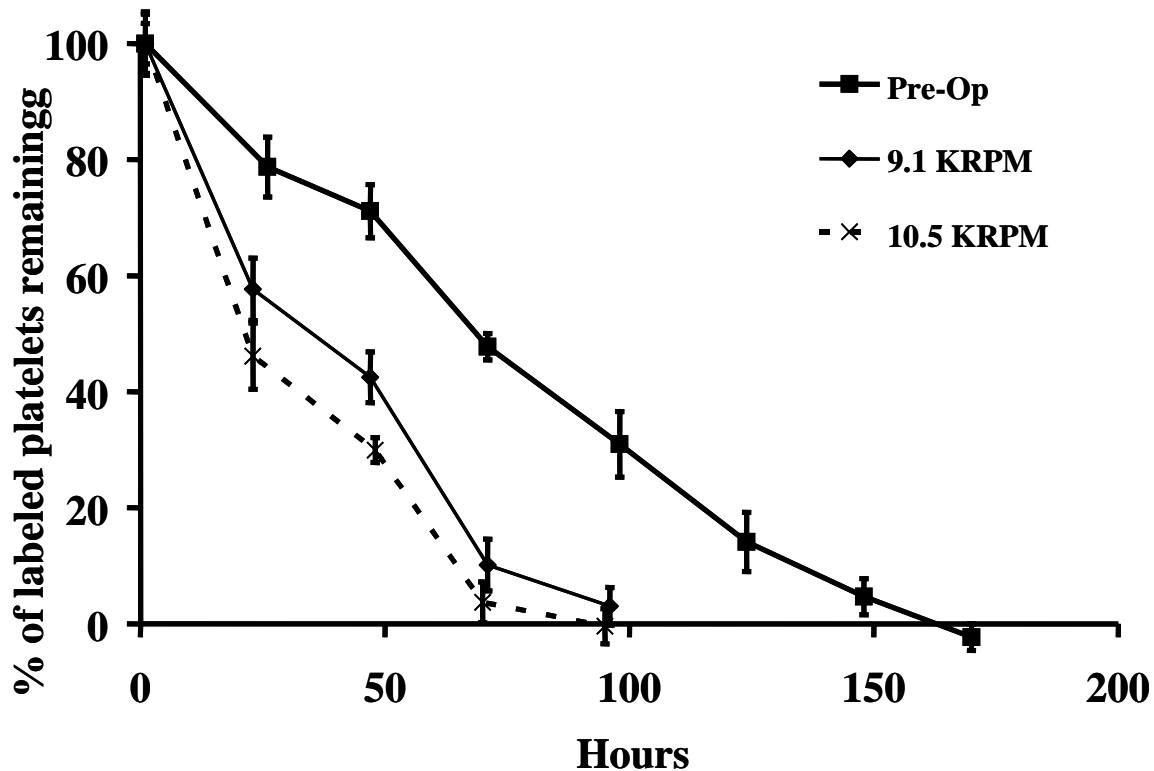


Figure 3-15. Data from three platelet life span determinations are shown.

3.2.2.7 Surface Comparisons

As described in Section 3.0, two types of pump surfaces were examined in these animal studies. The first were “textured pumps” with titanium beads sintered to the inflow conduit, inflows stators, outflow stators, and outflow conduit. The second were “smooth pumps” utilizing a polished titanium surface throughout the pump. In both cases the apical inflow cannula, and inflow and outflow elbows did have the sintered titanium applied to the surface.

Data collection was limited to 6 smooth pump studies. In one study, with an eight day duration, there was massive bleeding and blood samples were not available for most of the study. Only 1 of the other 5 studies would meet the criteria for an uneventful post-operative course. This was mostly due to echocardiographic confirmation of suction in four of the studies. Septal scarring was prevalent and all but one animal had large infarcts (> 10 mm diameter) found in the kidneys during necropsies. Statistical comparisons of the two groups did not reveal any significant differences. Thus, it appears that the adverse flow conditions encountered during

these studies overwhelmed the potential benefit modifying the blood-contacting surface of the pump. However, after stopping a clinical trial utilizing the textured pump, Thoratec has re-initiated clinical trials using the smooth pump version.

3.3 LEUKOCYTE PLATELET AGGREGATES AND MONOCYTE TISSUE FACTOR

3.3.1 Methods

Leukocyte platelet aggregates and monocyte tissue factor expression were quantified in four animals receiving the “smooth” Heartmate II pump. As before, samples were collected pre-operatively, daily in the immediate post-operative period, and twice weekly thereafter.

3.3.2 Results

The combined data from the four studies is shown in Figure 3-16. Similar to the platelet activation indices, there was a consistent pattern of low pre-operative values, followed by substantial increases following surgery and a downward trend to a plateau level that remained elevated versus pre-operative control. Granulocyte platelet aggregates did not increase above 20%, and only declined to about 15% through the post-operative period. Monocyte platelet aggregates and monocytes expressing tissue factor were usually very similar. It was likely that the two indicators were marking the same population of activated monocytes.

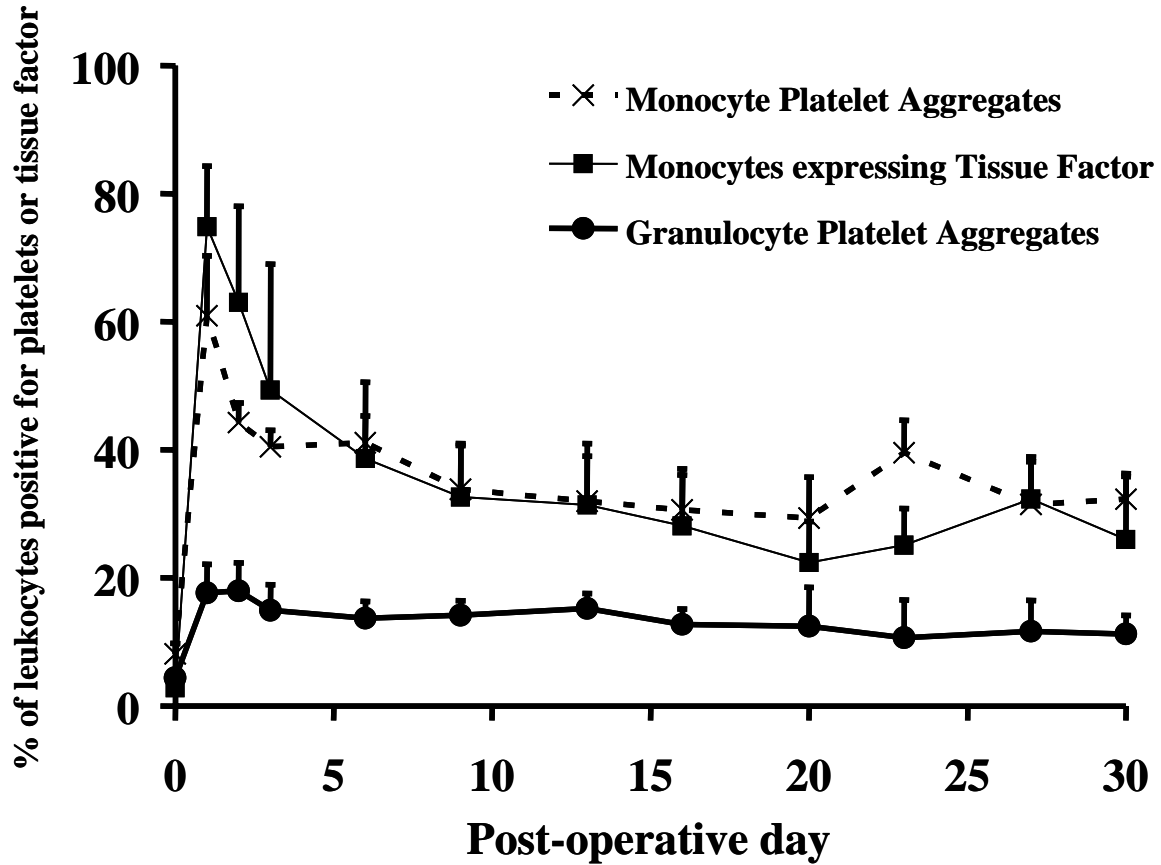


Figure 3-16. Combined temporal data from 4 Heartmate II implanted animals is shown.

3.3.3 Discussion

These three assays do provide some insight into the inflammatory process related to rotary VAD support. These assays had not been developed when the sham surgical procedures were performed. However, it is reasonable to assume that the ongoing leukocyte activation and aggregation was associated with Heartmate II VAD support, as significant elevation in all three assays persisted beyond the three week recovery period. The formation of leukocyte platelet aggregates demonstrates the interaction between the inflammatory and thrombotic process. Isolating the cause(s) of inflammation during VAD support can be at least as challenging as identifying the cause of thrombosis. In the future, identification and quantification of potential inflammatory stimuli must be clarified before methods to alleviate inflammation can be incorporated into the research and design of new cardiovascular devices.

3.4 FLOW VISUALIZATION OF THE HEARTMATE II

Wu and colleagues previously performed flow visualization on the Heartmate II [106]. They demonstrated the presence of flow vortices in the outflow stator region at nearly all flow rates and RPMs, while the development of adverse flow conditions in the inlet stator region was dependent on the flow rate and RPM. These results were first replicated, under steady flow conditions, and then the effects of pulsatile flow were considered.

3.4.1 Methods

A “smooth” Heartmate II modified with a transparent housing was placed in a mock flow loop consisting of a fluid reservoir and PVC tubing, (3/8” and 1/2” diameter) and flow restrictor valve. Pressure was measured at the inlet and outlet of the pump using clinical transducers (CR Bard, Murray Hill, NJ) and patient monitor (Servomed, Stockholm, Sweden). An ultrasonic flow meter (Transonics, Ithaca, NY) was placed on the tubing to quantify the fluid flow rate. For the non-steady portion of the study, a Thoratec pneumatic VAD was inserted into the flow loop between the fluid reservoir and the HMII. Actuation of the Thoratec was controlled via a TLC-II driver which allows operator adjustment of pulse rate and driving pressure. The test fluid was a Newtonian blood analogue consisting of 30% glycerin in water, which mimics the asymptotic viscosity of blood. Neutrally buoyant 30 μm fluorescent polystyrene beads (Duke Scientific, Palo Alto, CA) were added to the test fluid for to visualize flow patterns within the front and rear stator portions of the pump. A Nd:Yag diode continuous laser (532 nm wavelength, Millennia II, Spectra Physics Inc., Mountain View, CA, USA), illuminated the flow area of interest within the pump by splitting the laser beam into a light sheet through a cylindrical lens, exciting the illuminated fluorescent particles as the region of interest was imaged with a charge-coupled device camera (PCO SensiCamQE, PCO Image, UK). Flow patterns within the Heartmate II were imaged under steady flow conditions, covering a flow range 0-7 LPM at 8-12 kRPM and under pulsatile flow mimicking typical conditions encountered during the previous animal studies. A schematic of the flow visualization set-up is shown in Figure 3-17.

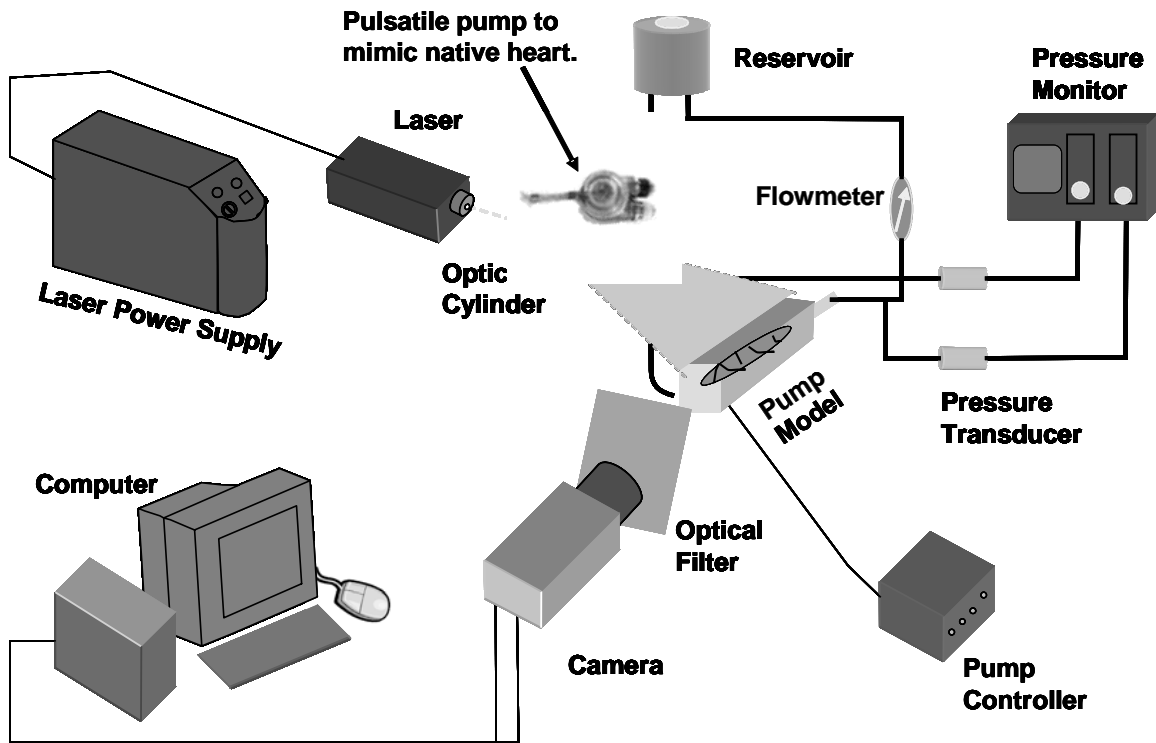


Figure 3-17. The schematic shows the set-up for flow visualization imaging of the flow through the Heartmate II.

3.4.2 Results

The flow characteristics within a rotary pump (Heartmate II) under steady and pulsatile flow conditions were studied by flow visualization method. Figure 3-18 shows the two flow patterns under steady flow conditions with a different flow rates at same rotational speed. The flow

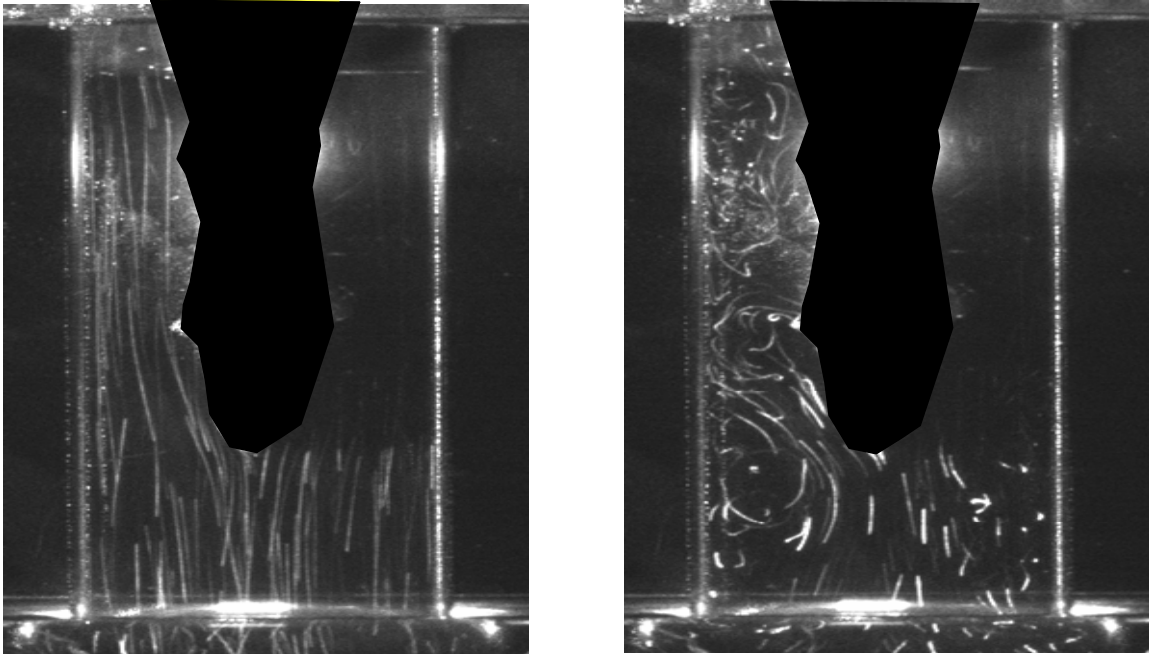


Figure 3-18. The images show particles tracks indicating the flow patterns within the pump.

The left image shows rectilinear flow at 9000 RPM with a flow rate of 4.8 LPM. The right image shows disturbed flow at 9000 RPM with a flow rate of 2 LPM. Black silhouettes were added over the stators and bearings for clarity.

features in the image clearly indicate disturbed flow conditions with several vortices in the inlet region of the pump. Under non-steady (pulsatile) flow conditions, disturbed flow temporarily became laminar during pulsatile VAD systole (fluid ejection). The initial wave of pulsatility served to displace the vortices, washing them downstream. Figure 3-19 summarizes the results of the flow visualization studies on the Heartmate II inlet. Disturbed flow occurred at the low end of the flow range, but could be produced with any RPM. Laminar flow could not be produced at very low flow rates (<2 LPM) for either flow condition. Conversely, disturbed flow was not observed at the higher flow rates. In the middle range, the presence or absence of disturbed flow is highly dependent on the flow rate, speed, and transient nature of the flow.

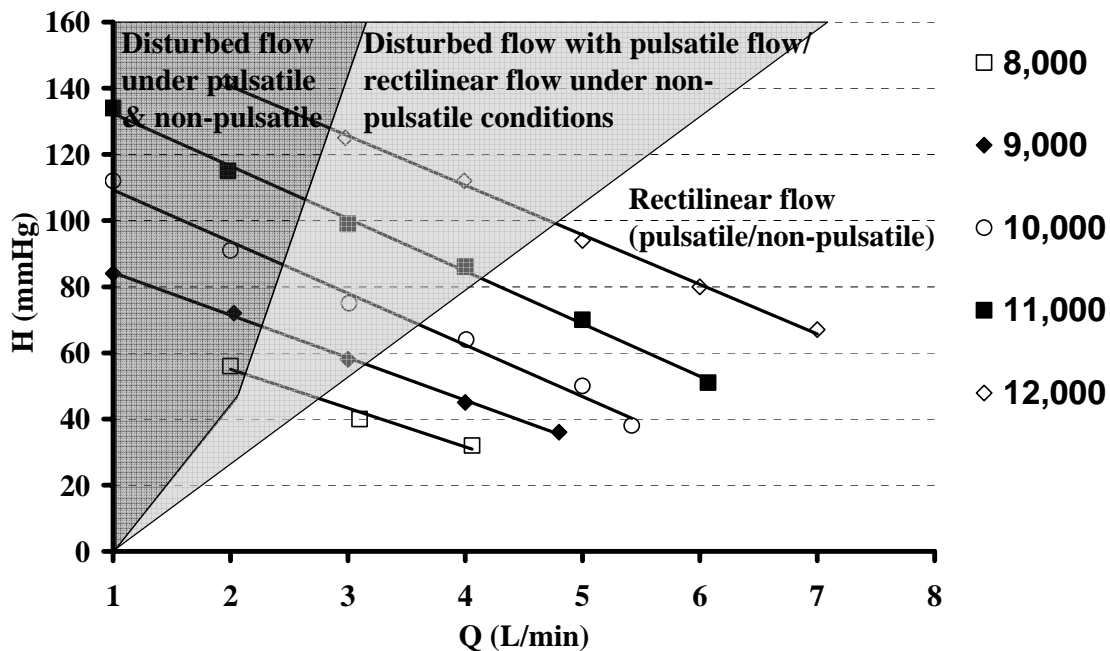


Figure 3-19. A summary H-Q curve displaying under what conditions disturbed flow occurred in the inlet of the Heartmate II.

Imaging of the outflow region of the pump was more problematic because of the three dimensional nature of the curved outflow stators. However, disturbed flow regions in the outflow stators were present at all flow rates, although the radial extent of the chaotic flow region varied with flow rate and RPM.

3.5 DISCUSSION OF THE OVERALL HEARTMATE II FINDINGS

Three lines of evidence demonstrate that Heartmate II support in bovines was associated with ongoing platelet activation and aggregation. Accounting for the effects of surgery, circulating activated platelets remain elevated throughout the implant duration. Platelet life span was substantially decreased following VAD implant after the effects of surgery have dissipated. Finally, every animal implanted with a VAD that survived for at least one week had evidence of

renal infarcts. No animal receiving a sham surgical procedure was ever found to have a renal infarct. Thus, some of the potential sources of platelet activation and aggregation were investigated.

The high shear stresses generated within the pump could contribute to platelet activation. The step increases in RPM were undertaken to begin investigating this effect. In these studies animal and pump (blood-contacting surfaces) would obviously remain the same, so that the only changes would be the RPM (and thus the shear rate at the blade tips) and the flow rate. Unfortunately, in all three cases suction occurred when the RPM was increased, and the RPM change had to be reduced or the initial step increase limited to 1,000 RPM. This difficulty in avoiding suction at higher RPMs or regurgitant flow at lower RPMs appeared to have plagued the Heartmate II throughout these studies [107].

Many animals had flow probes on the pulmonary artery (PA) as well as the pump outflow cannula. In most cases the PA flow was at least 9 LPM and was usually closer to 15 LPM. The animal's cardiac output was sufficient so that, based on the pump H-Q curves, it was thought that the pump speed could have been increased to 12,000 and possibly higher without encountering suction. However, operation of the pump at 11,000 RPM in most animals caused suction as verified by echocardiography. There was evidence of suction events at lower speeds as well. Examining the flow visualization data, a flow rate of 2 LPM generated disturbed flow for any RPM 8,000 or higher. Thus, when suction occurred, there was a combination of low flow rates with adverse flow conditions in the pump, conditions certainly likely to result in thrombus formation.

The textured surface of the inflow cannula can act as a serrated edge at the orifice, rubbing and cutting into the septum. This, of course, produces local tissue damage likely leading to exposure of tissue factor (see the Extrinsic Coagulation Cascade in Section 1.2.1.3) as well as the extracellular matrix, to which platelets may adhere. Clots were not observed on the damaged area of the septum during any necropsy, but frequently areas of red thrombus were present around the orifice of the cannula. Any thrombus that did form on the septal surface may have been pulled into the cannula and the pump. Thus, in most of these studies the following scenario developed: Blood was required to flow past injured tissue, possibly leading to some platelet activation and/or thrombus formation. Due to the partial obstruction of the orifice, the flow rate was limited, and vortices and flow separation would occur, so the "hot" (potentially activated)

blood entering the inflow cannula, then must transit through the adverse flow patterns in proximity of the inflow stators. The now “hotter” blood would then pass into the impeller region and be exposed to extreme shear rates. The blood would exit the impeller region and encounter another disturbed flow regime around the outflow stators. If the flow had a pulsatile component, the higher flow rate would then wash the vortices, and potentially, some aggregates or thrombus downstream. In retrospect, under these conditions it is not surprising the results were often poor.

The question remains as to why septal impingement occurred so frequently. There are obvious differences in the mechanical properties of a healthy bovine heart versus a failing, dilated human heart. Perhaps during systole the cannula orifice was brought into close proximity to the septum and then during diastole, with left ventricular blood volume at the lowest point, the pump could generate negative pressure and suck down onto the septum. The orientation of the cannula could also contribute to this effect. It would seem the desirable orientation would have the cannula tilting slightly away from the septum, towards the ventricular outflow tract.

The bovines in these studies also frequently lay on their sternum. In shifting back and forth while lying sternally, the animals were probably torquing the pump with respect to the position of the heart. During the implant, the pump was sewn to a rib, so it seems reasonable that as the rib cage expands and contracts during respiration and changes orientation to the heart with position changes, that the likelihood of the inflow cannula orifice interacting with the septum could be increased.

Although the precise reason for the frequency of septal impingement was not apparent, clearly it contributed to the poor outcomes in many of the studies. The situation further illustrates that investigators must attempt to consider how the animal model selected for preclinical studies differs from the intended human population and how those differences can impact the design and performance of the device undergoing evaluation.

It was not possible to image the flow the pump during the *in vivo* studies, yet through the examination of several lines of evidence, it may be demonstrated that undesirable flow conditions occurred during the bovine studies. Our colleagues demonstrated that during diastole the blood flow through a continuous flow pump could decline to zero (indicating stasis) for a portion of the cardiac cycle [108, 109]. The systolic blood flow rate through the pump was unchanged with assist rates, defined as the percent of pulmonary artery blood flow rate passing through the pump, varying from 68-100%. The diastolic pump flow rate and the native cardiac

output were inversely related, so that considering the pulmonary artery blood flow usually exceeded 9 lpm, while the pump flow was frequently less than 5 lpm, suggests very low (< 2 lpm) flow rates during diastole of most cardiac cycles. This was somewhat confirmed by the occasional observation of negative (retrograde) flow through the pump [107]. It is reasonable to conclude that adverse flow conditions were usually present during these studies. Thus, flow disturbances likely contributed to some extent to the platelet activation and thrombosis found during the Heartmate II studies.

The potential effects of the blood-contacting surface and the high shear environment remain a concern as well. While the Ti6Al4V ELI alloy used for the blood-contacting surface of the pump has been used in many cardiovascular devices with good clinical outcomes, many studies have demonstrated the application of coatings or the use of alternative titanium alloys could reduce platelet deposition or intrinsic coagulation cascade activation [110-112]. The textured surface titanium surface did not appear to produce the same response as that which occurs in the Heartmate I. The abluminal surface of the inflow cannula usually generated some areas of pseudo-neointima or coagulum. Isolated “islands” of white glossy material, assumed to be fibrous coagulum, appeared on the luminal surface of the inflow cannula and the connecting elbows. In pumps with the textured surface applied to the stators, there was never apparent deposition resembling a pseudo-neointima, although occlusive red thrombus was often present. In many of the studies, the contractor requested the pump and cannula not be disassembled so that interior surface either could not be visualized or incompletely visualized.

There was also a susceptibility to exuberant coagulum/pannus deposition at pump and cannula connections, as well as on the compressed polymer graft in the strain relief portion of the inflow cannula. This was evident in the five studies in which the luminal diameter was substantially reduced (see Figure 3-11 and accompanying description). Comparison data with Heartmate II cannula without the textured surface was not available; however, the benefit of incorporating the textured surface onto the Heartmate II cannula was not demonstrated.

The question of the effect of high shear applied micro- to millisecond time durations remains incompletely answered, but every relevant investigation of the shear environment of rotary pumps has demonstrated some level of platelet activation and platelet lysis following the exposure to the elevated shear environment. The extent of activation and the mechanism by

which the activation occurs are the issues at dispute. The attempt to investigate these issues will be described in Section 6.0 .

In weighing the influence of the various factors, the primary concerns with the Heartmate II appeared to be to avoiding inflow obstruction and low flow rates. When these conditions were averted, there was some degree of platelet activation, but this level was not incompatible with successful outcomes, as evidence by the uneventful post-operative course studies. The persistence of platelet activation suggests further efforts should be undertaken to develop an appropriate antithrombotic regimen to lessen the likelihood of thromboembolic events during clinical use of the current device implementation.

4.0 BIOCOMPABILITY ASSESSMENT OF THE SUNMEDICAL EVAHEART CENTRIFUGAL VAD

The EVAHEART centrifugal pump, shown in Figure 4-1, featured a unique purge seal [67-69, 113]. Sterile water was circulated through the pump housing to remove heat, and to the face of the pump shaft seal to remove heat as well as any blood constituents which may have penetrated the seal. This fluid then circulated out of the pump through an ultrafiltration unit and into a

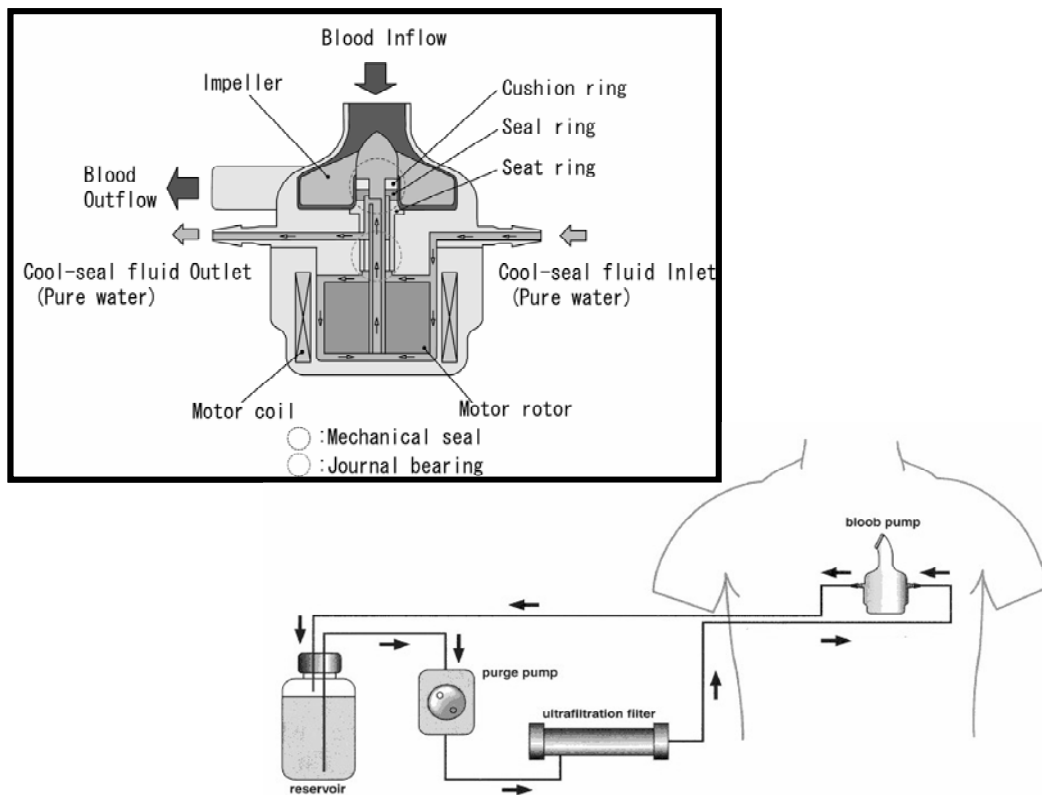


Figure 4-1. The upper image shows a view of the interior of the EVAHEART. The lower image shows the recirculating Cool-Seal purge flow system.

reservoir for collection prior to circulating back into the pump housing. The tubing for this system was incorporated with the wiring for power and control of the pump, so that only a single cable connected the pump to the extracorporeal driver unit.

The EVAHEART VAD interfaced with the circulation through an inflow cannula placed in the left ventricle and anastomosed to the aorta. The inflow cannula consisted of a beveled Ti6Al4V portion which extended from the apex of the left ventricle through the myocardial tissue to the pericardial space. The titanium section was attached to either a gelatin-sealed knitted polyester graft (GelSeal, Sulzer Vascutek Ltd., Scotland, UK), expanded polytetrafluoroethylene (ePTFE) graft (Gore-Tex, W. L. Gore & Assoc. Inc., Flagstaff, AR or Atrium, Atrium Medical Corp., Hudson, NH), or Dacron graft (Hemashield, Boston Scientific, Natick, MA). The same grafts were also used for the outflow cannulae. The blood-contacting surfaces of the pump were polished Ti6Al4V. The titanium portions of the cannula and pump were coated with either diamond-like carbon (DLC) or 2-methacryloyloxyethyl phosphorylcholine (MPC). The MPC is a biomembrane mimetic polymer applied by alcohol dehydration that has been used in several applications [73].

The EVAHEART VAD was specifically developed to be compatible with the smaller average stature of the Asian population. The pump dimensions were 55 x 64 mm, with a three bladed 40 mm diameter impeller. The VAD operates at 1,500 - 2,500 RPM, generating flows up to 9 LPM. The recirculating purge flow rate was maintained between 50-125 mL/min. Purge fluid leakage was usually < 0.5 mL/day.

4.1 SPECIFIC AIMS

- 4.1.1 Quantify Circulating Activated Platelets, Platelet Microaggregates, Platelet Life Span, Leukocyte Platelet Aggregates, and Monocytes Expressing Tissue Factor.**
- 4.1.2 Compare DLC vs. MPC Coated Pumps.**
- 4.1.3 Assess the Impact of Using No Post-Operative Anticoagulation.**

4.2 BIOCOMPATIBILITY ASSAYS

4.2.1 Methods

Blood samples were collected as described in Section 3.2.1.4. The majority of EVAHEART implanted animals did have a vascular access line throughout the study period.

4.2.2 Results

Figure 4-2 shows a plot of the temporal data from the circulating activated platelet and platelet microaggregate assays from a study with an uneventful post-operative course (See Section 3.2.2.1). BAQ125, GC5, annexin V, and platelet microaggregates display a similar pattern as

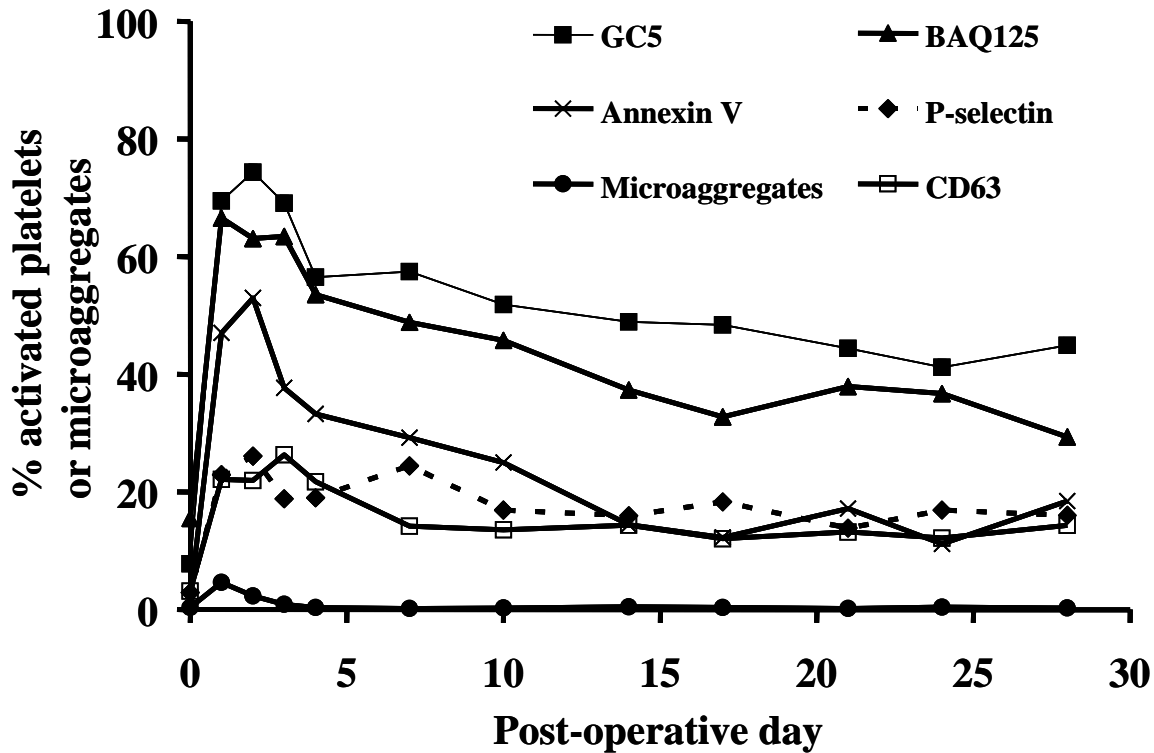


Figure 4-2. Temporal circulating activated platelet and platelet microaggragate data collected from an uneventful post-operative course animal is shown.

observed with the Heartmate II implants. That is relatively low pre-operative values followed by dramatic increases in activated platelets assay values following surgery with a decline to lower, but still elevated versus pre-operative control, levels. Microaggregates increased following surgery but returned to pre-operative values by POD7. The percent of platelets expressing p-selectin and CD63 increased following surgery but not to the same extent as the other indicators. Platelets expressing CD63 decreased to about 15% by POD7 and remained at that level throughout the study duration. Platelets expressing p-selectin increased from POD4 to POD7, but otherwise appeared to follow a similar trend to the CD63 levels. In this case the percent of platelets expressing annexin V, CD63, and p-selectin were nearly equal from POD15 onward. This was not necessarily typical, but may suggest these markers are labeling the same population of platelets, at least after the effects of the implant have diminished. The reason for the disparity between BAQ125 and GC5 and the annexin V, p-selectin, and CD63 levels is not apparent. It

has been shown that circulating activated platelets lose surface expressed p-selectin but may continue to circulate [114]. Thus, it is possible that the p-selectin and CD63 were binding to recently activated platelets, whereas other activated platelets had shed these markers and continued to circulate. It may be speculated that the epitope to which BAQ125 and GC5 bind remained on the platelet surface and was not shed.

Leukocyte platelet aggregates and monocytes expressing tissue factor were increased throughout the post-operative period as shown in Figure 4-3. In this case, nearly all monocytes

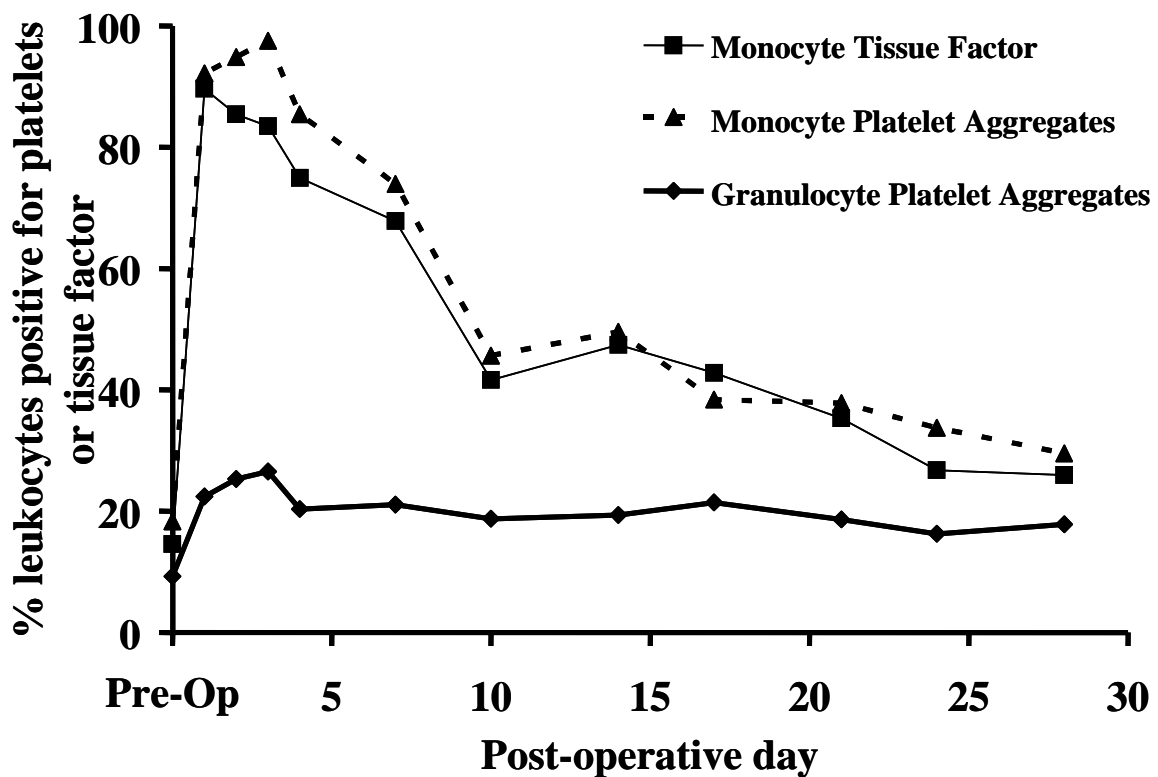


Figure 4-3. Temporal graph of leukocyte platelet aggregates or monocyte tissue factor is shown for study D054.

were positive for platelets or tissue factor indicative of a substantial inflammatory response. The percent of granulocytes positive for platelets peaked around 25%, and never increased to the extent the monocyte activation indicators did.

Ex vivo blood biotinylations were performed in three animals. The average pre-operative life span was 5.8 days, while the average post-operative life span was 4.7 days, which corresponded to a 7% increase in platelet consumption. The post-operative biotinylations were carried out on days 31, 48, and 128, so the effects of surgery had dissipated [84].

4.3 SURFACE COMPARISON OF DLC VS. MPC

Following the decision to switch from a DLC coating to the MPC coating, a manuscript was published which claimed to provide supporting data for the change [73]. The paper distinguished between the two surface treatments primarily through the presence or absence of thrombus on the ring seal around the impeller shaft and anecdotal reports regarding the number and size of infarcts in the kidneys. A statistical comparison of a grading of the amount of infarcted area in the kidneys revealed no significant difference between the two coatings. Other measures including plasma free hemoglobin, hematocrit, hemoglobin, plasma fibrinogen, osmolality, blood and plasma viscosity, deformability index, and oxygen delivery index demonstrated no significant differences between the two coatings. Only plasma total protein was significantly different between the coatings; however, the values for each group were within normal limits (5.7 ± 0.7 g/dL for MPC and 6.4 ± 0.6 g/dL for DLC, with the normal value being 6.0 g/dL). The meaning of the difference in plasma total protein is also not apparent as other measures of liver function (not reported in manuscript, but available in individual animal reports) were within normal limits. Unfortunately, the paper accurately reflects the currently accepted evaluation techniques for VADs, demonstrating the inadequacy of these measures to assess more subtle differences in device compatibility.

DLC and MPC are considered relatively biocompatible materials. DLC has been most frequently used because of its relatively high wear resistance, although it has been reported to reduce cellular deposition on biomaterials [115]. MPC attempts to incorporate the phosphoryl choline portion of the cell membrane as a coating to present a surface encountered by blood components in normal physiologic states [116]. Thus, attempting to distinguish between two relatively biocompatible materials posed a substantial challenge.

4.3.1 Methods

Blood samples were collected as described in Section 3.2.1.4. Four animals receiving DLC-coated components and 16 animals receiving MPC-coated components were compared as described in Section 3.2.1.5. The following assays were applied in the DLC-coated studies; thus, limiting the statistical comparison to these assays: BAQ125, GC5, Annexin V, anti-CD62P, and platelet microaggregates. The study durations were 30 to 196 days. Several studies which did not reach 30 days were excluded.

4.3.2 Results

Annexin V and anti-CD62P antibody binding to circulating platelets was significantly lower in animals receiving MPC-coated components beginning on POD24 and POD21, respectively, shown in Figure 4-4. The assays remained significantly different through POD49. The shortest duration DLC-coated study was 50 days, and after this time point there were three DLC-coated studies versus eight MPC-studies. An additional MPC study was electively terminated on POD59, leaving three DLC studies versus seven MPC studies. Platelet microaggregates were not significantly different and followed the previous trend of increases following implantation, then a return to pre-operative levels in 7 to 10 days. The other two antibodies, BAQ125 and GC5, were not significantly different for any time point.

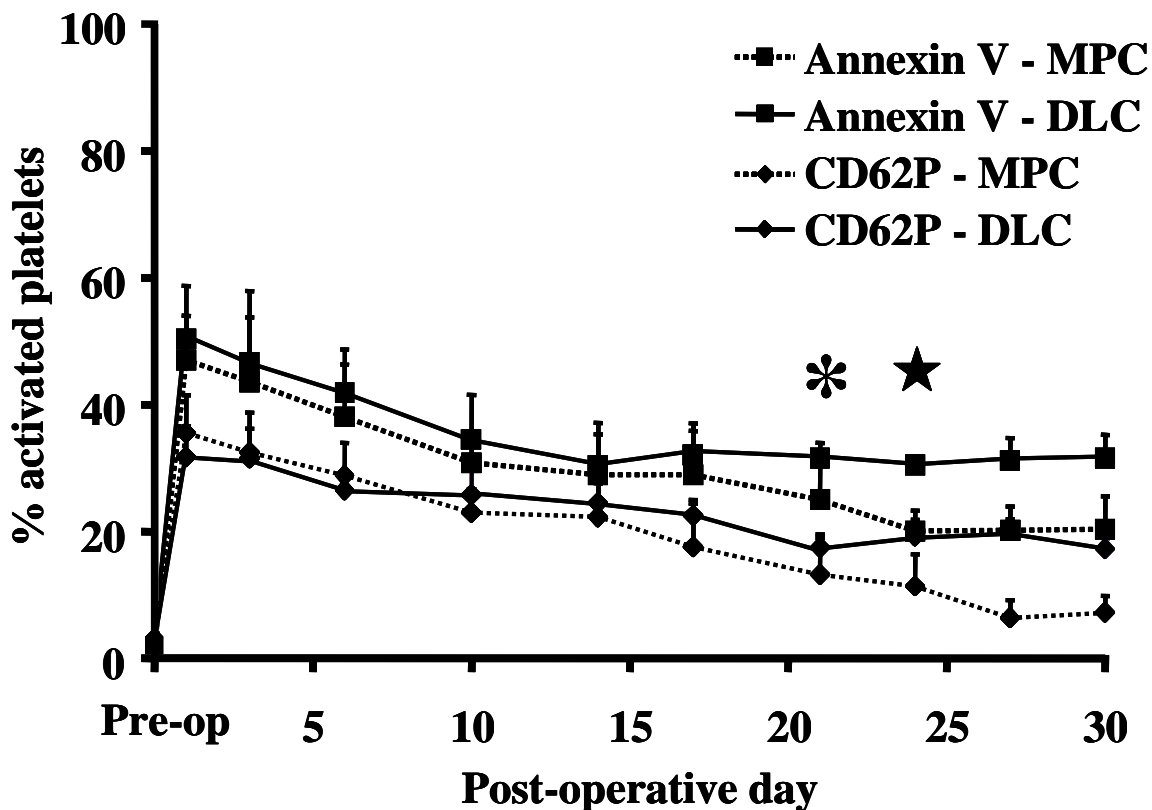


Figure 4-4. Temporal plots of annexin V and anti-p-selectin binding to platelets from studies using DLC- (solid lines) or MPC- (dashed lines) coated components.

* indicates $p < 0.05$ for anti-p-selectin. ★ indicates $p < 0.05$ for annexin V.

4.4 NO POST-OPERATIVE ANTICOAGULATION

Appropriate antithrombotic regimens for patients receiving VADs remain open to debate. Nevertheless, there are a variety of conditions that do arise during VAD support which require withholding antithrombotic agents. Thus, demonstration that a VAD may be operated safely without platelet or coagulation inhibitors would be a desirable attribute.

4.4.1 Methods

Three animals implanted with MPC-coated EVAHEART components received a bolus of 1.5 mg/kg heparin initially, and then sufficient heparin to maintain an ACT greater than 400 seconds during the VAD implant procedure, then no further anticoagulation with one exception noted below. The study durations were 30 to 36 days. Blood collection and antibody labeling was performed as described in Section 3.2.1.4.

4.4.2 Results

The three studies all reached the desired duration and were electively terminated. Kidney infarcts were rated moderate, which was typical for the EVAHEART experience. One pump was completely free of thrombus, while the two others had a small ring thrombus on the shaft seal. There were ring thrombi present on the cannula connections. The results from one of the studies are shown in Figure 4-5. In the D033 study, the pump stopped on POD30. 30,000 units of

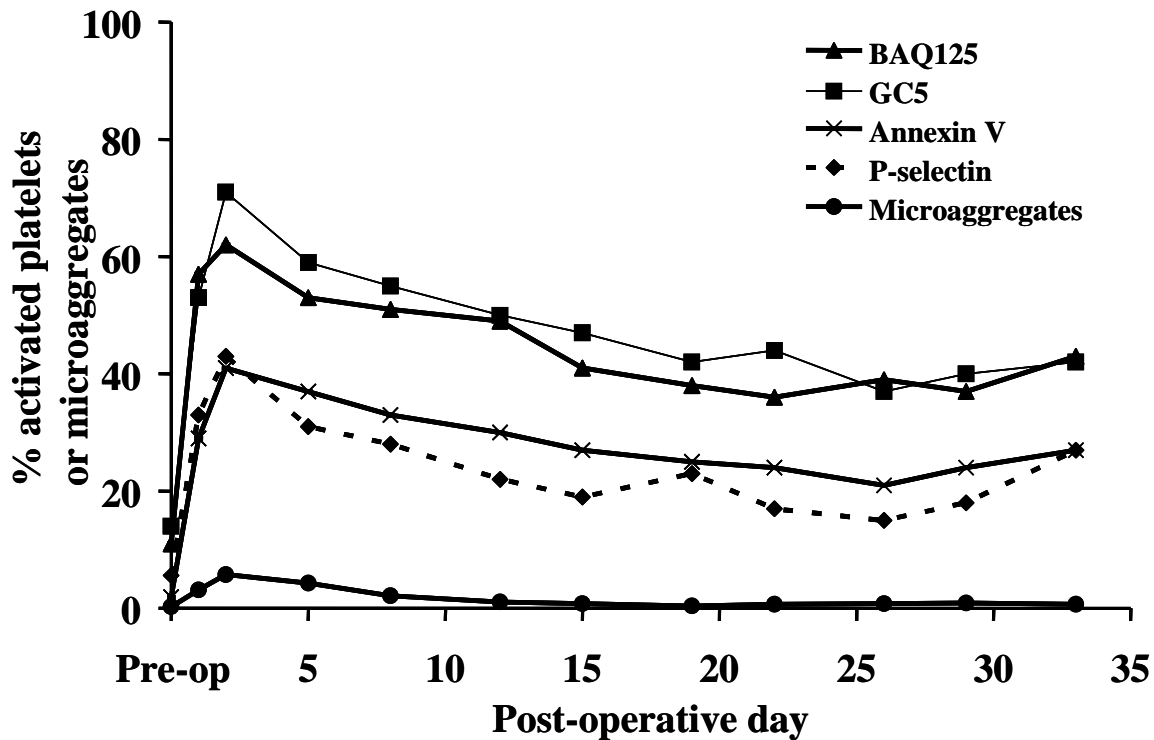


Figure 4-5. Temporal antibody and annexin V binding data for study D033.

heparin were administered and the pump was restarted 20 mins later. There was a qualitative increase in several of the assays at the next data point.

4.5 DISCUSSION OF OVERALL EVAHEART FINDINGS

As with the Heartmate II studies, there were three lines of evidence of ongoing thrombosis – flow cytometric quantification of circulating activated platelets, diminished platelet lifespan, and renal infarcts identified during the necropsies. Although suction events did occur occasionally in the EVAHEART studies, the investigators identified the importance of maintaining positive pump flow during diastole [108, 109] and frequently used echocardiography to verify the inflow orifice was free of septal occlusion during the entire cardiac cycle. Many of the studies focused

on assessing variations on cannula and cannula connections. The connections were nearly always the site of a ring thrombus. Emboli shedding from these sites could have contributed to the renal infarcts observed during necropsies.

The ability of two of the platelet flow cytometric assays employed in these studies, annexin V and anti-CD62P, to differentiate between two relatively biocompatible coatings demonstrated a unique capability. Conventional measures of biocompatibility, including those required by regulatory agencies, were not able to differentiate between these coatings. An interesting finding of the comparison between DLC and MPC was that the MPC polymer was shed from the pump surface over 30 to 90 days [73]. This probably may have resulted in gradual passivation of the titanium surface over several weeks. The ability to discriminate between the coatings was partially attributable to the relatively consistent results obtained with the juvenile bovine model, rather than the highly variable conditions under which humans receive VADs. It must be acknowledged, however, that the differences in the cannula employed with the different coatings may have contributed to some of the observed difference. There are no references in the literature comparing the long-term *in vivo* effect on the generation of activated platelets of the two different cannula materials.

The applied flow cytometric assays demonstrated that operating the EVAHEART without antithrombotic treatments did not produce significantly different results from operation with coumadin anticoagulation. Although the relative numbers were low, the ability of the assays, particularly annexin V and anti-CD62P, to be able to detect more subtle effects, contributes to the belief that the EVAHEART could be safely operated in bovines without post-operative anticoagulation.

5.0 BIOCOMPATIBILITY ASSESSMENT OF THE STREAMLINER VAD

The Streamliner VAD was a mixed-flow turbodynamic third-generation VAD utilizing a magnetically-levitated impeller [117]. The particular prototypes tested *in vivo* were the HG3C generation. The devices possessed a stationary axial spindle onto the front of which were mounted four inflow stators similar to those of the Heartmate II. The rear of the spindle attached to a hub containing an axial position sensor. Between the exterior of the hub and the housing were five outflow stators. The impeller had a hollow cylinder running through its axial length through which it was placed around the stationary spindle. The impeller was physically constrained between the front inflow stators and the rear hub. This configuration resulted in a by-pass flow path where a portion of the blood exiting from the impeller region could pass between the impeller and the rear hub, then in a retrograde direction axially between the impeller

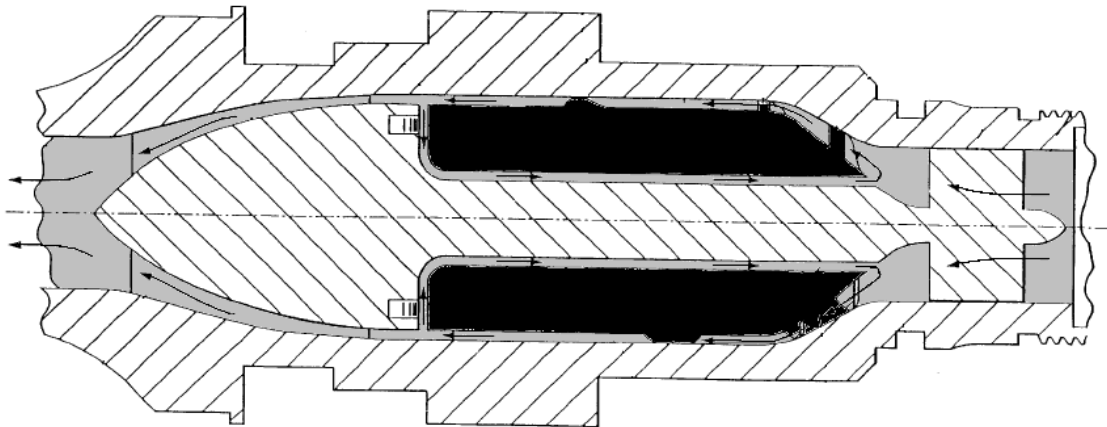


Figure 5-1. A cross-section of the Streamliner is shown.

The blood fluid path appears gray, while the impeller is shaded black, while the hatched areas are stationary. The arrows indicate the direction of blood flow in local regions.

and the spindle exiting at the rear of the inflow stators and front of the impeller, as shown in Figure 5-1. This alternate flow path was due to the higher pressure at the rear of the impeller versus the inlet. The flow rate through the bypass could be up to 20% of the total flow rate through the pump.

The Streamliner was implanted in five calves. The first implant was an acute study lasting only four hours. The second study was terminated four hours post-operatively due to excessive bleeding from incomplete suturing of the aortic anastomic site. Another study was stopped on POD2 due to problems with repeated pump stoppage. The remaining two study durations were 30 and 34 days. Data from the two chronic 30+ day studies is presented below. The implants all used a Thoratec animal inflow cannula (Thoratec, Pleasanton, CA) and 14 mm diameter woven Dacron outflow graft (Impra – CR Bard, Murray Hill, NJ). The pump speed was adjusted from 5,000 – 8,000 to maintain flow rates of five to seven lpm.

5.1 SPECIFIC AIMS

5.1.1 Quantify Circulating Activated Platelets, Platelet Microaggregates, and Platelet Life Span in Bovines Implanted with the Streamliner VAD.

5.1.2 Investigate the Effect of the Impeller Blade Tip Gap Width on Blood Damage and Platelet Activation.

5.2 BIOCOMPATIBILITY ASSAYS

5.2.1 Methods

Blood samples were collected as described in Section 3.2.1.4. BAQ125, GC5, annexin V, and platelet microaggregate assays developed in Chapter 2.0 were applied to the blood samples. Platelet life span determinations were performed pre-operatively and post-operatively on POD22 of the 30 day study and POD26 of the 34 day study.

5.2.2 Results

In both studies the pattern of circulating activated platelets and platelet microaggregates appeared similar to that observed with other VADs. There was a substantial increase in activated platelets following the implant procedure, followed by a decline with recovery from the surgery to a lower, but still elevated level, after about two weeks. Data from the 34 day study is shown in Figure 5-2. Platelet microaggregates were elevated versus pre-operative control until POD6.

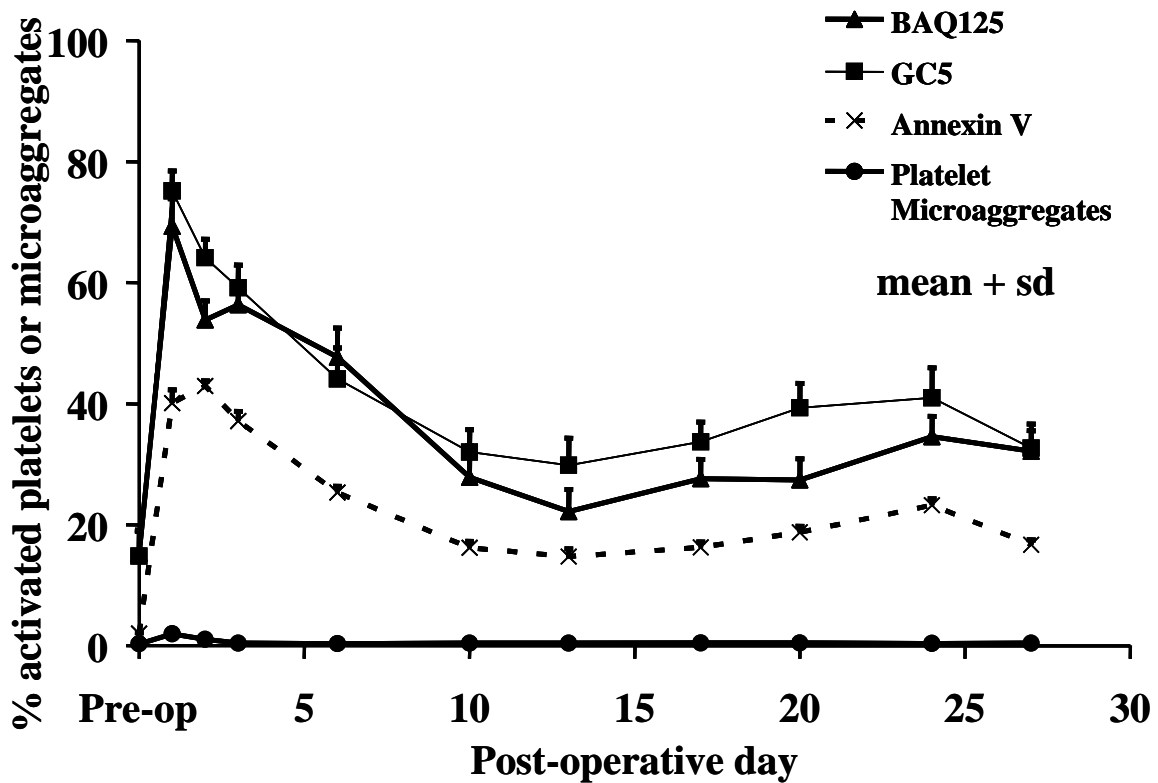


Figure 5-2. Three indicators of circulating activated platelets and platelet microaggregates for Streamliner study T004 are shown.

Data displayed indicate the percent of platelets binding the activated platelet indicators (BAQ125, GC5, or Annexin V) or the percent of platelet positive events occurring in the microaggregate size range.

The 30 day study results were similar. Pre-operative platelet life spans were 6.6 and 6.9 days, respectively for the 34 and 30 day studies. The POD26 life span was 3.6 days and the POD22 life span was 3.8 days.

During the necropsies ring thrombi were found at the cannula-pump junctions. There were also small thrombi at the junction of some of the stators with the pump housing. Renal infarcts covered 10% of the renal surface in the 34 day study, with slightly fewer renal infarcts and about 5% of the renal surface covered with infarcts in the 30 day study. During the 34 day study the pump stopped repeatedly, usually for less than five mins. There were also several periods of low flow during the final week of the study, lasting from two to ten mins. In both studies there was evidence of the inflow cannula rubbing against the ventricular septum suggesting either suboptimal positioning of the inlet of the cannula, which can be related to the animal lying sternally rather than improper surgical placement or orientation, or occasional suction events.

5.2.3 Discussion

Examination of the pump revealed that the press fit of the stators onto the pump housing left small crevices in which thrombi formed. It was very likely that thrombi formed in the defects at the stator-housing and cannula-pump junctions, then embolized, and subsequently reformed in a cyclic process. Low flows and retrograde flow (during pump stoppage) would likely enhance this process. Repeated emboli generation was evidenced by the large number of renal infarcts observed during the necropsies. The level of circulating activated platelets in the later half of the study qualitatively compares favorably with the results from other VADs, in spite of the large number of renal infarcts.

The inflow cannula had a caged inlet with a polyurethane blood contacting surface. The combination of the shape of the cannula with a softer surface composition made septal scarring much less likely to occur compared to the sintered titanium inflow of the Heartmate II. Evidence of the cannula rubbing against the septum in conjunction with periods of low flow also suggests occasional suction events.

Extensive oil dot and particle-based flow visualization of the Streamliner indicated desirable flow characteristics at the best efficiency point (6 lpm against 100 mm Hg at 6,000

RPM) [118]. At lower flow rates, recirculation zones and chaotic flow patterns become more pronounced. Thus, the observed platelet activation, decreased platelet life span, and thromboembolism revealed by renal infarcts were likely attributable to a combination of flow effects, contact with a foreign surface, and particularly with the Streamliner prototypes, stagnation zones caused by known defects in the pump construction.

5.3 INVESTIGATION OF THE EFFECTS OF IMPELLER BLADE TIP GAP ON PLATELET ACTIVATION AND BLOOD DAMAGE

5.3.1 Introduction

Every study of VADs encountered in the literature which has applied measures of platelet cellular activation, coagulation, or thrombosis, be it in humans or animals, has found some degree of activation. To attempt to improve VAD technology to decrease the associated level of thromboembolism, the underlying causes of the observed hemostatic derangements require identification and elucidation. The previous studies described in this dissertation suggest that the presence of a foreign surface, adverse flow characteristics, and potentially supraphysiologic shear rates all contributed to the observed platelet activation. The step increase in RPMs with the Heartmate II presented in Section 3.2.2.6 was intended to investigate the effects of increased shear rate on platelet activation; however, this could not be accomplished due to the confounding effects of septal impingement, ventricular suction, and low flow rates.

The Streamliner offered a method to begin investigating the effects of increasing shear rates while avoiding the confounding factors encountered in the Heartmate II studies. As a third generation VAD, the Streamliner's impeller was levitated within the pump. The position of the impeller is maintained radially by passive magnets. The axial position of the impeller was controlled by an active voice coil. There was 0.010" of available axial translation of the impeller between abutting the front stator spindle and contacting the face of the outlet stator mount. During normal operation, the impeller position was actively maintained near the center of this available travel (the virtual zero point), leaving about 0.005" of axial motion in the fore or aft direction before touchdown (impeller contact with the adjacent housing) would occur. Through

a minor adjustment to the pump, the impeller could be displaced from the center alignment. As the impeller was driven forward, the gap between the impeller blade tips and the pump housing is reduced. The position of the impeller could be determined from the voltage output of the axial position sensor located in the outlet stator hub.

The shear rate in the blade tip gap can be approximated as the circumferential velocity of the blade tip divided by the gap width. Thus, by maintaining a constant impeller RPM, and decreasing the impeller tip gap, the shear rate can be changed substantially while maintaining a relatively constant exposure time within the tip gap by maintaining a consistent pump flow rate. The time exposure could be manipulated through changing the flow rate through the pump (by manipulating the pressure differential across the pump or altering the impeller RPM), but as described previously deviations from the best efficiency point result in degradation of the flow characteristics [118]. An acute *in vivo* study was carried out to begin to examine the effects increases in the shear rate on platelet activation and blood damage.

5.3.2 Methods

5.3.2.1 Streamliner Implant, Operation, and Blood Sample Collection

An 80 kg sheep was anesthetized as in Snyder et al [84]. The heart was accessed through a left thoracotomy. There was a layer a subcutaneous fat two to three inches thick, which increased the anticipated time to prepare the animal for implant. The 5th rib was removed to provide easier access to the heart. Heparin was administered to produce an ACT exceeding 900 seconds. The aorta was partially clamped and a 12 mm Hemashield collagen impregnated graft was attached by end to side anastomosis. During this time levitation of the impeller could not be achieved. The sheep was maintained under sedation while the pump was repaired. Approximately two hours later, the pump was functioning properly and the implant procedure continued. The outflow graft was primed with saline and attached to the pump. The pump was connected to the 12 mm inflow cannula as used in the previous Streamliner studies (provided by Dr. Antaki). The apex was incised, then cored with a 14 mm coring tool (a 12 mm tool was not available). The inflow cannula was inserted into the left ventricle and the pump conduit was de-aired through an 18 gauge, 1 ½” needle placed in the proximal section of the outflow graft. The pump impeller was levitated and the impeller started at 4000 revolutions per min (RPM). A transonic flow

probe (Transonic, Ithaca, NY) was attached around the outflow cannula, but no flow measurement could be obtained. The heart fibrillated and several shocks were administered. Manual massage was begun, and then additional shocks applied. 13 mins after pump operation began, the animal was stable. It was decided to allow 20 more mins to insure the animal remained stable. Ten mins later, the surgeon noted that the lung upon which the pump was resting was burned. It was determined that this was due to a short in the pump, and an insulator was placed between the pump and the animal's tissue. The animal fibrillated following the lung burn and could not be restored to a sinus rhythm, even with multiple shocks. The arterial pressure trace indicated a flat waveform with no pulse pressure or sign of aortic valve closing. After repeated attempts, it was decided to allow the animal to remain in fibrillation with no further efforts to obtain a sinus rhythm. The pump speed was increased to 5,000 RPM. While it was not intended to disrupt the native cardiac function, this condition did present a few advantages for the study. The pump generated all of the cardiac output, thus all of the sampled arterial blood had passed through the device. The absence of ventricular contraction and the constant arterial blood pressure resulted in a constant pressure difference across the pump, so that the impeller position was relatively stable and the flow rate was nearly constant. A heparin infusion was used to maintain an ACT exceeding 400 seconds.

The initial blade tip gap was 125 μm . Forty mins after pump operation was begun, the impeller axial position was adjusted to produce a 100 μm blade tip gap. Then after one hour, the impeller position was altered to generate a 50 μm blade tip gap. After 40 mins operating with this setting, the impeller crashed and the pump had to be restarted. After pump operation was re-initiated, touchdown (by auscultation) occurred when attempting to maintain the 50 μm gap. The pump was operated to deliberately produce touchdown for about five mins while blood samples were collected from the central venous pressure line and the arterial line were collected. Potassium chloride overdose was then administered and pump operation was halted.

During the study, blood was periodically collected from an arterial line placed a carotid artery. Ten mL of blood was drawn through the line, and then a sample was drawn into a new syringe. The blood was then transferred to a monovette for the platelet studies. Three mL was placed into silicon-coated vacutainers containing no additive (Fisher) for plasma free hemoglobin measurements. The 10 mL of blood previously obtained was re-infused and the line was flushed with saline containing 10 U/mL heparin. One sample was collected through the

central venous pressure (CVP) line of a Swan-Ganz catheter which was placed before the thoracic cavity was accessed. Blood samples were collected with the conditions indicated in Table 5-1.

Table 5-1. Blood samples collected during acute Streamliner study.

Sample No.	Description
1	Post-aortic clamp
2	Pump ON, RPM 4,000, Gap 125 μ M
3	30 min later RPM increased to 5,000
4	30 min later sample collected, then gap decreased to 100 μ m
5	30 min later sample collected, gap remained 100 μ m
6	30 min later sample collected, then gap decreased to 50 μ m
7	30 min later sample collected, gap remained 50 μ m
8 CVP	10 min later, Touchdown occurring
9 Arterial	Collected immediately following sample 8, Touchdown occurring

5.3.2.2 Blood Biocompatibility Assays

Ovine platelets expressing CD62P were determined using methods developed by Carl Johnson in our laboratory. Five μ L of blood was added to 35 μ L tyrode's buffer containing 1% bovine serum albumin, 5 μ L GB20A (7.5 μ g/mL VMRD) and 5 μ L polyclonal rabbit anti-human CD62P (30 μ g/mL Becton-Dickinson (BD), LaJolla, CA) or 5 μ L polyclonal rabbit IgG (BD) to serve as a labeling control. The samples were incubated for 20 mins and washed with 1000 μ L of the above tyrode's buffer. Five μ L goat anti-mouse PE (30 μ g/mL, Molecular Probes-Invitrogen, Carlsbad, CA) and 5 mL goat anti-rabbit alexa 488 (30 μ g/mL, Molecular Probes-Invitrogen) were added and the samples were incubated for 20 min. The samples were washed again and fixed with 500 μ L 1% filtered paraformaldehyde.

Platelet counts were determined by centrifuging ovine blood to produce platelet-rich plasma (PRP). 10.0 μ L of PRP was added to a diluent cup containing 20.0 mL isoton II buffer

(Coulter). Cell counts were collected on a Multisizer II (Coulter) using a 50 μm diameter aperture tube and a 100 μL sample volume. All counts were performed in triplicate. Particles falling between 1.5 and 3.0 μm in diameter were assumed to be single platelets.

Plasma free hemoglobin quantification was performed by Dr. Marina Kameneva's laboratory. Because the hematocrit varied from 17.5 to 32.5, all samples were adjusted to a standard hematocrit of 36. Plasma free hemoglobin measurements were carried out as previously described [27].

5.3.3 Results

5.3.3.1 Changes in Circulating Activated Platelets and Platelet Count with Decreases in Impeller Gap

The percent of activated platelets indicated by CD62P expression is shown in Figure 5-3. CD62P appeared on over 60% of platelets following aortic cross-clamping in spite of the prolonged ACT value during this part of the procedure. Circulating activated platelets did not

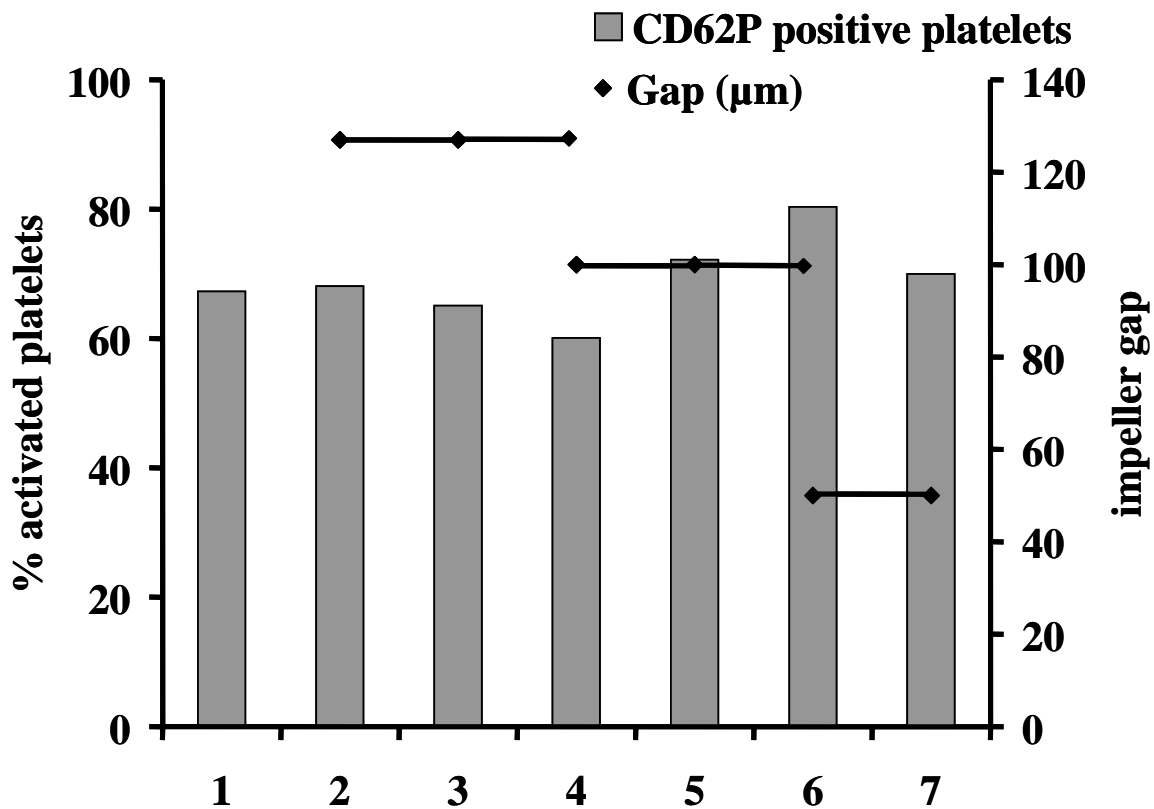


Figure 5-3. Change in circulating activated platelets as indicated by CD62P expression with variation in the impeller blade tip gap.

The numbers on the x-axis correspond to the sample descriptions given in Table 5-1.

increase after pump insertion and initiation of pumping. During pump operation with a 125 μm gap, the percent of activated platelets remained fairly constant, or perhaps declining slightly. After decreasing the gap to 100 μm , circulating activated platelets increased from 60 to 80%, a one third increase in only one hour. During operation of the pump with a 50 μm gap, the percent of activated platelets decreased to 70%.

Platelet counts for each time point are shown in Figure 5-4. The platelet count increased following the pump insertion. However, the normal range for an ovine platelet count is 200,000 to 800,000/ μL , so all of the platelet count values remained within normal. Sheep also sequester

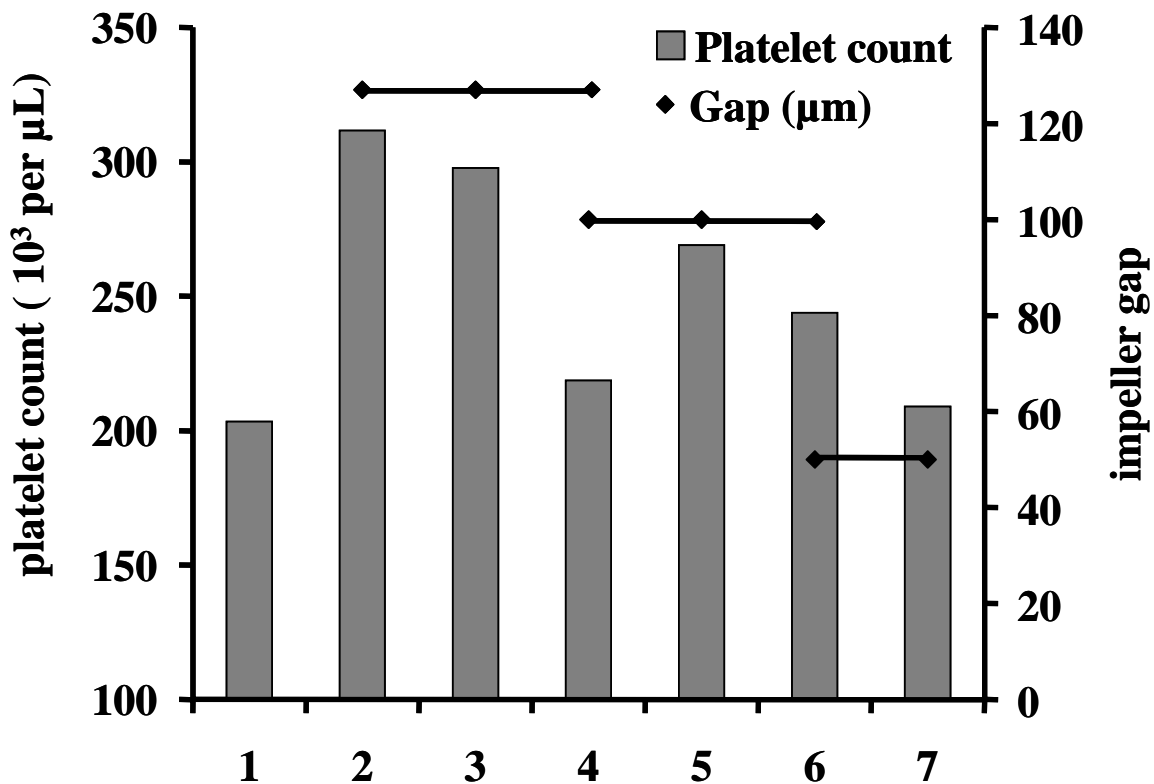


Figure 5-4. Platelet counts for the time points described in Table 5-1 are shown.

blood cells, presumably including platelets, in response to stress or anesthesia. There was likely some degree of deposition on the outflow graft. During any open heart procedure bleeding will

occur. The animal also received continuous infusion of fluids during the procedure which produces hemodilution. Thus, a decrease in the platelet count after initiating pump support was not unexpected. While the cell counting technique employed in this study yields results with high accuracy, the daily variation in platelet counts in healthy human individuals can exceed 50,000/ μ L [119]. Overall the results indicate a downward trend in the platelet count, which can be attributed to several factors associated with the surgical procedure so that effects of the operation of the pump on platelet counts could not be determined.

5.3.3.2 Effect of Decreases in the Impeller Blade Tip Gap on Plasma Free Hemoglobin

Figure 5-5 shows the change in plasma free hemoglobin over the course of the study. The results show low levels of hemolysis (indicated by plasma free hemoglobin release) during operation of

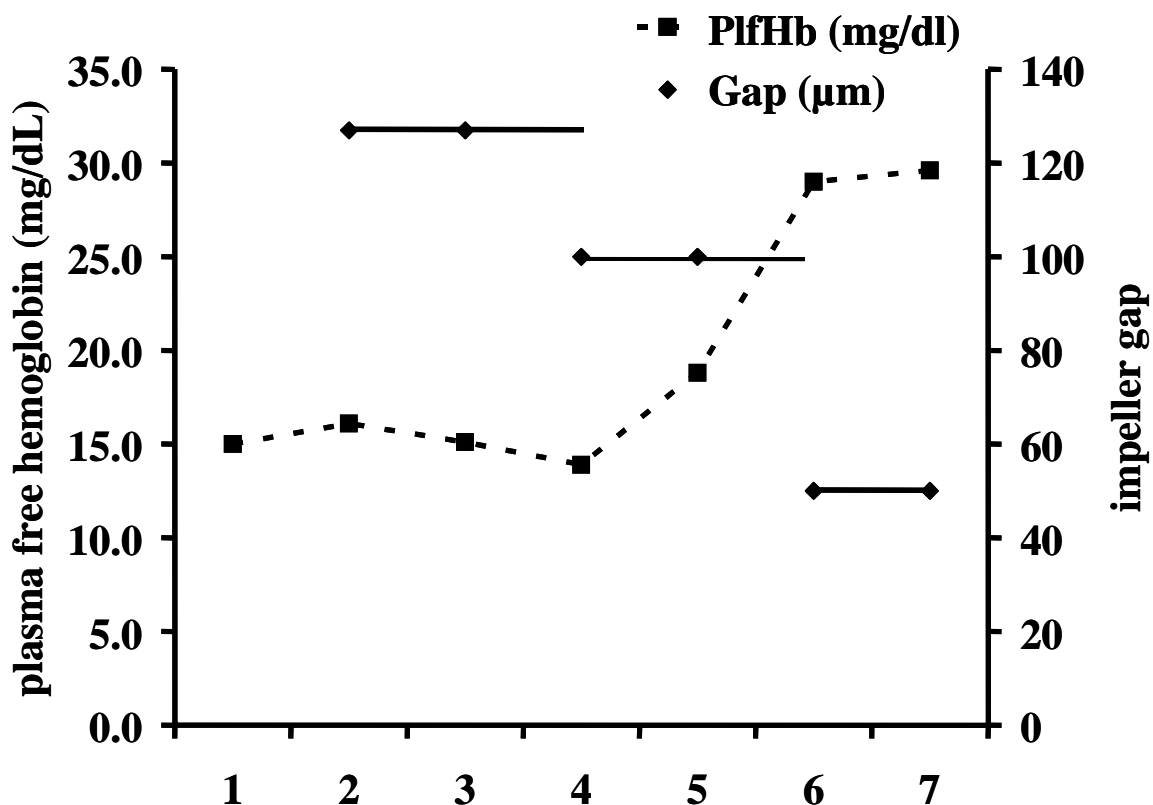


Figure 5-5. Plasma free hemoglobin (PlfHb), standardized to a hematocrit of 36%, the time points are described in Table 5-1.

the Streamliner with the impeller located in the middle of its potential axial travel path. This finding is supported by the results from the previous *in vivo* studies in bovines in which plasma free hemoglobin liberation always remained low. When the gap was decreased to 100 μm , there was a 100% increase in plasma free hemoglobin in only one hour. A further decrease in the impeller blade tip gap resulted in only a slight (2%) increase in plasma free hemoglobin in 30 mins. Plasma free hemoglobin release associated with blood pumps is normally reported as the normalized index of hemolysis, which is the amount of hemoglobin released per unit of volume of blood pumped normalized by the hematocrit. Unfortunately, the blood flow rate could not be determined in this study.

5.3.3.3 Effect of Impeller Touchdown on Circulating Platelet Activated and Platelet Count

After 40 min of operation with a 50 μm gap, the pump stopped. Upon restarting the pump, and while maintaining touchdown of the impeller, samples were collected from venous (CVP) and arterial lines, attempting to capture the effect of a single pass through a VAD incurring severe touchdown. The increase in circulating activated platelets from the CVP to arterial samples is shown in Figure 5-6. Platelets expressing CD62P nearly doubled following passage through the

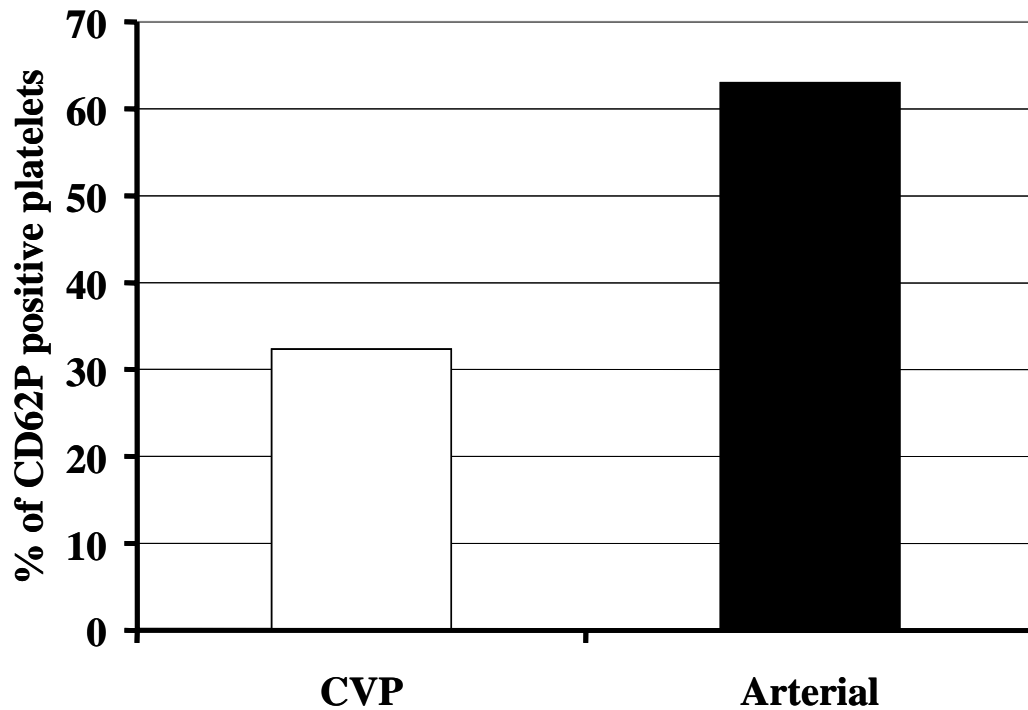


Figure 5-6. The percent of platelets expressing CD62P from venous and arterial samples during continuous touchdown of the Streamliner impeller is shown.

pump during continuous touchdown. The platelet count obtained from these samples is shown in Figure 5-7. The platelet count was about 10% lower in the arterial sample after passage through the pump, although the samples were collected nearly simultaneously.

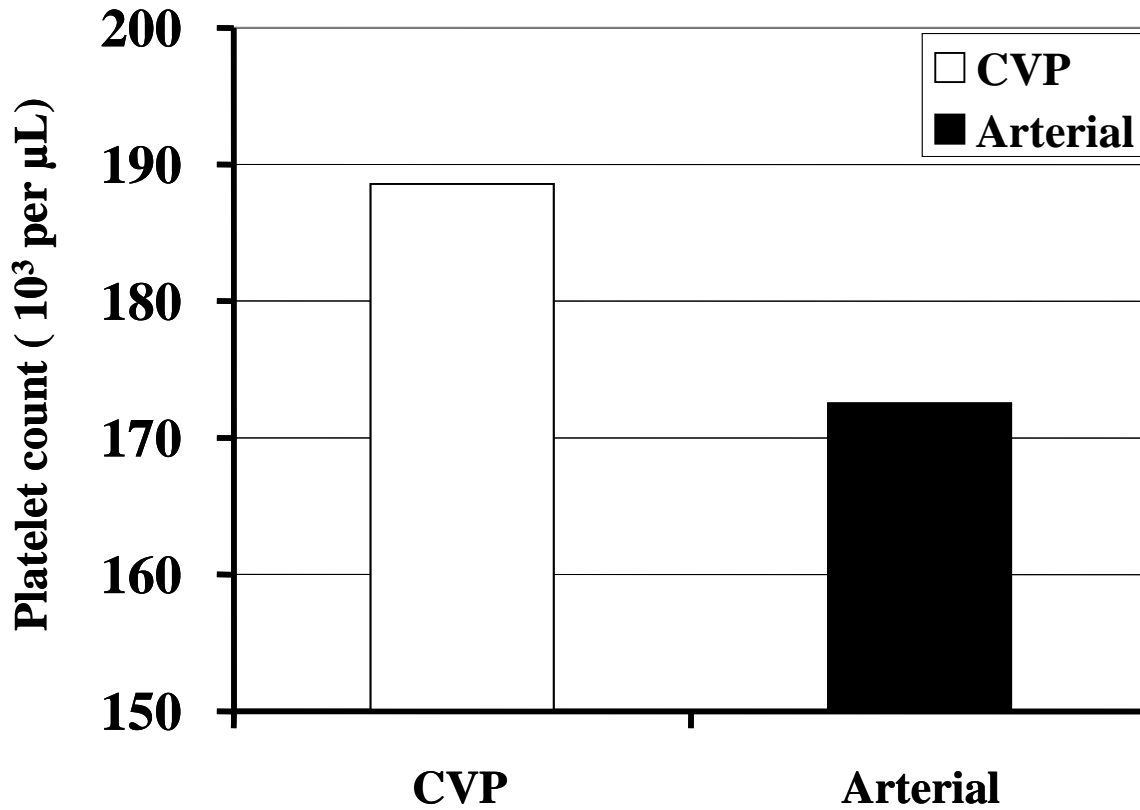


Figure 5-7. Platelet counts from venous (CVP) and arterial blood samples collected during continuous touchdown of the Streamliner impeller.

The change in plasma free hemoglobin values from the CVP and arterial sample are shown in Figure 5-8. The plasma free hemoglobin increased from 24.0 to 28.1 g/dL following passage through the pump during touchdown.

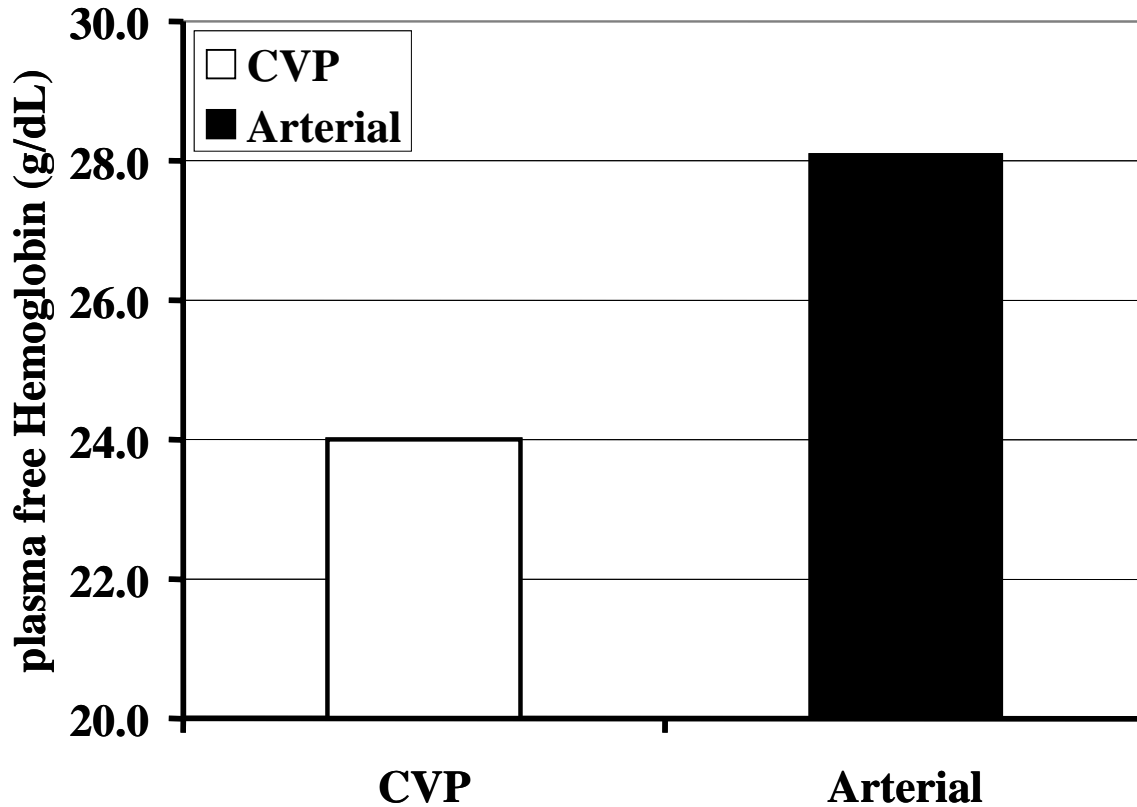


Figure 5-8. The plasma free hemoglobin, standardized to a 36% hematocrit, for venous (CVP) and arterial samples during continuous touchdown of the Streamliner impeller is shown.

5.3.4 Discussion

When operated with a 127 μm gap, the Streamliner did not produce an increase in plasma free hemoglobin or platelet activation. It is possible that haptoglobin could have masked an increase in the plasma free hemoglobin. However, the relatively high baseline level of 15 mg/dL, compared to a normal level in a healthy animal (< 10 mg/dL), suggests that the haptoglobin would have already bound as much hemoglobin as feasible. When the gap was reduced to 100 μm , plasma free hemoglobin increased 15 mg/dL in one hour, actually doubling. After decreasing the gap to about 50 μm , the plasma free hemoglobin remained nearly unchanged.

The hematocrit varied from 17.5 to 32.5 during the experiment, so the plasma free hemoglobin was standardized to a hematocrit of 36%. This also confirms an observation that Dr. Kameneva passed along previously that sheep sequester a significant portion of their red blood cells (RBCs), and presumably platelets, when anesthetized. The cells are released to the circulation after a few hours. Thus, the delay in the pump implantation during the second study may have been fortuitous as the hematocrit had returned to 32.5% at pump implantation. The hematocrit ranged from 22 to 29 mg/dL during pump operation. The variation could have been due to fluid volume delivered to the animal during the study following pump implantation, bleeding, and potential fluid shifts in the animal. Platelet counts similarly varied from 170,000 to 310,000 platelets/ μ L.

Platelet activation levels were relatively high prior to the pump implantation. This can be attributed to the large injury produced by the thoracotomy, effects of clamping the aorta, placement of intravenous lines, etc. The percent of activated platelets remained the same or decreased slightly following pump implantation and operation with a 125 μ m gap. A decrease can be attributed to removal of activated platelets, either through deposition or clearance by the spleen or to an increase in unactivated platelets, as might occur with the release of sequestered cells into the circulation. Platelet activation increased during operation with a 100 μ m gap, reaching 80% after one hour. Platelet activation declined somewhat with the decrease in the gap to 50 μ m.

Five mins of impeller touchdown produced a 4 mg/dL increase in plasma free hemoglobin and a 30% increase in platelet activation. Clearly, touchdown has detrimental effects in terms of blood damage and should be avoided.

During these studies, the shear rate at the impeller blade tip increased from 42,000 s^{-1} (gap = 127 μ m) to 52,000 s^{-1} (gap = 100 μ m) to 105,000 s^{-1} (gap = 50 μ m). Calculating the exposure time was more problematic, since the flow rate was not measured. However, the flow rate was relatively stable as evidenced by the lack of variance in the arterial pressure and the RPMs were also held constant. A consensus in the literature has emerged in applying a power-law model to predict shear-related blood damage, with some variation in the regression fit coefficients. As described in Section 1.2.2.2 a damage index is predicted based on the product of the shear stress, raised to a regression fit exponent, and the exposure time, also raised to an exponent. The flow rate through the impeller blade tip gap decreases approximately linearly

with a decrease in the gap width for this pump topology [120]. The exposure time likely remained nearly constant, which the volume passing through the high shear zone between the impeller blade tips and the pump housing would have declined.

Thus, the damage index will vary based on the increase in shear stress as the impeller gap was decreased. Damage indices from blood pumps are generated following application of CFD to predict flow related parameters in pump, due to the complex three-dimensional character of the flow field. In these analyses blood is assumed to be a Newtonian fluid, due to the high shear rates encountered in the flow field [121]. Of course, for a Newtonian fluid the shear stress can simply be calculated as the product of the fluid viscosity and the shear rate. While in actuality the shear stress is not a scalar quantity but a tensor, including Reynolds stresses, the magnitude of the shear stress due to the radial velocity gradient in the blade tip gap is several orders of magnitude higher than other stresses, so they can be ignored [122]. Thus, the predicted damage index in this situation would be proportional to the shear rate (with the appropriate exponent). A power-law model of blood damage would have incorrectly predicted the most blood damage with the smallest gap (thus, the highest shear rate). Obviously, this experiment is only a single result and requires additional confirmation, but it points to significant limitations in the current understanding of blood damage in rotary blood pumps.

As the blade tip impeller gap decreases, the Farhenius-Lindqvist effect suggests a decrease in the hematocrit of the fluid passing through the gap volume. It is well known that in laminar tube flow, the motion of red blood cells force platelets and leukocytes toward the wall. Models of platelet deposition, such as those developed by Sorenson et al., account for this effect with enhanced platelet diffusivity [123, 124]. The viscosity of blood varies with the hematocrit, as well. Thus, in the blade tip gap, the local concentration of cells can be lower than in the bulk fluid, and thus, the local viscosity is decreased. These factors do not describe an inherent weakness of the power-law approach; however, it does demonstrate that the implementation of such models with the commonly applied assumptions in CFD analyses does not necessarily capture phenomena relevant to predicating blood damage that may occur by modeling blood as a colloidal suspension in plasma.

From this limited study, it can be suggested that there was likely a cell exclusion effect that occurred with a blade tip gap smaller 100 μm in sheep blood. Sheep red blood cells are 5 μm in diameter compared to 8 μm diameter human red blood cells and this size difference

probably contributed to the critical gap size when cell exclusion became extensive. In addition to the potentially detrimental effects in terms of mechanical damage to the pump, touchdown also provoked substantial hemolysis, platelet activation, and possibly platelet lysis. This emphasizes the requirement to develop a robust magnetic suspension in third generation VADs, and suggests these devices should possess a control mechanism to exit the touchdown state, should it occur during clinical use.

6.0 BLOOD SHEARING DEVICES

As discussed in Section 1.2.2.2 many investigators have attempted to develop devices to generate the high shear, very short time exposure flow conditions encountered in artificial organs and heart valves. Giersiepen proposed coefficients for a power-law damage index based on the previous efforts of Wurzinger and colleagues [59-62, 125]. However, the couette device used in the Wurzinger studies, had a hard mechanical seal in the flow path which caused thermal and friction-induced blood trauma. They concluded that shear-induced platelet activation was due to the release of platelet agonists from mechanically compromised red blood cells and other platelets. Since those studies were performed, an entire body of literature has developed describing shear-induced platelet activation and aggregation that results from von Willebrand factor binding to the GPI_b-V-IX receptor on platelets under high shear conditions [126]. Dr. Reul and colleagues developed a different couette shearing device, utilizing a fluid seal, and their results called into question the reliability of using the Wurzinger data to predict blood trauma [63]. Subsequent work from their laboratory has supported their hypothesis that the Giersiepen version of the power-law equation overestimates hemolysis [127, 128].

Concurrent with efforts of the Reul group, our laboratory attempted to develop a blood shearing device to examine these phenomena, and specifically investigate platelet activation in high shear flow.

6.1 SPECIFIC AIMS

6.1.1 Develop a Device to Expose Blood to the High Shear, Millisecond Exposure Time Environment Which Occurs in Rotary Blood Pumps.

6.1.2 Measure the Heat Generation and Reduce this Generation to Acceptable Levels for Blood Testing.

6.1.3 Characterize the Flow Field in the Device.

6.1.4 Apply Biocompatibility Assays to Quantify Activated Platelets and Microaggregates in Blood Passing through the Blood Shearing Device.

6.2 THE HEMOLYZER

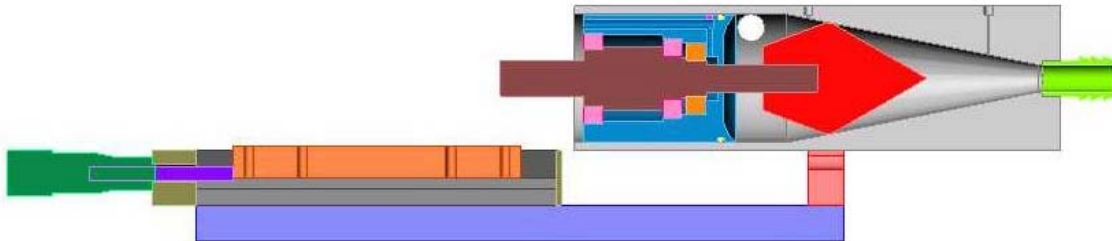


Figure 6-1. A high-shear couette flow device, the hemolyzer, is shown.

The left-hand side of the device is a micrometer (dark green) attached to a sliding platform on which the motor (not shown), shaft (brown), and rotor (red) could be moved in relation to the stationary lexan housing (gray). The arrangement permitted precise adjustment of the gap between the conical shaped rotor and the housing. The rotor could be turned up to 10,000 RPM. The magnitude of the shear field was determined by the rotational speed and the gap width between the rotor and the housing. The pressure drop across the gap controlled exposure time. Blood collection ports were placed just upstream of the rotor and immediately behind the end of the test section on the rotor.

The hemolyzer blood shearing device is shown in Figure 6-1. It consisted of a conical shaped rotor within a conforming housing. The rotor was tapered with two angles. A 0.125" test section

shared the same angle as the housing (14° , the arctangent of 0.25), while the front section of the cone had a steeper angle so that the shear rate in the gap between the test section and the housing was significantly higher than in surrounding areas. The rotor, shaft, shaft housing, and motor were mounted on a sled which was advanced until the rotor contacted the housing and then was withdrawn with a micrometer so that there was a gap of known width between the rotor and the housing. The angle of the housing was selected so that a four unit axial translation of the rotor resulted in a one unit change in the radial gap between the rotor and the housing.

The shaft was mounted on two sets of 17 mm ID, 26 mm OD, 5 mm wide radial ball bearings (pink in the Figure). The shaft was sealed at the junction of the shaft housing and the blood fluid path with a 0.5" ID, 0.875" bore, 0.879" OD, 0.125" wide, nitrile lip seal (HM14R, CR Seals, Chicago, IL). 3/8" diameter tubing was connected to a barbed inlet (light green in the figure). Two 3/8" barbed connectors extending perpendicularly from the rear portion of the lexan housing served as the fluid outlets. The rotor and shaft were constructed from Ti6Al4V. The lexan housing was vapor polished with methylene chloride.

The original design as proposed incorporated a fluid purge seal between the shaft and housing; however, the design was modified to reduce construction costs. The final device was constructed by Vascor, Inc. and donated to the University of Pittsburgh.

6.2.1 Heat Generation Testing

6.2.1.1 Introduction

Upon receipt of the hemolyzer, it was noted that during preliminary tests with air or water, the device rapidly became hot to the touch. Recirculation of 600 mL of water (the amount of blood available for most of the planned tests) through the device resulted in water temperatures exceeding 50°C after 10 to 15 mins of operation. Heating blood beyond 40°C results in an increased mechanical fragility of red blood cells. Additional heating produces hemolysis and other blood cell dysfunction, thus the blood contacting surfaces of the hemolyzer could not exceed 40° . Sources of heat generation in the device included motor heating due to excessive torque requirements to rotate the shaft and friction in the bearings or at the shaft-seal interface.

6.2.1.2 Methods

A temperature probe (Model #DP25-TC, Omega Engineering, Stamford, CT) was used to measure the surface temperature of various components of the hemolyzer after 30 and 60 mins of operation. The bearings were lubricated with Lubriplate food grade lubricating grease (FGL-00, Lubriplate, Newark, NJ).

The hemolyzer was operated under three conditions: 1) Motor uncoupled from the shaft; 2) Motor coupled to the shaft with a shaft coupler (FC Bellows couple, Sterling Instrument, Hyde Park, NY). Rotor not attached to the shaft, with air as the fluid medium ; 3) Motor coupled to the shaft as above, seal was lubricated with Super Lube synolon PTFE lubricant (Synco Chemical Corp., Bohemia, NY), fluid medium was air. The temperature was measured after at the locations listed in Table 6-1.

Table 6-1. Locations of hemolyzer temperature measurements.

A	Motor
B	Aluminum motor mount
C	Shaft couple
D	Rotor shaft adjacent to shaft couple
E	Aluminum shaft housing mount
F	Ti6Al4V shaft housing adjacent to aft bearing
G	Ti6Al4V shaft housing adjacent to fore bearing
H	Shaft at rotor mount

For each condition the hemolyzer motor was operated at 10,000 RPM (the maximum RPM intended for blood studies). All surfaces were verified to be within $\pm 0.5^{\circ}$ C prior to initiating the test.

6.2.1.3 Results

The ambient air temperature during the tests was 22.5-23.3° C. The RPM for each test was 9720 for condition 1) and 2) and 9600-10140 for condition 3). The temperatures for each location at 30 mins are shown in Figure 6-2. The results at 60 mins were very similar indicating the heat generation had attained a steady state. The results demonstrate that the motor reached 33.1° C

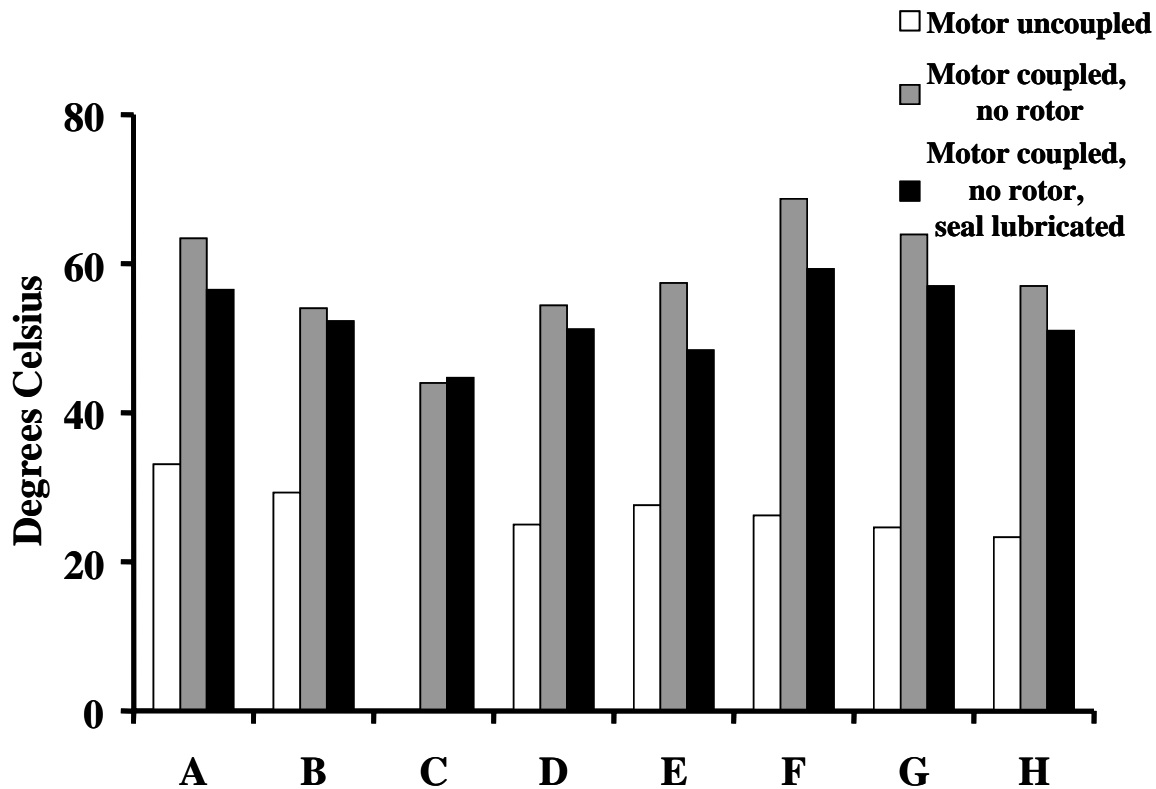


Figure 6-2. Temperature of the hemolyzer surfaces, indicated in Table 6-1, after 30 mins of motor operation are shown.

after 30 min with no load. Heat transfer from the motor to the shaft and shaft housing, though the aluminum mounts and structure was not a concern. Operation of the motor, coupled to the shaft, produced substantial increases in surface temperatures. The shaft couple, indicated by C in the figure, was cooler than either the motor mount or shaft, indicating that heat was not being

effectively transferred for the motor to the shaft housing. Lubricating the seal face resulted in a decrease in temperatures at all surfaces except the shaft couple.

Based on these results, the bearings were replaced with ABEC 7 rated spindle bearings and the nitrile seal was replaced with fluoroelastomer seal (both from the same suppliers as the previous materials). After 30 mins of operation at 10,000 RPM, the housing surface temperature varied from 41.8 to 45.0° C with air as the fluid or 34.9 to 37.1 with a blood analogue fluid (30% glycerol in water).

6.2.1.4 Discussion

The results demonstrated that the motor, the bearings, and the seal all contributed to the heat generation. Selecting bearings and seals more appropriate for this demanding application and with lubrication use reduced heat generation in two ways. Primarily, friction with both the seal and bearings were reduced, decreasing the local heat generation. The reduced friction lowered the torque requirement on the motor, leading to less heat generation. Thus, with this simple approach, the heat generation issues of the hemolyzer could be resolved.

6.2.2 Visualization of the flow patterns within the Hemolyzer.

6.2.2.1 Introduction

The underlying principle behind the design of the hemolyzer was to develop an apparatus that exposed passing blood to a uniform shear field with a known time exposure history. The concept which evolved into the hemolyzer design was based on intuition, requiring verification of the anticipated results.

6.2.2.2 Methods

Flow visualization of the hemolyzer flow field was carried out using the methods described in Wu et al [118]. Neutrally buoyant 30 µm diameter fluorescent beads suspended in a blood analogue (30% glycerol in water) were illuminated by a sheet of laser light through the transparent lexan housing to image the flow. Preliminary CFD analysis was performed by Dr. Greg Burgreen.

6.2.2.3 Results

During the flow visualization studies pressure versus flow rate data was also collected. The data revealed that the device was actually a relatively powerful pump, capable of generating a flow

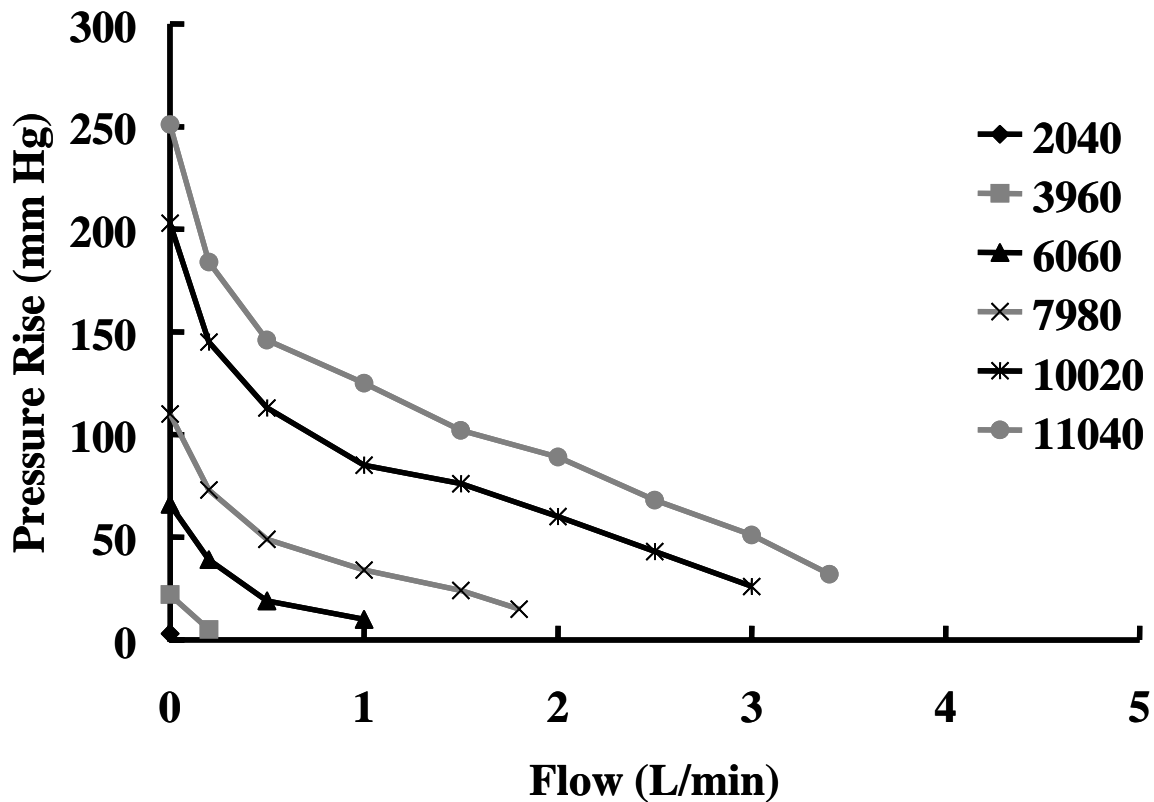


Figure 6-3. H-Q for the hemolyzer with a 0.005" rotor gap.

rate, Q, exceeding 5 lpm, depending on the gap between the rotor and the housing as well as the rotor RPM, with a static pressure rise of over 250 mm Hg.

Flow visualization revealed several areas of concern. Blood flow in the inlet was laminar as shown in Figure 6-4. However, it was readily apparent that large areas of recirculation existed

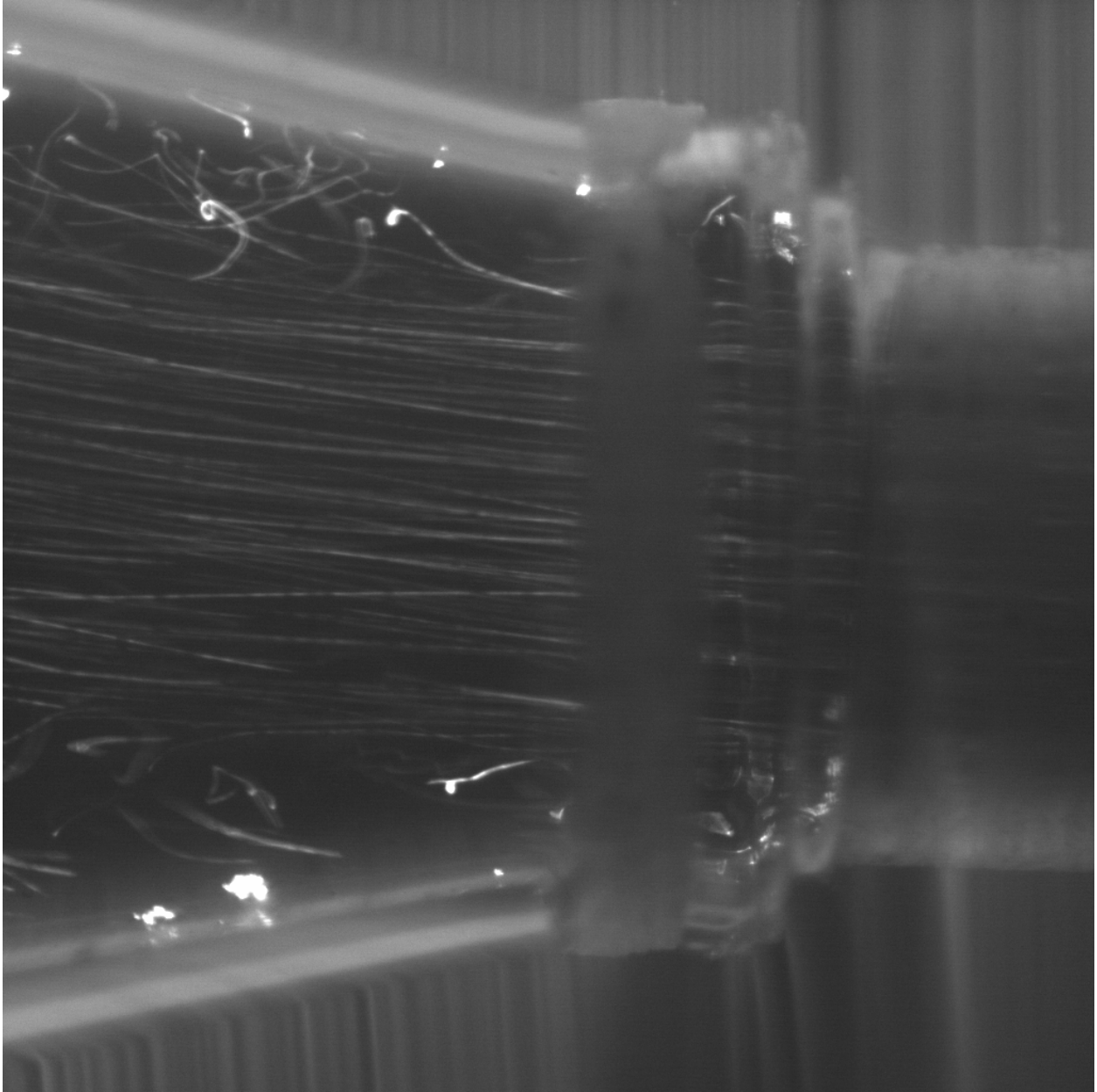


Figure 6-4. Flow through the inlet of the hemolyzer with a 0.010" rotor gap, 10,500 RPM, Q=4.5 lpm

at the divergent portion of the flow path. This finding was also demonstrated in the CFD results as shown in Figure 6-5. Both the flow visualization and the CFD analysis showed that the

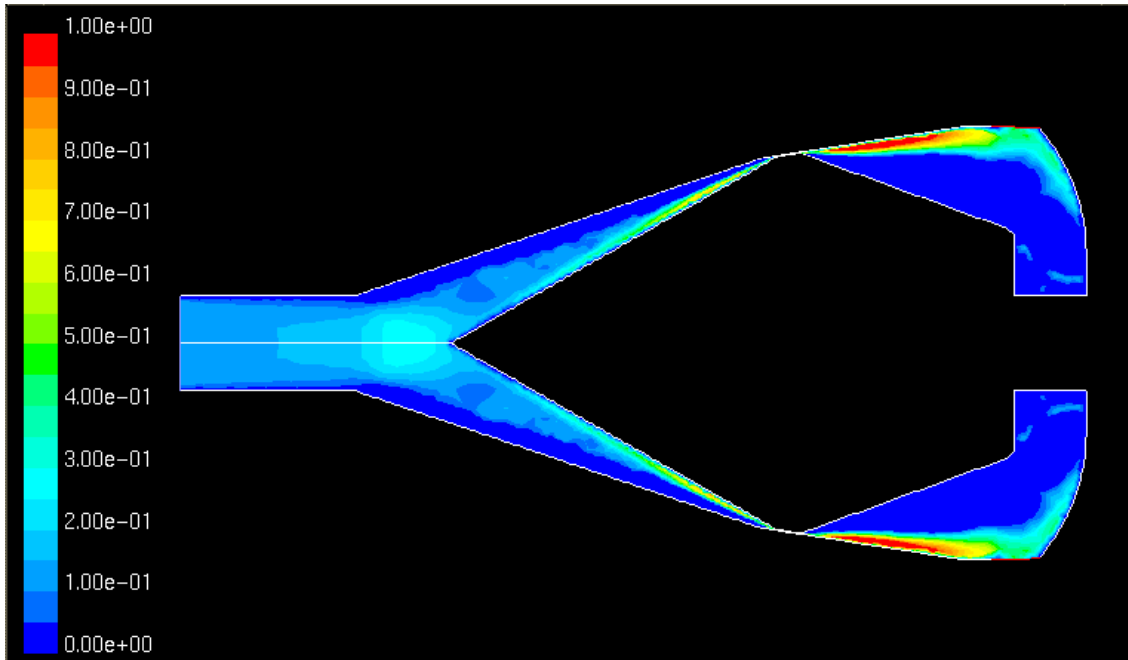


Figure 6-5. CFD prediction of the axial velocity of the primary flow path in the hemolyzer.

The scale indicates axial velocity in m/s. The impeller RPM is 10,000 and the flow rate is 1 lpm.

axial core flow remained laminar until encountering the primarily circumferential flow (oriented perpendicular to the axial flow) at the rotor, generating vortices and another recirculation zone as shown in Figure 6-6. The location of this interaction in relation to the rotor was dependent on the flow rate and pressure drop. At lower flow rates the interaction was proximal to the rotor tip, while at higher flow rates the effect was not as severe, occurring past the rotor tip, where the a portion of the axial flow had begun circumferential rotation, so only the outer portion of the core axial flow interacted with the circumferential flow.

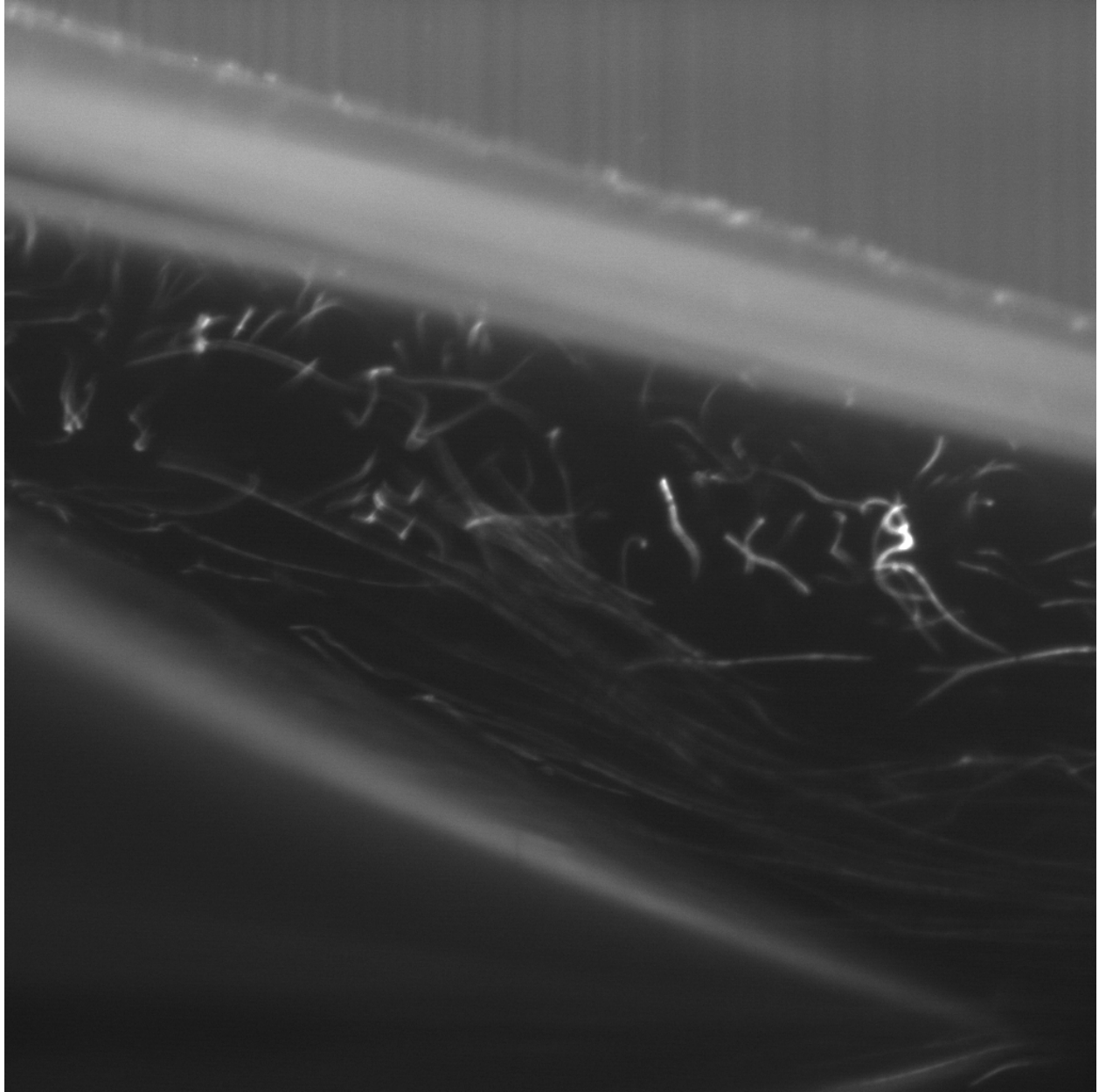


Figure 6-6. A disturbed flow pattern at the tip of the rotor.

The flow adjacent to the rotor was well-adhered and flow separation or vortices were absent. Moving radially towards the housing wall, the flow deteriorated, exhibiting chaotic flow paths as shown in Figure 6-7.



Figure 6-7. The flow pattern from the rotor surface extending to the housing is shown for the same conditions as in Figure 6-5.

The flow through the gap appeared to be uniform in the flow visualization and the CFD analysis as seen in Figure 6-8. Taylor vortices were not observed or predicted. The Taylor numbers for this device are several orders of magnitude below the critical Taylor number for blood [129].

The flow visualization images unfortunately were not clear. The reason for this can also be seen in the left image in Figure 6-8. The lexan housing had rapidly developed subsurface

crazing due to residue stresses remaining from the machining process and the stresses experienced during flow experiments. The small fractures prevented clear focus through the housing and diffracted some of the laser light.

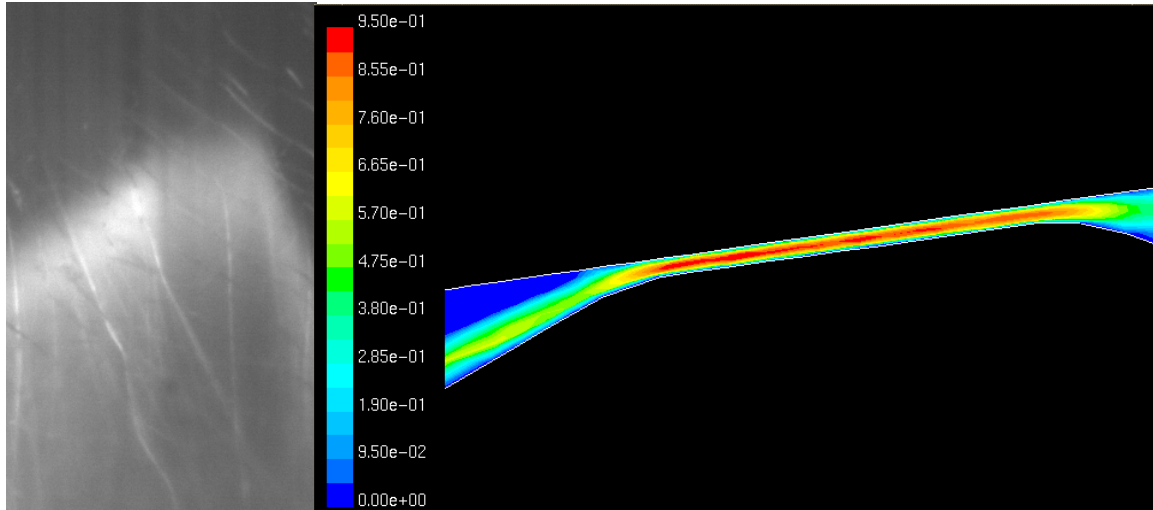


Figure 6-8. Flow visualization (left) and CFD predicted axial velocity contours (right) of the flow through the high shear gap in the hemolyzer.

6.2.2.4 Discussion

Incorporating the findings together, it was observed that there was a strong axial core flow entering from the inlet. This core remained intact until encountering the circumferential flow generated by the rotor. As the flow approached the small fluid gap, a portion of the flow was forced towards the housing and then in the retrograde direction towards the inlet forming the large recirculation zones apparent in Figure 6-4 and 6-6 and correctly predicted in the CFD analysis in Figure 6-5. In spite of these recirculation zones the flow through the gap was relatively uniform.

The overall findings suggested that blood passing through the device would be likely to encounter some degree of recirculation or chaotic flow. Thus, it was decided that the hemolyzer could be used for single pass studies, but would likely introduce considerable artifact in multiple pass studies due to adverse flow conditions.

6.2.3 Platelet Activation and Microaggregate Formation Following Exposure to High Shear for Short Time Durations

6.2.3.1 Introduction

Although the flow characteristics of the hemolyzer were not optimal, they were deemed acceptable for single pass experiments to begin investigation of the effects of high shear ($> 100,000 \text{ s}^{-1}$) for short durations ($< 5 \text{ msec}$).

6.2.3.2 Methods

Blood was collected via jugular venipuncture from healthy, non-device implanted bovines as described in Section 2.3.1.1. The surgical grade Tygon tubing (S-50-HL; Norton Performance Plastics, Akron, OH) was attached to the hemolyzer and the blood bag. The hemolyzer and tubing were primed with saline. The motor was started at a low RPM. The tubing clamps were released, and after the saline/blood interface reached the rotor, the speed was increased to the level specified for the test and samples were collected. The pre-shear exposure sample was collected approximately 2" upstream of the shear gap. The post-exposure sample was collected from about 0.25" distal to the rotor gap. The samples were collected into the citrated monovettes used in the previous studies with a double-sided 20 gauge needle, so that blood could be directly drawn into the blood tube. Control samples were obtained from the blood bag prior to initiating the test. Flow cytometric quantification of activated platelets and platelet microaggregates was performed with BAQ125, GC5, annexin V, and anti-CD62P as described in Section 2.2. The test was carried out 12 times.

The exposure history of the blood samples was determined from the flow rate, rotor speed, and radial gap. Time exposure was calculated as the volume of the shear gap divided by the flow rate as measure by an in line ultrasonic flow probe. The shear rate was calculated as the average rotor surface speed divided by the radial gap. The rotor speed was output from the motor controller to a multimeter. The viscosity and hematocrit of the blood in these tests was estimated, but not directly measured.

Samples from the control, upstream (before passage through the shear gap), downstream (post-passage through the shear gap) were compared with paired Student's t-test assuming unequal variances with Bonferroni correction.

6.2.3.3 Results

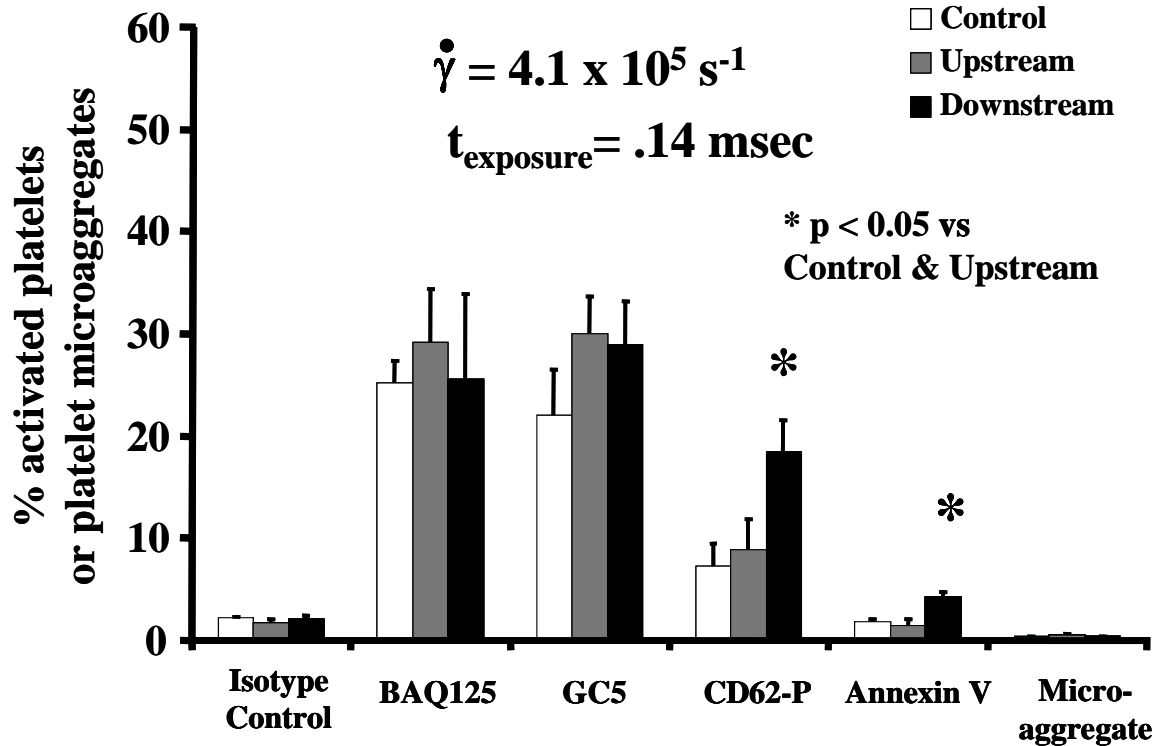


Figure 6-9. Changes in activated platelets and microaggregates following hemolyzer passage.

Upstream sample was collected before the blood reached the rotor, while the down stream sample was collected after the blood had traversed the shear gap.

Sample results from one of the studies are shown in Figure 6-9. No significant differences were found between upstream and downstream samples with BAQ125, GC5, or microaggregates. In several samples either annexin V binding or CD62P or both were significantly increased in the downstream sample. The results from all 12 studies are shown in Figure 6-10. The combined

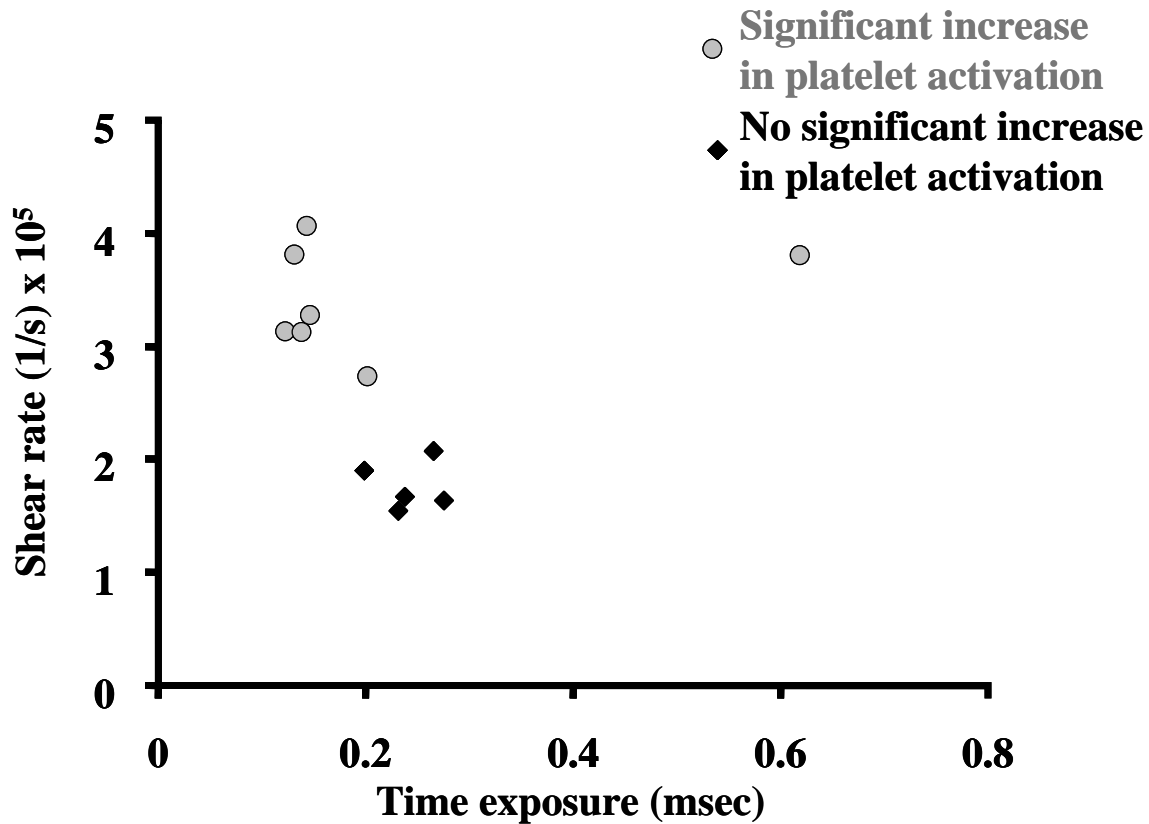


Figure 6-10. The platelet activation dependency on shear rate and exposure time is shown.

A significant increase was defined as at least one of the two assays (annexin V or anti-CD62P binding) demonstrating a significant increase of the downstream sample versus the upstream and control samples.

results tend to suggest a threshold for activation with a shear rate exceeding $2.5 \times 10^5 \text{ s}^{-1}$. Unfortunately after these initial results, the lexan housing fractured through the downstream sampling access point due to the subsurface crazing and the difficulty of mating the lexan housing to the shaft housing. Thus, additional studies could not be completed.

6.2.3.4 Discussion

The early results suggest a threshold for shear activation of platelets, tending to support the hypothesis proposed by Paul and colleagues [128]. Thresholds have also been proposed for hemolysis as reviewed by Grigioni [50]; although this hypothesis is contradictory to the more commonly accepted hypothesis that shear-induced damage to red blood cells is time dependent.

However, neither this study nor Paul's work elucidated the mechanism of platelet activation. The release of platelet agonists by platelet mechanical compromise or another mechanism, such as vWF binding, or a combination could have been involved. Thus, the work remains too preliminary to draw specific conclusions.

There were, of course, other potential sources of activation. Inserting a needle into the flow path creates a flow disturbance due to the high local velocity. To attempt to avoid the potential problems caused by the recirculation regions the collection site locations in the flow were carefully monitored. The upstream sample was collected from the centerline of the axial flow at the inlet. As shown in the flow visualization, the core of this flow was laminar and undisturbed by the recirculating regions adjacent to the housing. The downstream sample was collected just behind the rotor gap, prior to the blood entering the outlet area, which also contained recirculation regions. Anticoagulation, hematocrit, platelet count, blood-contacting surface composition, etc. were some of the factors that likely contributed to the platelet response to the high shear environments. Unfortunately, there was not an opportunity to investigate these issues.

Following the failure of the lexan housing, the overall suitability of the hemolyzer for the desired studies was examined and found wanting. The considerable recirculation regions and the presence of a mechanical seal in the blood flow path required improvement. Other issues with the device, such as ensuring concentricity of the rotor within the housing, the rotor-shaft junction, and the large reservoir between the rotor and the shaft housing required improvement or modification. Thus, it was decided to begin from scratch with a new design.

6.3 THE BLOOD SHEARING INSTRUMENT (BSI)

6.3.1 Introduction

Based on the issues discovered with the hemolyzer, several objectives were established for the BSI. The hemolyzer experienced substantial recirculation due, in part, to the rotor generating substantial flow and attempting to force several liters per min through gaps measured in thousandths of an inch. The conical rotor did not generate to desired isolation of high shear to

the gap region only. The mechanical seal required removal from the blood contacting fluid path. Incorporating these ideas the BSI was designed in collaboration with LaunchPoint Technologies (formerly Magnetic Moments, Goleta, CA).

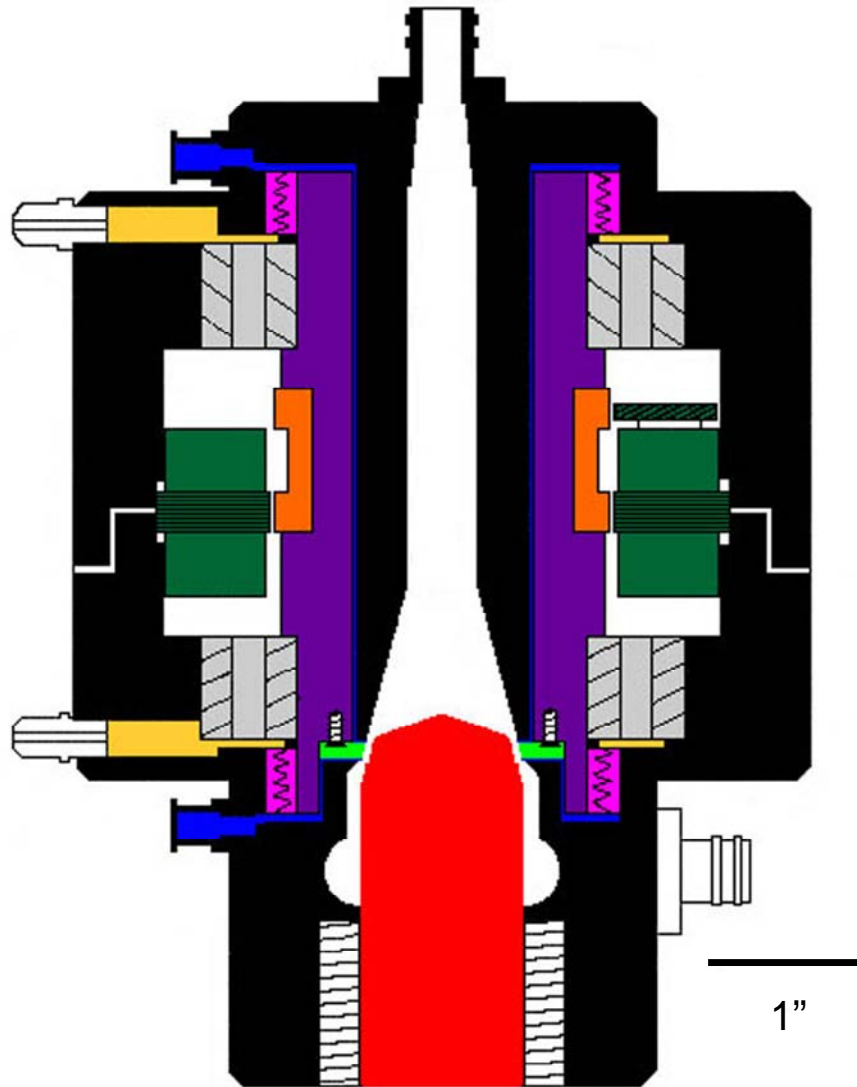


Figure 6-11. A schematic of the blood shearing device is shown in cross section.

A rotating ring (light green) is anchored to a spindle which connects the motor rotor (orange) to the bearings (gray hatched). The whole rotating member is separated from the stationary housing (black) by a narrow space, including the top and bottom face of the rotating ring. This space is filled with an aqueous solution (blue) which is driven by a positive displacement pump (not shown) and acts as a purge seal at the blood contacting face of the ring. The space adjacent to the bearings is filled with grease (yellow) to prevent water from penetrating the bearings or to the motor. The grease and the aqueous solution are separated with labyrinth seals (pink). The central hub (red) can be moved axially to adjust the gap between the ring and the hub. Blood enters the top of the device, passes through the central lumen (white), flows past the shear ring, and exits through the outlet port on the bottom right. Blood sampling ports (not shown) allow blood to be collected prior to and immediately after passing the rotating ring. All parts in black are Ti6Al4V, while 30 copies of the central hub have been constructed, so that different materials and coatings can be examined.

The device consists of a rotating ring constructed from Ti6Al4V and attached to the rotor of a brushless direct current (DC) motor (Bayside Motion Group, Port Washington, NY) which can rotate up to 15,000 revolutions per min (RPM). A non-rotating center hub can move axially to adjust the gap between it and the rotating ring. Adjusting the motor RPM and the gap increases or decreases the magnitude of the shear field. The rotating ring and hub have a slight taper so that they may be mated with a slight press fit to register their positions for each experiment. The bottom of the BSI housing was gauged and the hub has a surface mark so that the hub may be rotated in 1/25 of a turn increments. The hub screw thread density is 40 turns per inch. Thus the hub may be very accurately positioned in relation to the rotating ring. The rotor is attached to hybrid ceramic bearings (Champion Bearings, Fallbrook, CA), which provide axial and radial stability.

A fluid purge seal avoided a hard contacting seal in the blood flow path. To prevent plasma and blood element penetration between the rotating ring and the adjacent (stationary) housing two separate positive displacement pumps maintain a low positive flow (approximately 1 mL/hr) of fluid through the purge seal. Because of the slight taper of the rotating ring, some pressure is generated, depending on the experimental conditions (about 20 mm Hg at 10,000 RPM from preliminary calculations). Thus, two pumps were used to maintain constant purge flow on both sides of the ring in spite of pressure gradients across the ring. The device was connected by 3/8" surgical grade Tygon tubing to a flow circuit which re-circulates the blood by applying air pressure to the exterior surface three flexible blood reservoirs. By changing the pressure gradient across the device, the time exposure of blood to the high shear region can be adjusted. The device was been designed to generate shear rates up to $100,000 \text{ s}^{-1}$ for exposure times as low as 2 msec. It may be disassembled to gain access to blood contacting surfaces for further examination. Table 6-2 indicates the performance targets for the device and re-circulating loop. Please note that maximum (or minimum) quantities are not linked.

Table 6-2. Performance characteristics of the BSI.

Quantity	Maximum	Minimum
Shear Rate (s-1)	105,000	525
Exposure Time (msec)	100	1.5
Gap (inches)	0.005	0.05
Flow rate (liters/min)	1.5	0.1

The shear rate in the device can be calculated from the circumferential velocity of shear ring divided by the gap width. The velocity will be obtained by multiplying the rotation rate (from the motor RPM, which is output from an integrated Hall effect sensor) by the ring circumference. The time exposure can be calculated by dividing the volumetric flow rate, Q , by the volume of space between the shear ring and the center hub, V_s . The actual shear stress will depend on the viscosity of the test fluid, and is product of the viscosity times the shear rate (assuming Newtonian behavior of blood at high shear rates).

Alternately, these variables may be obtained by applying the superposition principle to predict the solution for the flow field; however, it will not be possible to accurately measure the pressure across the shear ring. The presence of only a single outlet means the flow field of the whole device is not axisymmetric, requiring a three dimensional solution. The non-Newtonian nature of blood viscosity will also impact the solution. While blood can be modeled as a Newtonian fluid at high shear rates, this will not hold in the inflow and outflow areas, especially at lower flow rates. This suggests either using the simpler method based on motor RPM and gap volume or CFD based analysis.

To investigate the flow field within the BSI, a CFD study was carried out by Dr. Jinchun Wu from LaunchPoint [130]. The analysis indicated that at a 1 lpm flow rate and with large shearing gap widths (0.020”) recirculation zones formed below the shear ring. With smaller gaps the shear field is fairly uniform, but still varied over the gap because of the no-slip conditions on the stationary hub and rotating ring. No one has yet designed an ideal resolution to this limitation.

The BSI represents the product of multiple design iterations, based on both our experiences and the experiences of others. The elimination of blood contact with mechanical seal was crucial to generate a controlled shear environment. Implementing an outer rotating ring prevented the formation of Taylor vortices. Use of a relatively small shear ring eliminated secondary flows due to centrifugal pumping action of the rotating element while specifically isolating the high shear region. The hybrid ceramic bearings not only possessed superior wear characteristics (versus conventional stainless steel bearings), but also provided precise alignment to aid in maintaining radial and axial stability. The device also has the flexibility to adjust the gap width, as well as to test multiple materials/coatings/surfaces under the same flow conditions. Overall, this design offers superior flow characteristics and flexibility, while minimizing the factors that limited the effectiveness of previous devices.

6.3.2 Sealing and heat generation issues

The design shown in Figure 6-11 weighed nearly 10 lbs. One of the goals of the BSI was to be able to use it in an *ex vivo* loop, which required mounting the BSI on or just above an animal to examine sub-lethal blood trauma. To attain feasibility for that application, the weight was reduced as much as possible by removing unneeded Ti6Al4V material from the housing. During this process the lube ports were inadvertently removed from the design. Thus, there was not a way to insert lubricant into the space between the labyrinth seal and the bearing. The labyrinth seals were then replaced with custom made Teflon lip seals (BalSeal, Foothill Ranch, CA). The lip seals adequately prevented fluid ingress into the bearing and motor chamber, however, heat generation was once again a problem.

Operating the BSI motor at 2,000 RPM with the seals in place caused rapid heating of the device to over 50° C in less than 90 seconds. The temperature increase occurred too quickly for the temperature probe previously used to provide accurate readings. These did not represent steady-state values as the BSI would exceed safe temperatures for handling with bare skin within a few minutes. The heating was a result of friction at the seals and the increasing torque load on the motor.

Several approaches were taken to address this issue. Lubricant was applied to the surface of seal. This did not appear to have an effect on heat generation, however, during the repeated

attempts to investigate the issue, it was noted that the heating caused loss of flexibility of the seal. The Teflon lip seals were then trimmed to reduce the inner diameter by 0.5 mm to decrease the friction at the seal interface. This resulted in seal failure. An overmold was then made of an unused seal by the Swanson Center for Product Innovation at the University of Pittsburgh. “Soft” polyurethane seals were then made from the mold with varying durometers. The polyurethane seals required a wear-in period to provide a seal with minimal applied pressure. Unfortunately, most of the fabricated seals never met the desired function well enough to prevent fluid ingress under either static or rotating conditions. The wear-in period was reflective of abrasion to the seals, as the abrasion continued the seals wore-out and their sealing ability quickly degraded. Thus, the polyurethane soft seal approach was discarded.

Since the original design was intended to use a labyrinth seal, a system was devised to essentially replace the lube ports that were dropped from the design. Small holes were drilled into the cavities between the labyrinth seals and the bearings. Blocks were temporarily placed over these holes as shown in Figure 6-12. Male luer ports were placed in the blocks. Syringes

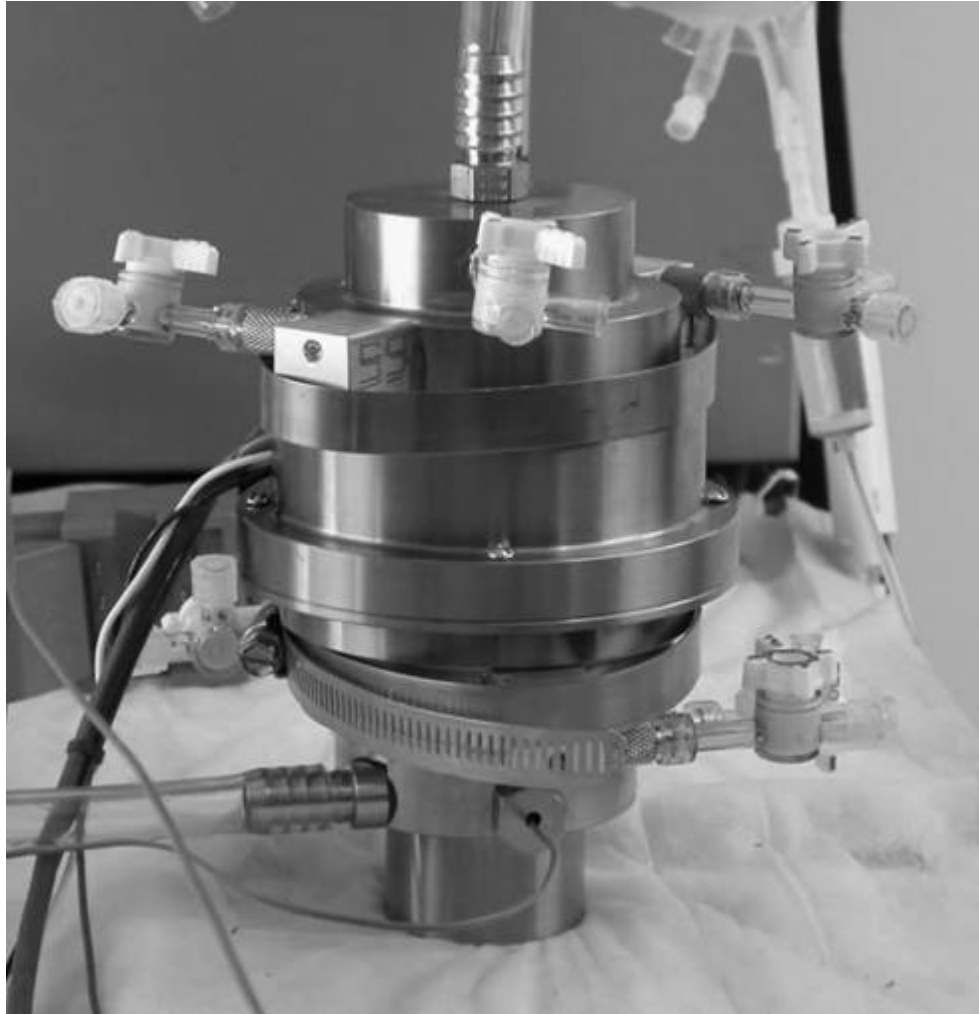


Figure 6-12. The modified BSI with temporary blocks added to permit introduction of lubricant into the cavities between the labyrinth seal and the bearings to prevent purge fluid ingress into the motor chamber.

were used to inject lubricant into the cavity. However, this failed to prevent purge fluid ingress into the cavity. This was because the lubricant (a grease) has a higher density than the purge fluid (saline/water), thus when rotation was begun, the grease was forced radially outward, away from the seal face, while the lighter water was forced inward and was able to pass through the seal. In attempting to address this issue, it became apparent that labyrinth seal design was not intended for the set-up within the BSI and that the design was not appropriate to implement the sealing desired.

Since then, a new custom seal has been designed by Gallagher Fluid Seals Inc. (King of Prussia, PA) to attempt to balance the sealing requirement combined with the need for a low friction, low torque solution. The seals were not yet available to complete the intended studies with the BSI.

The plan will be to use the BSI to examine the effect of the high shear, short time exposure environment on platelets. A primary goal is to attempt to elucidate the underlying cause of the platelet activation. This will be accomplished by testing whole blood, PRP, and platelet suspensions in the device. The PRP will exclude the potential effects of red blood cell lysis and subsequent ADP release on platelet activation. A washed platelet suspension will eliminate the contribution of plasma proteins, including vWF and fibrinogen, in the shear-induced platelet activation. Proteins of interest can be added back to the platelet suspensions to identify effects of individual proteins in observed platelet activation. Other approaches including ADP-scavengers and g-protein inhibitors can be implemented to further investigate any findings of interest.

As part of a pediatric VAD development program a blood shearing device will be constructed from a modified pump prototype. The device will incorporate a magnetically levitated impeller, modified to investigate rotary VAD related blood damage. Until this device is prepared a Streamliner prototype will serve as the test vehicle for pump induced blood damage. The use of magnetically levitated components will eliminate the bearing, sealing, and heat generation issues encountered in previous devices.

7.0 BIOCOMPATIBILITY ASSESSMENT OF AN INTRAVASCULAR ARTIFICIAL LUNG

7.1 SPECIFIC AIMS

7.1.1 Quantify Circulating Activated Platelets and Platelet Microaggregates with the Artificial Lung Following Implantation in Bovines.

7.1.2 Development and Implementation of a Rapid Method for Assessing the Relative Biocompatibility of Several Coatings Applied to Hollow Fiber Membranes.

7.2 BIOCOMPATIBILITY ASSAYS

7.2.1 Introduction

The Hattler Catheter is an artificial lung device that consists of a mat of hollow fiber membranes (HFM) scrolled around a polyurethane balloon. It is deployed into the vena cava through the jugular or femoral vein. Oxygen and carbon dioxide are exchanged through microporous polypropylene HFMs. The balloon is rapidly pulsated (up to 300 beats per min) to augment gas exchange by reducing the boundary layer thickness around the HFMs. Patient support is provided by improving oxygen delivery or enhancing carbon dioxide removal in a variety of clinical settings characterized by acute lung failure.

7.2.2 Methods

7.2.2.1 Device Insertion and Blood Sampling

The devices were inserted in the jugular vein of 11 bovines for periods ranging from 6 to 96 hours. The insertion procedure has been previously described [131]. Briefly, the device was constrained in a sheath. The jugular vein was isolated and following a small incision, the device was inserted in the vein and advanced through the superior vena cava, so the distal end of the device resided near the renal veins and the proximal end was either just below or transversed the right atrium. Balloon pumping was then initiated.

Blood samples for biocompatibility assays were collected from an access line placed in the femoral vein and either a line placed to measure central venous pressure (CVP) or pulmonary artery (PA) pressure through a Swan-Ganz catheter line (Edwards Lifesciences, Irvine, CA). At least 10 mL of blood was drawn through the line, then with a fresh syringe the sample was collected and transferred to a monovette as described previously. Samples were collected pre-operatively, following blood access line placement, two hours post-implantation, and at least once daily thereafter.

7.2.2.2 Anticoagulation

A bolus of 4 mg/kg heparin was administered intravenously immediately prior to device insertion. In two animals with implant durations of 96 hours, 1 g of acetylsalicylic acid dissolved in 500 mL of saline was also given. Post-operatively, intravenous heparin was given to maintain an ACT of 200-450 secs with the target ACT determined prior to each study.

7.2.2.3 Quantification of Circulating Activated Platelets and Platelet Microaggregates

Circulating activated platelets and platelet microaggregates were quantified using the BAQ125, GC5, annexin V, and anti-bovine CD41/61 as described in Section 2.2.

7.2.2.4 Post-Explant Analysis

Immediately prior to study termination, a bolus of heparin was administered along with an overdose of barbiturate and potassium chloride. The lateral chest wall was removed to expose the thoracic organs. The position of the catheter within the vena cava was noted and then the

vessel was sliced axially to expose the device. The positioning of the device in relation to the portal and renal veins was recorded. SVC and IVC diameters and lengths to relevant anatomic landmarks were measured. The animal was then exsanguinated by jugular incision (opposite from catheter insertion site). The device was then removed and immediately transferred to a column of saline containing 50 U/mL heparin. A syringe was attached to the balloon luer port and used to inflate and deflate the balloon for about a min. The heparinized saline was discarded, fresh saline was added, and the balloon was inflated and deflated to rinse again. This process was repeated until the saline remained clear after balloon pulsation. The process did not remove any visible clot. Animals were thoroughly examined for distal embolic thrombus.

The intact explanted device was digitally photographed, noting any bending or kinking of the device that would be a result of anatomic variations in the vena caval tract. The front and rear manifolds of the device were then cut off to free the fiber mat, which was cut along the longitudinal axis, parallel to the direction of the HFMs and cutting through the nylon weft fibers. The fiber mat was then removed from around the balloon, leaving the fiber mat in stacked sections where each section corresponded to one concentric layer of wrapped HFMs. Pieces of the mat (1 cm²) were cut from the proximal, middle, and distal (in relation to the communicating gas delivery line) portions of the mat for scanning electron microscopy (SEM) analysis in 10 of the devices. Individual layers from the remaining mat were then separated and laid out for digital imaging. Any areas of significant gross thrombotic deposition were noted and imaged.

Images of the laid out fiber mat were analyzed with IPLab (Scanalytics, Bethesda, MD). The color image was converted to binary using a color intensity threshold so that areas of thrombotic deposition were converted to black (positive) and the remaining areas changed to white (negative). The percent of the whole mat and individual layer areas positive for deposition was then calculated. This process was repeated on two additional images of the mat and averaged.

7.2.2.5 Scanning Electron Microscopy

The pieces previously excised from the mat and a 1 cm² section of the balloon were prepared for scanning electron microscopy. Individual layers were separated and placed in saline in 6 well tissue culture plates. Fixation was accomplished by placing samples in 2.5% glutaraldehyde (Taab Laboratories, Berkshire, England) for 60 min at 2-8° C. The samples were rinsed with

saline and then placed in 4% osmium tetroxide (Sigma, St. Louis, MO) for 60 min. After rinsing three times with saline, the samples were serially dehydrated by immersion for 10 min in 30, 50, 70, 90, and 100% (the latter three times) ethanol (Sigma). The samples were then placed in an Emscope 450 (Emscope Laboratories, Ashford, UK) for carbon dioxide critical point drying, following by sputter coating with gold-palladium. Samples were imaged with a Jeol JEM-6335F field emission gun scanning electron microscope (Jeol, Peabody, MA).

7.2.2.6 Statistical Analysis

Statistical comparisons for the flow cytometric assays were performed using one-way ANOVA with post-hoc Scheffé testing. The percent of surface thrombus deposition for the various coatings was normalized for each experiment by dividing by the percent of surface thrombus deposition on the uncoated Celgard fiber sample, which served as the control, to account for variability in the condition of the blood. The Levene test for homogeneity of the sample variances was performed. The surface deposition results were then compared using one-way ANOVA using the Welch statistic and post-hoc Dunnett's T3 testing assuming unequal variances. Significance was assumed for $p \leq 0.05$. Statistical testing was carried out using SPSS 13 for Windows (SPSS Inc., Chicago, IL).

7.2.3 Results

7.2.3.1 Flow cytometric assays

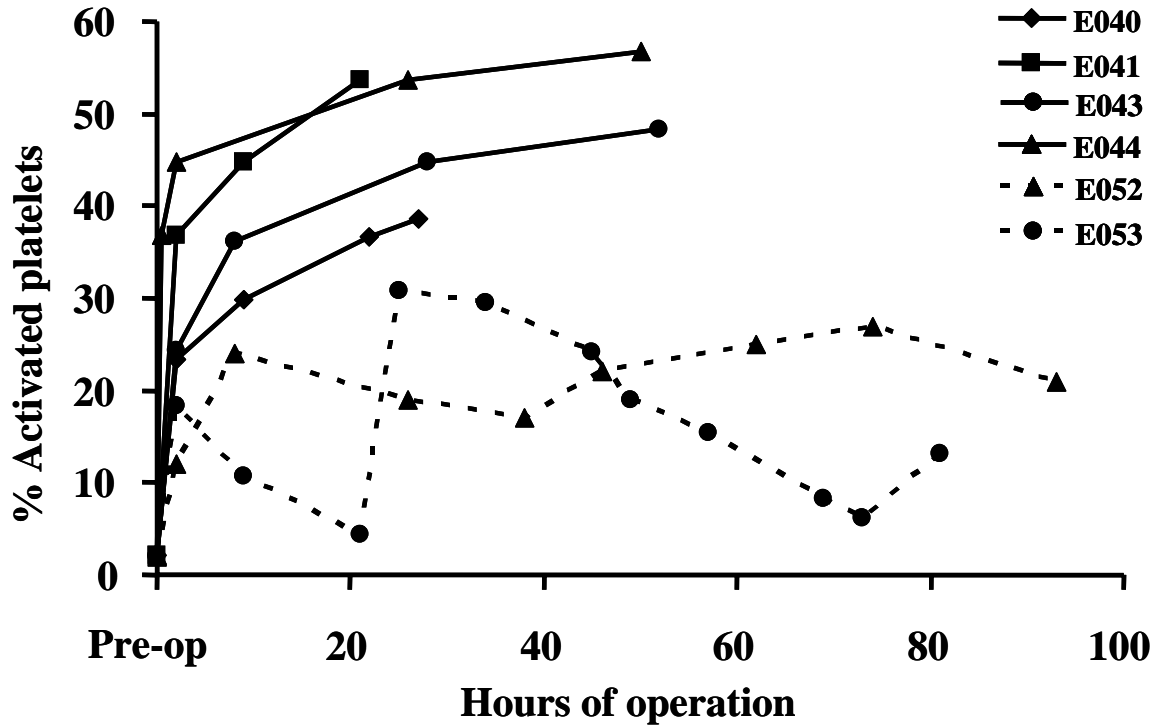


Figure 7-1. The plot shows the percent of circulating activated platelets, as indicated by annexin V binding, versus the time from implant.

E040-E053 refer to the study number. The dashed lines indicate the 96 hour studies, while the solid lines indicate shorter duration studies. All studies display a substantial increase following device insertion that continues to increase with implant duration in the four studies lasting less than 52 hours. The two 96 hour studies display a different response, but remain under 32%, a level exceeded by the four shorter studies.

Platelet activation was elevated in all studies following device implantation. Circulating activated platelets were elevated in animals with implant durations exceeding 6 hours, but who did not complete the full 96 hour duration as shown in Figure 7-1. In four studies there was a

significant ($p < 0.05$) increase in platelet microaggregates in blood collected after device contact (PA samples) versus blood collected proximal to the device (FEM samples) as shown in Figure 7-2.

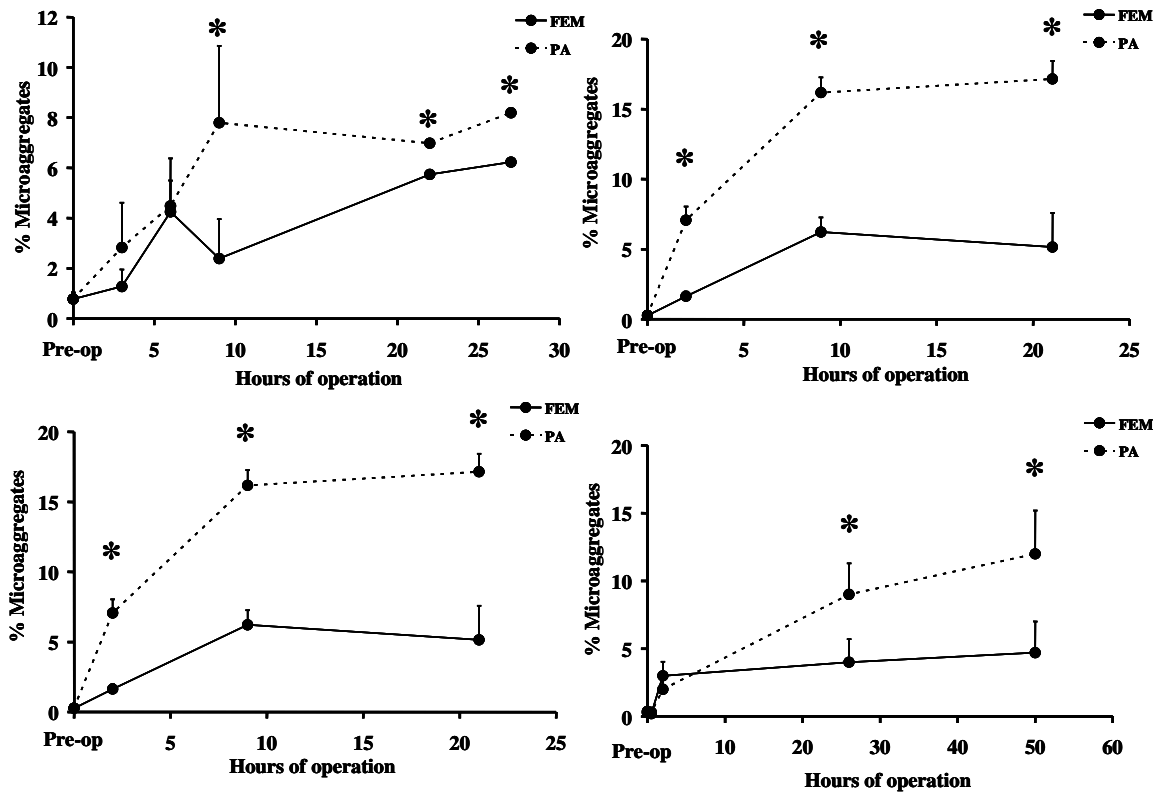


Figure 7-2. The plots show the percent of circulating platelet microaggregates versus the implant duration.

A)E040 – a 27 hour study, B)E041 – a 28 hour study, C)E043 – a 52 hour study, and D)E044 – a 52 hour study. The solid line represents blood collected from an access line in the femoral artery (FEM), prior to passing through the device, while the dashed line indicates blood collected from a line placed in the pulmonary artery (PA), after device contact. Data shown are mean + standard deviation. * indicates $p < 0.05$ for FEM vs. PA data.

7.2.3.2 Post-Explant Analysis

During device recovery anatomic landmarks were noted, and then the device was excised from the vena cava. Some degree of thrombus was usually apparent on the device. After removal of the device hubs, freeing the HFM mat, it was clearly evident that the nidus for thrombus formation was the nylon weft fiber as seen in Figure 7-3.

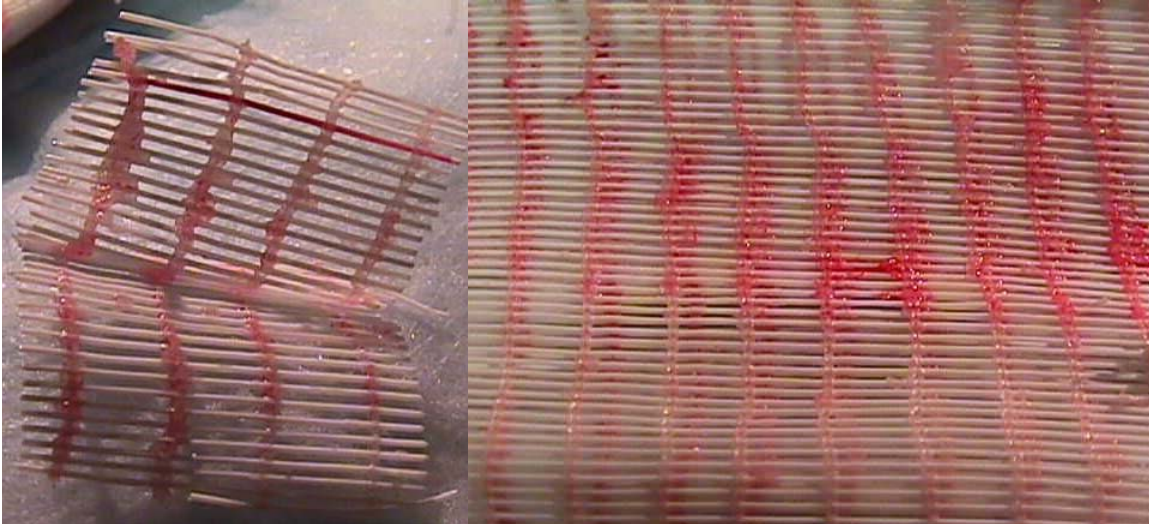


Figure 7-3. The images show the appearance of sections excised from the device following explant after a 6 hour study.

The image on the right shows thrombus on the weft fibers, which acts to adhere adjacent fiber layers together. The image on the right displays how alignment of weft fibers can result in the formation of alternating channels of thrombus covered areas with relatively unoccluded areas in the fiber mat.

Visible thrombus deposition was $20\pm 3\%$ in nine devices with study durations of less than 53 hours. One device which completed a 96 hour study had 3% visible surface deposition. The other device which completed a 96 hour study was immediately taken for *in vitro* gas exchange studies and was not analyzed to quantify surface deposition, although it appeared very similar for the other 96 hour, with little readily evident thrombus.

7.2.3.3 Scanning Electron Microscopy Findings

The scanning electron microscopy also demonstrated thrombus was nearly always apparent on nylon weft fibers. In examining the propylene HFMs that appeared to be free of deposition to the naked eye, it was revealed that there was cellular deposition on nearly all fibers. The deposition ranged from widely scattered patches of platelets and leukocytes (see Figure 7-4) to a monolayer of white thrombus, with occasionally entrapped red blood cells. Larger thrombus was usually confined to the weft fibers or areas in which it was evident that the HFMs had been bent

by the animal anatomy. Occasionally the thrombus from one weft fiber extended along a polypropylene fiber to reach the adjacent weft fiber.

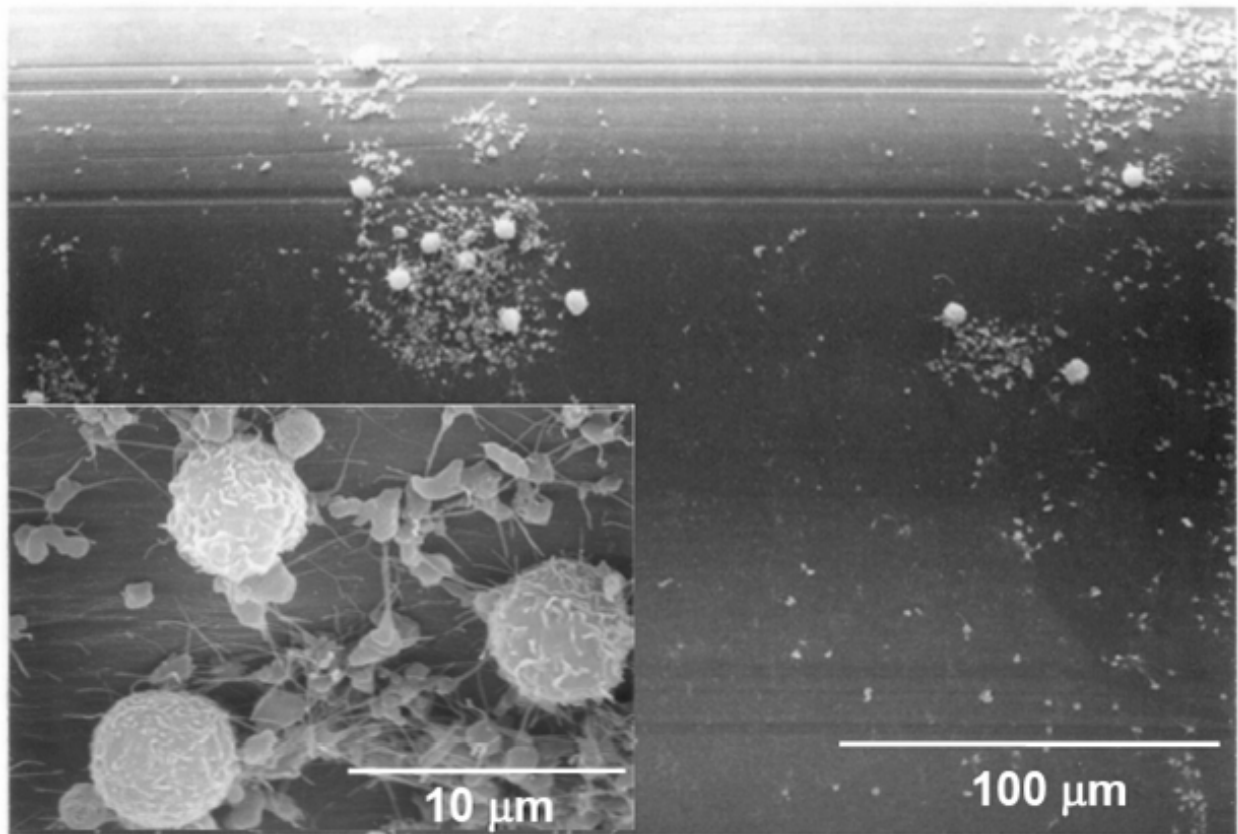


Figure 7-4. A micrograph is shown of the device which completed the 96 hour study.

The image is from an HFM without thrombus visible to the naked eye. The main image shows scattered cellular deposition. The inset shows a higher magnification of the deposition, indicating the composition is primarily platelets and leukocytes. The platelets have extended pseudopodia and some fibrin strands indicating platelet activation.

7.2.4 Potential Coatings for the Artificial Lung HMFs

Having observed some degree of deposition on all of the devices, a screening method was established to rapidly compare several coatings applied to the fibers mats used to construct the

devices at the same time. These studies were conducted in parallel with assessments of the effects of the coatings on gas exchange properties of the fibers in Dr. Federspiel's laboratory.

7.2.4.1 Methods

Three cm diameter circular sections of Celgard (x30-240, Celgard Inc., Charlotte, NC) matted fibers with or without various coatings (described below) were placed individually in 16 x 100 mm siliconized glass tubes (Fisher Scientific, Pittsburgh, PA). Blood was collected from healthy juvenile bovines via jugular venipuncture with an 18 gauge 1 ½" needle (Becton-Dickinson) into a 600 mL blood transfer pack (Baxter Healthcare). Heparin was added to the transfer pack prior to blood collection for a final concentration of 0.75 U/mL. The anticoagulation level for these studies was determined by attempting to produce a similar deposition pattern to that observed from device explant studies. Eight mL of blood was then added to each glass tube containing a matted fiber section and the tubes were placed on a hematology mixer (Fisher Scientific) for two hrs at 37° C. After this contact period the fiber samples were removed and rinsed in heparinized saline. The percent of the surface covered with thrombus deposition was calculated as described above. All 10 fiber/coating combinations were tested in parallel.

Commercial coatings were applied to the matted Celgard fibers, some of which had been previously coated with a thin siloxane membrane (Senko, Medical Instrument Mfg., Tokyo, Japan). The coating combinations investigated are listed in Table 7-1.

Table 7-1. Fiber/coating combinations tested in the *in vitro* rocker studies

Coating	Abbreviation	Company
None	CG	N/A
Siloxane	SX	Senko
PhotoLink Heparin	CG-H SX-H	Surmodics, Eden Prairie, MN
PhotoLink Polyvinyl Pyrrolidone	CG-PVP/H	Surmodics
X-coating	CG-X SX-X	Terumo, Tokyo, Japan
Heparin Complex T-2	CG-T2	TUA Systems, Merritt Island, FL
Duraflo II	CG-D	Edwards Lifesciences
Bionet	CG-B	Edwards Lifesciences

7.2.4.2 Results

Figure 7-5 displays the results of the fiber deposition tests normalized to the uncoated Celgard fiber results. The test results indicate the application of heparin coatings significantly reduced thrombus deposition on the fibers *in vitro*. Application of a siloxane layer to the HFMs alone did not result in a significant decrease in deposition.

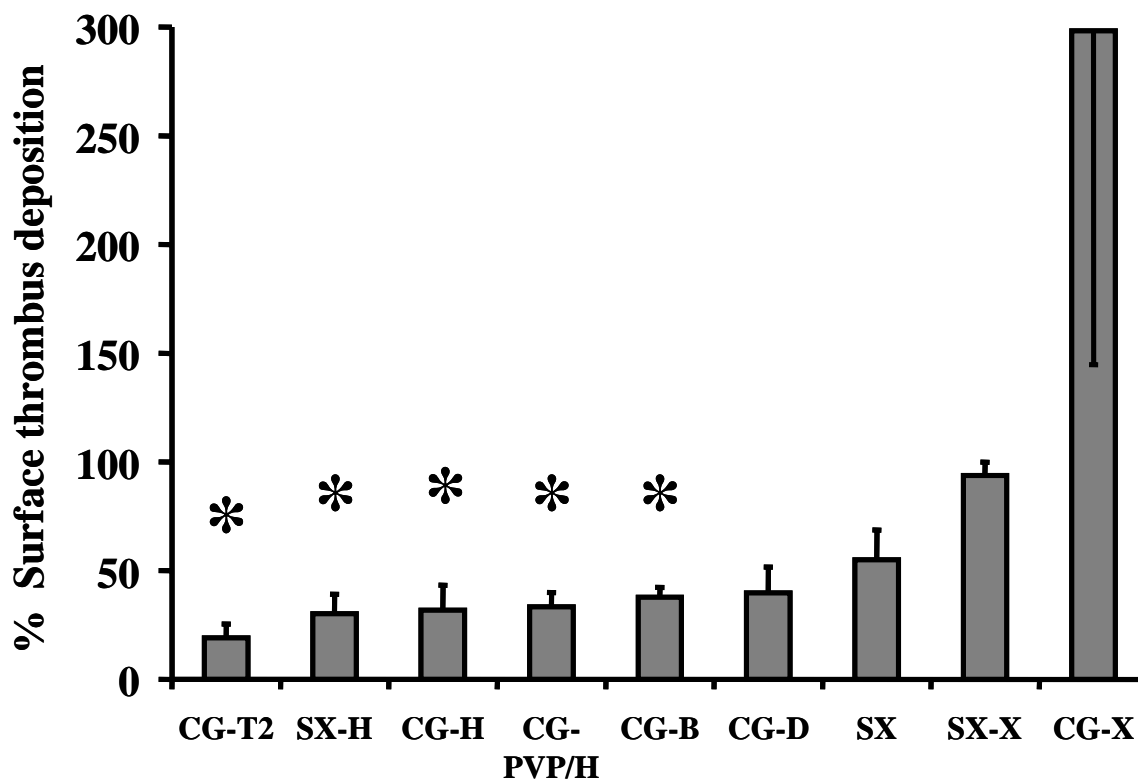


Figure 7-5. The chart displays the percent of surface area covered by visible thrombus following rocking a 3 cm diameter swatch of knitted hollow fiber membranes in bovine blood for 2 hours.

The description of the coatings appears in Table 7-1. The data were normalized so that the percent of deposition on the uncoated Celgard fibers equaled 100. Data shown are the means + standard error, except the CG-X for which the standard error is shown in the negative. * indicates $p \leq 0.05$ versus the uncoated Celgard.

7.3 DISCUSSION

The results demonstrated by flow cytometry and the post-explant visual and microscopic analysis, that the artificial lung does provoke a thrombotic response. However, the level of circulating activated platelets indicated by flow cytometry in many of the studies which was less than that observed in bovines implanted with VADs which are now being successfully used clinically. Both the application of coatings the HFMs and the use of aspirin and combined with heparin administration could alleviate some of the thrombus formation.

Of concern however, was the pattern of thrombus formation. The deposition on the nylon weft fibers caused adhesion of adjacent layers and the formation of channels through the device. While radial flow through the device, generated by the balloon inflation, likely would not have been affected, axial flow through the bundle would probably have been obstructed. The deposition pattern could induce blood flow to be shunted around the fiber bundle limiting gas exchange. Thus, limiting the amount of thrombus deposition is probably required to maintain adequate gas exchange.

8.0 SUMMARY

8.1 CONCLUSIONS

Thromboembolism and bleeding remain significant complications of ventricular assist device support. Attempting to identify the underlying cause(s) of hemostatic derangements in the target VAD population can be overwhelming. The patients present a multitude of co-morbidities and pre-existing conditions which contribute to an increased likelihood of thrombotic complications including heart attacks and strokes. The VAD implant procedure, including significant time supported by cardiopulmonary bypass, introduces additional confounding factors and presents its own set of complications and maladies, both acute and chronic in duration. Placement of a VAD, including inflow cannula, outflow graft, and the pump itself into this complex milieu obscures the ability to isolate and identify the causes of detrimental or beneficial effects of the device. Clearly, the restoration of adequate end-organ perfusion provides a substantial benefit to the patient. The benefit is accompanied by wide range of effects on multiple systems in the body [132].

The complications associated with supporting moribund patients are largely absent in the animal models selected for preclinical studies. However, the wide range of assays available in humans to assess various systems are lacking for large animal models, such as the bovine. In this work, a range of assays was developed to assess platelet responses to several cardiovascular artificial organs. First, the relative health of the study animals, especially with regards to platelet activation, was confirmed. This finding already distinguishes the bovine recipients of artificial organs from their human counterparts. The sham surgical procedure and subsequent recovery demonstrated that in healthy animals the effects of the implant procedure dissipate over two to weeks. Differences in the response of VAD-implanted bovines from those undergoing sham surgical procedures after the recovery period can thus be attributed to the presence and operation

of the device. The consistent observation of ongoing platelet activation and decreased platelet life span beyond the recovery period was thus attributable to the implanted VADs. While data was not collected for the leukocyte assays for the sham surgical procedure, it is reasonable to attribute the elevated of these assays to chronic inflammation in response to the VADs.

The relatively clean bovine model also permitted evaluation of device and operational changes. The ability of two platelet activation indicators to discriminate between two biocompatible coatings with relatively low subject numbers was a remarkable demonstration of the potential power of applying novel biocompatibility assays to preclinical studies. These were still limited in the ability to identify the underlying causes the observed platelet and leukocyte activation. Flow conditions; shear induced activation and cell trauma; blood-contacting surfaces; and antithrombotic regimen probably each contribute to the observed responses to the artificial organs. Unfortunately, the attempts to devise a system to further investigate the potential contributions of each of these effects fell short of the intended goals. The issue is not trivial, and it can be argued that no one as of yet has adequately investigated these concerns.

In conclusion a multi-modal system to evaluate and quantify the response of platelets and leukocytes to novel cardiovascular devices was implemented. The use of a sham surgical procedure provided a mechanism to account for the severe effects of the implant procedure. Ongoing platelet and leukocyte activation and decreased platelet life spans beyond the recovery period could thus be attributed to the implanted devices. The assays also proved valuable for the evaluation device modifications and operation. Thus, the application of sophisticated biocompatibility assays may be utilized to develop safer artificial organs.

8.2 FUTURE STUDIES

The overall goal of this work was to develop methods leading to safe artificial organs. To continue that pursuit biocompatibility must be integrated into the design process as much as possible. Refining and implementing blood damage models into a CFD based design optimization approach holds promise for developing better, safer artificial organs and getting those devices to the clinic faster. Currently there exists a dichotomy in blood model development in that most models focus on either the biochemical factors or mechanical forces,

but do not unite the two. Anand has coalesced a comprehensive model of thrombosis, which addresses some previous limitations [133]. However, to adequately unite the multiple inputs which may result in platelet activation, a unified model requires focus on the common aspect of the pathways, factors, agonists, and forces which influence platelet behavior, perhaps the intracellular calcium concentration. Thus, a comprehensive model of blood flow would incorporate mechanical effects, such as mechanically-induced hemolysis, shear-induced platelet aggregation, sublethal trauma, and biochemical effects such as local thrombin generation, with other factors including the thrombogenicity of the surface and the influence of antithrombotic agents. Overall, the goal of the future studies is to use the assays that have been developed (with further expansion as needed) to refine blood models for enhanced suitability for artificial organ design, while continuing to use the assays as tools to evaluate the devices and their modifications. Incorporating biocompatibility testing into the research and development phase will lead to production of safer artificial organs.

BIBLIOGRAPHY

1. Poulter N. Coronary heart disease is a multifactorial disease. *Am J Hypertens.* 1999;12(10 Pt 2):92S-95S.
2. Harper AM, Rosendale JD, McBride MA, Cherikh WS, Ellison MD. *Clinical Transplants.* 1998:73-90.
3. Taylor DO, Edwards LB, Boucek MM, Trulock EP, Keck BM, Hertz MI. The registry of the international society for heart and lung transplantation: Twenty-first official adult heart transplant report – 2004. *J Heart Lung Transplantation.* 2004;23(7):796-803.
4. Howard RJ, Schold JD, Cornell DL. A 10-year analysis of organ donation after cardiac death in the United States. *Transplantation.* 2005;80(5):564-8.
5. Bove AA, Kashem A, Cross RC, Wald J, Furukama S, Berman GO, McClurken JB, Eisen HJ. Factors affecting survival after heart transplantation: Comparison of pre- and post-1999 listing protocols. *J Heart Lung Transplant.* 2006;25(1):42-7.
6. El-Banayosy A, Arusoglu L, Kizner L, Tenderich G, Minami K, Inoue K, Korfer R. Novacor left ventricular assist system versus Heartmate vented electric left ventricular assist system as a long-term mechanical circulatory support device in bridging patients: a prospective study. *J Thorac Cardiovasc Surg.* 2000;119(3):581-7.
7. Mann DL, Willerson JT. Left ventricular assist devices and the failing heart: a bridge to recovery, a permanent assist device, or a bridge too far? *Circulation.* 1998;98(22):2367-9.
8. Pennington DG, Oaks TE, Lohmann DP. Permanent ventricular assist device support versus cardiac transplantation. *Ann Thorac Surg.* 1999;68(2):729-33.
9. Cooley DA. The total artificial heart. *Nature Med.* 2003;9(1):108-111.
10. Joyce LD, DeVries WC, Hastings WL, Olsen DB, Jarvik RK, Kolff WJ. Response of the human body to the first permanent implant of the Jarvik-7 total artificial heart. *Transact Amer Soc Artif Intern Organs.* 1983;29:81-5.
11. Burns GL. Infections associated with implanted blood pumps. *Int J Artif Organs* 1993;16(11):771-6.

12. Dowling RD, Gray Jr LA, Etoch SW, Laks H, Marelli D, Samuels L, Entwistle J, Couper G, Vlahakes GJ, Frazier OH, Hetzer R. Initial experience with the Abioco^r implantable replacement heart system. *J Thorac Cardiovasc Surg.* 2004;127(1):131-141.
13. FDA Center for Devices and Radiological Health, Medical Devices Advisory Committee, Circulatory Systems Device Panel Meeting, Gaithersburg, Md June 23rd, 2005. www.fda.gov/ohrms/dockets/ac/05/transcripts/2005-4149t2.htm
14. Starzl TE, Weil III R, Iwatsuki S. FK 506 for human liver, kidney and pancreas transplantation. *Lancet.* 1989;2:1000-4.
15. Todo S, Fung JJ, Starzl TE. Liver, kidney, and thoracic organ transplantation under FK 506. *Ann Surg.* 1990;212:295-305.
16. Griffith BP, Hardesty RL, Kormos RL. Temporary use of the Jarvik-7 total artificial heart before transplantation. *New Eng J Med.* 1987;316(3):130-4.
17. Arabia FA, Smith RG, Rose DS, Arzouman DA, Sethi GK, Copeland JG. Success rates of long-term circulatory assist devices used currently for bridge to heart transplantation. *ASAIO J.* 1996;42(5):542-6.
18. Hampton CR, Verrier ED. Systemic consequences of ventricular assist devices: Alterations of coagulation, immune function, inflammation, and the neuroendocrine system. *Artif Organs.* 2002;26(11):902-8.
19. Gross DR. Concerning thromboembolism associated with left ventricular assist devices. *Cardiovasc Res.* 1999;42(1):45-7.
20. Lutwick LI, Vaghjimal A, Connolly MW. Postcardiac surgery infections. *Crit Care Clin.* 1998;14(2):221-50.
21. Chinn R, Dembitsky W, Waton L, Chillcott S, Stahovich M, Rasmusson B, Pagani F. Multicenter experience: Prevention and management of left ventricular assist device infections. *ASAIO J.* 2005;51(4):461-70.
22. Dowling RD, Park SJ, Pagani FD, Tector AJ, Naka Y, Icenogle TB, Poirier VL, Frazier OH. Heartmate VE LVAS design enhancements and its impact on device reliability. *Euro J Cardiothorac Surg.* 2004;25(6):958-63.
23. Wheeldon DR, LaForge DH, Lee J, Jansen PGM, Jassawalla JS, Portner PM. Novacor left ventricular assist system long-term performance: Comparison of clinical experience with demonstrated *in vitro* reliability. *ASAIO J.* 2002;48(5):546-51.
24. Farrar DJ. The thoratec ventricular assist device: a paracorporeal pump for treating acute and chronic heart failure. *Semin Thorac Cardiovasc Surg.* 2000;12(3):243-50.
25. Song X, Throckmorton AL, Untaroiu A, Patel S, Allaire PE, Wood HG, Olsen DB. Axial flow blood pumps. *ASAIO J.* 2003;49(4):355-64.

26. Fossum TW, Morley D, Benkowski R, Tayama E, Olsen DB, Burns G, Miller MW, Franks J, Martinez E, Carroll G, Edwards J, Vinnerqvist A, Lynch B, Stein F, Noon GP, DeBakey ME. Chronic survival of calves implanted with the DeBakey ventricular assist device. *Artif Organs*. 1999;23(8):802-6.
27. Kameneva MV, Watach MJ, Litwak P, Antaki JF, Butler KC, Thomas DC, Taylor LP, Borovetz HS, Kormos RL, Griffith BP. Chronic animal health assessment during axial ventricular assistance: importance of hemorheologic parameters. *ASAIO J*. 1999;45(3):183-8.
28. Kawahito K, Mohara J, Misawa Y, Fuse K. Platelet damage caused by the centrifugal pump: *in vitro* evaluations by measuring the release of α -granule packing proteins. *Artif Organs*. 1997;21(10):1105-9.
29. Williams MS, Collier BS, Vaananen HK, Scudder LE, Sharma SK, Marmur JD. Activation of platelets in platelet-rich plasma by rotablation is speed-dependent and can be inhibited by abciximab (c7E3 Fab; Reopro). *Circulation*. 1998;98(8):742-8.
30. Takami Y, Makinouchi K, Nakazawa T, Yamane S, Glueck J, Nose Y. Mechanical white blood cell damage in rotary blood pumps. *Artif Organs*. 1997;21:138-42.
31. Bonaros N, Mueller MR, Salat A, Schima H, Roethy W, Rocher AA, Wolner E, Wieselthaler GM. Extensive coagulation monitoring in patients after implantation of the MicroMed DeBakey continuous flow axial pump. *ASAIO J*. 2004;50(5):424-31.
32. Koster A, Loebe M, Hansen R, Potapov EV, Noon GP, Kuppe H, Hetzer R. Alterations in Coagulation after implantation of a pulsatile Novacor LVAD and the axial flow Micromed DeBakey LVAD. *Ann Thorac Surg*. 2000;70:533-7.
33. Loebe M, Koster A, Sanger S, Potapov EV, Kuppe H, Noon GP, Hetzer R. Inflammatory response after implantation of a left ventricular assist device: comparison between the axial flow MicroMed DeBakey VAD and the pulsatile Novacor device. *ASAIO J*. 2001;47:272-4.
34. Rothenburger M, Wilhelm MJ, Hammel D, Schmidt C, Tjan TDT, Bocker D, Scheld HH, Schmid C. *Circulation*. 2002;106(13S):I189-92.
35. Frazier OH, Myers TJ, Gregoric ID, Khan T, Delgado R, Croitoru M, Miller K, Jarvik R, Westaby S. Initial clinical experience with the Jarvik 2000 implantable axial-flow left ventricular assist system. *Circulation*. 2002;105:2855-60.
36. Westaby S, Banning AP, Saito S, Pigott DW, Jin XY, Catarino PA, Robson D, Moorjani N, Kardos A, Poole-Wilson PA, Jarvik R, Frazier OH. Circulatory support for long-term treatment of heart failure, experience with an intraventricular continuous flow pump. *Circulation*. 2002;105:2588-91.

37. Westaby S, Frazier OH, Beyersdorf F, Saito S, Siegenthaler MP, Pigott DW, Catarino PA, Jarvik R. The Jarvik 2000 heart. Clinical validation of the intraventricular position. *Eur J Cardiothorac Surg.* 2002;22:228-32.
38. Delgado III RD, Frazier OH, Myers TJ, Gregoric ID, Robertson K, Shah, Kar B. Direct thrombolytic therapy for intraventricular thrombosis in patients with the Jarvik 2000 left ventricular assist device. *J Heart Lung Transplant.* 2005;24(2):231-3.
39. Brontman DJ, Deitcher SR, Yip GY. Virchow's triad revisited. *Southern Medical J.* 2004;97(2):213-4.
40. Vroman L. The life of an artificial device in contact with blood: initial events and their effect on its final state. *Bull New York Acad Med: J Urban Health.* 1988;64(4):352-7.
41. Horbett TA. Proteins: Structure, properties, and adsorption to surfaces. *Biomaterials Science: An introduction to materials in medicine.* pp. 133-141, Ratner BD, Hoffman AS, Schoen FJ, Lemons JE, editors. San Diego: Academic Press 1996.
42. Bloom AL, ed., *Haemostasis and Thrombosis*, 3rd Ed. Edinburgh; New York: Churchill Livingstone, 1994.
43. Wu Y, Simonovsky FI, Ratner BD, Horbett TA. The role of adsorbed fibrinogen in platelet adhesion to polyurethane surfaces: comparison of surface hydrophobicity, protein adsorption, monoclonal antibody binding, and platelet adhesion. *J Biomed Mater Res – Part A.* 2005;74(4):722-38.
44. Wettero J, Bengtsson T, Tengvall P. Complement activation on immunoglobulin G-coated hydrophobic surfaces enhances the release of oxygen radicals from neutrophils through an actin-dependent mechanism. *J Biomed Mater Res.* 2000;51(4):742-51.
45. Shen M, Martinson L, Wagner MS, Castner DG, Ratner BD, Horbett TA. PEO-like plasma polymerized tetraglyme surface interactions with leukocytes and proteins: *In vitro* and *in vivo* studies. *J Biomat Sci, Poly Ed.* 2002;13(4):367-90.
46. Burchenal JEB, Deible CR, Deglau TE, Russell AJ, Beckman EJ, Wagner WR. Polyethylene glycol diisocyanate decreases platelet deposition after balloon injury of rabbit femoral arteries. *J Thrombosis Thrombolysis.* 2002;13(1):27-33.
47. Weber N, Wendel HP, Ziemer G. Hemocompatibility of heparin-coated surfaces and the role of selective plasma protein adsorption. *Biomaterials.* 2002;23(2):429-39.
48. Affeld K, Reininger AJ, Gadischke J, Grunert K, Schmidt S, Thiele F. Fluid mechanics of the stagnation flow chamber and its platelet deposition. *Artif Organs.* 1995;19(7):597-602.
49. Kerrigan JP, Yamazaki K, Meyer RK, Mori T, Otake Y, Outa E, Umezu M, Antaki JF. High resolution fluorescent particle-tracking flow visualization within an intraventricular axial flow left ventricular assist device. *Artif Organs.* 1996;20(6):534-40.

50. Grigioni M, Daniele C, Morbiducci U, D'Avenio G, Di Benedetto G, Barbaro V. The power-law mathematical model for blood damage prediction: Analytical developments and physical inconsistencies. *Artif Organs*. 2004;28(5):467-75.
51. Yeleswarapu KK, Antaki JF, Kameneva MV, Rajagopal KR. A mathematical model for shear-induced hemolysis. *Artif Organs*. 1995;19(7):576-82.
52. Song X, Throckmorton AL, Wood HG, Antaki JF, Olsen DB. Computational fluid dynamics prediction of blood damage in a centrifugal pump. *Artif Organs*. 2003;27(10):938-41.
53. Peterson DM, Stathopoulos NA, Giorgio TD, Hellums JD, Moake JL. Shear-induced platelet aggregation requires von Willebrand factor and platelet membrane glycoproteins Ib and IIb-IIIa. *Blood*. 1987;69:625-8.
54. Yap CL, Anderson KE, Hughan SC, Dopheide SM, Salem HH, Jackson SP. Essential role for phosphoinositide 3-kinase in shear-dependent signaling between platelet glycoprotein Ib/V/IX and integrin α IIb β 3. *Blood*. 2002;99:151-8.
55. Clementson KJ. Platelet Activation: signal transduction via membrane receptors. *Thromb Haemo*. 1995;74:111-5.
56. Miura S, Sakurai Y, Takatsuka H, Yoshioka A, Matsumoto M, Yagi H, Kokubo T, Ikeda Y, Matsui T, Titani K, Fujimura Y. Total inhibition of high shear stress induced platelet aggregation by homodimeric von Willebrand factor A1-loop fragments. *Brit J Haematol*. 1999;105(4-II):1092-1100.
57. Sakariassen KS, Hanson SR, Cadroy Y. Methods and models to evaluate shear-dependent and surface reactivity dependent antithrombotic efficacy. *Thromb Res*. 2001;104:149-174.
58. Wootton DM, Ku DN. Fluid mechanics of vascular systems, disease, and thrombosis. *Annu Rev Biomed Eng*. 1999;1:299-329.
59. Wurzinger LJ, Opitz R, Wolf M, Schmid-Schonbein H. Shear induced platelet activation: a critical reappraisal. *Biorheology*. 1985;22:399-413.
60. Wurzinger LJ, Blasberg P, Schmid-Schonbein H. Towards a concept of thrombosis in accelerated flow: rheology, fluid dynamics, and biochemistry. *Biorheology*. 1985;22(5):437-50.
61. Wurzinger LJ, Opitz R, Wolf M, Schmid-Schonbein H. Ultrastructural investigations on the question of mechanical activation of blood platelets. *Blut* 1987;54:97-107.
62. Wurzinger LJ, Opitz R. Hematological principles of hemolysis and thrombosis with special reference to rotary blood pumps. *Proc Int Workshop on Rotary Blood Pumps*. Eds. Schima H et al., Vienna, 1991.

63. Klaus S, Korfer S, Mottaghy K, Reul H, Glasmacher B. *In vitro* blood damage by high shear flow: Human versus porcine blood. *Int J Artif Organs*. 2002;25(4):306-12.
64. Sakariassen KS, Holme PA, Orvim U, Barstad RM, Solum NO, Brosstad FR. Shear-induced platelet activation and platelet microparticle formation in native human blood. *Thromb Res*. 1998;92(6,S2):S33-41.
65. Copeland JG, Arabia FA, Smith RG, Sethi GK, Nolan PE, Banchy ME. Arizona experience with CardioWest total artificial heart bridge to transplantation. *Ann Thorac Surg*. 1999;68(2):756-60.
66. Houel R, Mazoyer E, Kirsch M, Boval B, Drouet L, Loisançe DY. Resistance to aspirin after external ventricular assist device implantation. *J Thorac Cardiovasc Surg*. 2003;126(5):1636-7.
67. Yamazaki K, Kormos R, Mori T, Umezu M, Kameneva M, Antaki J, Outa E, Litwak P, Kerrigan J, Tomczak J, et al. An intraventricular axial flow blood pump integrated with a bearing purge system. *ASAIO J*. 1995;41(3):M327-32.
68. Yamazaki K, Litwak P, Kormos RL, Mori T, Tagusari O, Antaki JF, Kameneva M, Watach M, Gordon L, Umezu M, Tomioka J, Koyanagi H, Griffith BP. An implantable centrifugal blood pump for long term circulatory support. *ASAIO J*. 1997;43(5):M686-91.
69. Yamazaki K, Litwak P, Tagusari O, Mori T, Kono K, Kameneva M, Watach M, Gordon L, Miyagishima M, Tomioka J, Umezu M, Outa E, Antaki JF, Kormos RL, Koyanagi H, Griffith BP. An implantable centrifugal blood pump with a recirculating purge system (Cool-Seal system). *Artif Organs*. 1998;22(6):466-74.
70. Westaby S, Katsumata T, Houel R, Evans R, Pigott D, Frazier OH, Jarvik R. Jarvik 2000 heart: potential for bridge to myocyte recovery. *Circulation*. 1998;98(15):1568-74.
71. DeBakey ME. A miniature implantable axial flow ventricular assist device. *Ann Thorac Surg*. 1999;68(2):637-40.
72. Czlonkowska A, Ryglewicz D, Lechowicz W. Basic analytical parameters as the predictive factors for 30-day case fatality rate in stroke. *Acta Neurol Scand*. 1997;95(2):121-4.
73. Kihara S, Yamazaki K, Litwak KN, Litwak P, Kameneva MV, Ushiyama H, Tokuno T, Borzelleca DC, Umezu M, Tomioka, J, Tagusari O, Akimoto T, Koyanagi H, Kurosawa H, Kormos RL, Griffith BP. *In vivo* Evaluation of a MPC Polymer Coated Continuous Flow Left Ventricular Assist System. *Artif Organs* 2003;27(2):188-192.
74. Amrani DL, Christensen C, Hauerwas L, Rieder M, Mosesson MW, Schmidt D, Flemma R, Prophet GA, Pierce W. Hemostatic evaluation of Sarns/3M-VAD implantation in calves. *Trans Am Soc Artif Intern Organs* 1991;37:M308-M310.

75. Harasaki H, Fukamachi K, Benavides M, Manos J, Wika K, Massiello A. A comprehensive hematologic study in calves with total artificial hearts. *ASAIO J.* 1995;41: M266-71.
76. Soloviev MV, Okazaki Y, Harasaki H. Whole blood platelet aggregation in humans and animals: a comparative study. *J Surg Res.* 1999;82(2):180-7.
77. Sato M, Harasaki H. Evaluation of platelet and coagulation function in different animal species using the xylum clot signature analyzer. *ASAIO J.* 2002;48(4):360-4.
78. Baker LC, Davis WC, Autieri J, Watach MJ, Yamazaki K, Litwak P, Wagner WR. Flow cytometric assays to detect platelet activation and aggregation in device-implanted calves. *J Biomed Mater Res.* 1998;41(2):312-21.
79. Morel MC, Lecompte T, Champeix P, Favier R, Potevin F, Samama M, Salmon C, Kaplan C. PL2-49, a monoclonal antibody against glycoprotein IIb which is a platelet activator. *Brit J Haematol.* 1989;71(1):57-63.
80. Tzima E, Walker JH. Platelet annexin V: The ins and outs. *Platelets.* 2000;11(5):245-51.
81. Dewald O, Schmitz C, Diem H, Goehring P, Vetter HO, Roell W, Goedje O, Tschoepe D, Reichart B. Platelet activation markers in patients with heart assist device. *Artif Organs.* 2005;29(4):292-9.
82. White JG. The secretory pathway of bovine platelets. *Blood.* 1987;69(3):878-85.
83. Brooke GP, Sopp P, Kwong LS, Howard CJ. Molecular cloning of cattle CD63 and evidence for high level expression on subpopulations of dendritic cells. *Immunogenetics.* 1999;49(9):812-4.
84. Snyder TA, Litwak KN, Watach MJ, Wagner WR. Platelet activation, aggregation, and life span in calves implanted with axial flow ventricular assist devices. *Ann Thorac Surg.* 2002;73(6):1933-8.
85. Softeland E, Hervig T, Framstad T, Holmsen H. Simple method for labeling of porcine platelets with indium-111 oxine. *Laboratory Anim Sci.* 1995;45(2):195-8.
86. Manning KL, Novinger S, Sullivan PS, McDonald TP. Successful determination of platelet lifespan in C3H mice by *in vivo* biotinylation. *Laboratory Anim Sci.* 1996;46(5):545-8.
87. Baker LC, Kameneva MV, Watach MJ, Litwak P, Wagner WR. Assessment of bovine platelet life span with biotinylation and flow cytometry. *Artif Organs.* 1998;22:799-803.
88. Magnusson S, Hou M, Hallberg EC, Breimer ME, Wadenvik H. Biotinylated platelets have an impaired response to agonists as evidenced by *in vitro* platelet aggregation tests. *Thromb Res.* 1998;89(2):53-8.

89. Michelson AD, Barnard MR, Krueger LA, Valeri CR, Furman MI. Circulating monocyte-platelet aggregates are a more sensitive marker of *in vivo* platelet activation than platelet surface p-selectin: Studies in baboons, human coronary intervention, and human acute myocardial infarction. *Circulation*. 2001;104(13):1533-7.
90. Nijm J, Wikby A, Tompa A, Olsson AG, Jonasson L. Circulating levels of proinflammatory cytokines and neutrophil-platelet aggregates in patients with coronary artery disease. *Amer J Cardiology*. 2005;95(4):452-6.
91. Bertrand OF, Sipehia R, Mongrain R, Rodes J, Tardif JC, Bilodeau L, Cote G, Bourassa MG. Biocompatibility aspects of new stent technology. *J Am Coll Cardiol*. 1998;32(3):562-71.
92. Wilhelm CR, Ristich J, Kormos RL, Wagner WR. Monocyte tissue factor expression and ongoing complement generation in ventricular assist device patients. *Ann Thorac Surg*. 1998;65:1071-6.
93. Wilhelm CR, Ristich J, Knepper LE, Holubkov R, Wisniewski SR, Kormos RL, and Wagner WR. Measurement of hemostatic indices in conjunction with transcranial doppler sonography in ventricular assist device patients. *Stroke*. 1999;30: 2554-61.
94. Coomber BL, Nyarko KA, Noyes TM, Gentry PA. Neutrophil-platelet interactions and their relevance to bovine respiratory disease. *The Veterinary J* 2001;161(1):41-62.
95. Davis WC, Marusic S, Lewin HA, Splitter GA, Perryman LE, McGuire TC, Gorham JR. The development and analysis of species specific and cross reactive monoclonal antibodies to leukocyte differentiation antigens and antigens of the major histocompatibility complex for use in the study of the immune system in cattle. *Vet Immunol Immunopathol*. 1987;15(4):337-76.
96. Carson SD, Bach R, Carson SM. Monoclonal antibodies against bovine tissue factor, which block interaction with factor VIIa. *Blood*. 1985;66(1):152-156.
97. Bokarewa MI, Morrissey JH, Tarkowski A. Tissue factor as a proinflammatory agent. *Arthritis Res*. 2002;4:190-195.
98. Butler K, Thomas D, Antaki J, Borovetz H, Griffith B, Kameneva M, Kormos R, Litwak P. Development of the Nimbus/University of Pittsburgh axial flow left ventricular assist system. *Artif Organs*. 21:602-10 (1997).
99. Butler KC, Dow JJ, Litwak P, Kormos RL, Borovetz HS. Development of the Nimbus/University of Pittsburgh innovative ventricular assist system. *Ann Thorac Surg*. 68:790-4 (1999).
100. Griffith BP, Kormos RL, Borovetz HS, Litwak K, Antaki JF, Poirie VL, Butler KC. Heartmate II left ventricular assist system: from concept to first clinical use. *Ann Thorac Surg*. 2001;71(3 Suppl):S116-20.

101. Amin DV, Antaki JF, Litwak P, Thomas D, Wu ZJ, Watach M. Induction of ventricular collapse by an axial flow blood pump. *ASAIO J.* 1998;44(5):M685-90.
102. Rose EA, Levin HR, Oz MC, Frazier OH, Macmanus Q, Burton NA, Lefrak EA. Artificial circulatory support with textured interior surfaces. A counterintuitive approach to minimizing thromboembolism. *Circulation.* 1994;90(5 Pt 2):II87-97.
103. Frazier OH, Baldwin RT, Eskin SG, Duncan JM. Immunochemical identification of human endothelial cells on the lining of a ventricular assist device. *Texas Heart Inst J.* 1993;20(2):78-82.
104. Spanier T, Oz M, Levin H, Weinberg A, Stamatis K, Stern D, Rose E, Schmidt AM. Activation of coagulation and fibrinolytic pathways in patients with left ventricular assist devices. *J Thorac Cardiovasc Surg.* 1996;112:1090-7.
105. Frazier OH, Rose EA, Oz MC, Dembitsky W, McCarthy P, Radovancevic B, Poirier VL, Dasse KA, Couper G, Cummings N, Vargo R, Foray-Kaplon A, Vacha C, KAmis S, Yeager MM, Catanses K, Burton N, Hill A, Muncy K, Acker M, O'Hara ML, Long J, Pitt J, Marks J, Bagley A, Foy B, Martin K, Laff M, Peterson A, Scatena M, Beatty L, Maier G, Baker K, Flattery M, Mack M, McMellon T, Fuzesi L, Klapp L, Cortez E, Van Meter C, Hollenbach S, Uber P, Kersker L, Piccione W, Mattea A, Grady K, Icenogle T, Sato D, Himey S, Butters D, Puhlman M, Chilcott S, Murphy D, Davis P, Leighty S, Tector A, Dressler D, Schauer P, Matiak L, Jeevanandam V, Furukawa S, Todd B, Hargraves J, Myers T, Tamez D, Miller K, Boyce S, Sweet L, Walsh S, Holman W, Brantley L, Wainscott C, Richenbacher W, Vance S, Laxson C, Pagani F, Monaghan H, Mentzer R, Canver C, Jacobs L, Yakey J. Multicenter clinical evaluation of the HeartMate vented electric left ventricular assist system in patients awaiting heart transplantation. *J Thorac Cardiovasc Surg.* 2001;122(6):1186-95.
106. Wu ZJ, Antaki JF, Burgreen GW, Butler KC, Thomas DC, Griffith BP. Fluid dynamic characterization of operating conditions for continuous flow blood pumps. *ASAIO J.* 1999;45:442-9.
107. Kihara S, Litwak KN, Nichols L, Litwak P, Kameneva MV, Wu Z, Kormos RL, Griffith BP. Smooth muscle cell hypertrophy of renal cortex arteries with chronic continuous flow left ventricular assist. *Ann Thorac Surg.* 2003;75(1):178-83.
108. Akimoto T, Litwak KN, Yamazaki K, Litwak P, Kihara S, Tagusari O, Yamazaki S, Kameneva MV, Watach MJ, Umezu M, Tomioka J, Kormos RL, Koyanagi H, Griffith BP. The role of diastolic pump flow in centrifugal blood pump hemodynamics. *Artif Organs.* 2001;25(9):724-7.
109. Akimoto T, Yamazaki K, Litwak P, Litwak KN, Tagusari O, Mori T, Antaki JF, Kameneva MV, Watach MJ, Umezu M, Tomioka J, Kormos RL, Koyanagi H, Griffith BP. Continuously maintaining positive flow avoids endocardial suction of a rotary blood pump with left ventricular bypass. *Artif Organs.* 2000;24(8):606-10.

110. Yun YH, Turitto VT, Daigle KP, Kovacs P, Davidson JA, Slack SM. Initial hemocompatibility studies of titanium and zirconium alloys: Prekallikrein activation, fibrinogen adsorption, and their correlation with surface electrochemical properties. *J Biomed Mater Res.* 1996;32(1):77-85.
111. Maitz MF, Pham MT, Wieser E, Tsyganov I. Blood compatibility of titanium oxides with various crystal structure and element doping. *J Biomater Applications.* 2003;17(4):303-19.
112. Schaub RD, Kameneva MV, Borovetz HS, Wagner WR. Assessing acute platelet adhesion on opaque metallic and polymeric biomaterials with fiber optic microscopy. *J Biomed Mater Res.* 2000;49(4):460-8.
113. Yamazaki K, Mori T, Tomioka J, Litwak P, Antaki JF, Tagusari O, Koyanagi, Griffith BP, Kormos RL. The cool seal system: a practical solution to the shaft seal problem and heat related complications with implantable rotary blood pumps. *ASAIO J.* 1997;43(5): M567-71.
114. Michelson AD, Barnard MR, Hechtman HB, MacGregor H, Connolly RJ, Loscalzo J, Valeri CR. *In vivo* tracking of platelets: Circulating degranulated platelets rapidly lose surface P-selectin but continue to circulate and function. *Proc Natl Acad Sci USA.* 1996;93:11877-82.
115. Chen JY, Wang LP, Fu KY, Huang N, Leng Y, Leng YX, Yang P, Wang J, Wan GJ, Sun H, Tian XB, Chu PK. Blood compatibility and sp³/sp² contents of diamond-like carbon (DLC) synthesized by plasma immersion ion implantation-deposition. *Surf Coatings Tech.* 2002;156(1-3):289-94.
116. Ishihara K, Oshida H, Ueda T, Endo Y, Watanabe A, Nakabayashi N. Hemocompatibility of human whole blood on polymers with a phospholipid polar group and its mechanism. *J Biomed Mater Res.* 1992;26:1543-52.
117. Antaki JF, Paden B, Burgreen G, Groom NJ. "Blood Pump Having a Magnetically Suspended Rotor" US Patent No. 6,447,266 B2. Issued Sep 10, 2002.
118. Wu ZJ, Gottlieb RK, Burgreen GW, Holmes JA, Borzelleca DC, Kameneva MV, Griffith BP, Antaki JF. Investigation of fluid dynamics within a miniature mixed flow blood pump. *Experiments in Fluids.* 2001;31(6):615-619.
119. Ross DW, Ayscue LH, Watson J, Bentley SA. Stability of hematologic parameters in healthy subjects: Intraindividual versus interindividual variation. *Am J Clin Pathol.* 1988;90:262-267.
120. Wu J, Antaki JF, Snyder TA, Wagner WR, Borovetz HS, Paden BE. CFD analysis of blade tip clearances on hydrodynamic performance and blood damage in a miniature pediatric blood pump. Submitted to *Artif Organs.*

121. Burgreen GW, Antaki JF, Wu ZJ, Holmes AJ. Computational fluid dynamics as a development tool for rotary blood pumps. *Artif Organs* 2001;25(5):336-40.
122. Arora D, Behr M, Pasquali M. A tensor-based measure for estimating blood damage. *Artif Organs* 2004;28(11):363-5.
123. Sorensen EN, Burgreen GW, Wagner WR, Antaki JF. Computational simulation of platelet deposition and activation: I. Model development and properties. *Ann Biomed Eng* 1999;27(4):436-48.
124. Sorensen EN, Burgreen GW, Wagner WR, Antaki JF. Computational simulation of platelet deposition and activation: II. Results for poiseuille flow over collagen. *Ann Biomed Eng* 1999;27(4):449-58.
125. Giersiepen M, Wurzinger LJ, Opitz R, Reul H. Estimation of shear stress-related blood damage in heart valve prostheses – in vitro comparison of 25 aortic valves. *Int J Artif Organs*. 1990;13(5):300-6.
126. O'Brien JR, Shear-induced platelet aggregation. *Lancet* 1990;335:711-713.
127. Klaus S, Korfer S, Mottaghy K, Reul H, Glasmacher B. In vitro blood damage by high shear flow: human versus porcine blood. *Int J Artif Organs*. 2002;25(4):306-12.
128. Paul R, Apel J, Klaus S, Schugner F, Schwindke P, Reul H. Shear stress related blood damage in laminar couette flow. *Artif Organs*. 2003;27(6):517-29.
129. McMillan DE, Strigberger J, Utterback NG. Blood's critical Taylor number and its flow behavior at supercritical Taylor numbers. *Biorheology*. 1987;24(4):401-410.
130. Wu J, Antaki JF, Wagner WR, Snyder TA, Paden BE, Borovetz HS. Design optimization of blood shearing instrument by computational fluid dynamics. *Artif Organs*. 2005;29(6):482-9.
131. Hattler BG, Lund LW, Golob J, Russian H, Lann MF, Merrill TL, Frankowski BF, Federspiel WJ. A respiratory gas exchange catheter: *In vitro* and *in vivo* tests in large animals. *J Thorac Cardiovasc Surg*. 2002;124:520-530.
132. Thompson LO, Leobe M, Noon GP. What price support? Ventricular assist device induced systemic response. *ASAIO J*. 2003;49(5):518-526.
133. Anand M, Rajagopal K, Rajagopal KR. A model incorporating some of the mechanical and biochemical factors underlying clot formation and dissolution in flow blood. *J Theoretical Med*. 2003;5(34):183-218.